Interface Motion in the Ostwald Ripening and Chemotaxis Systems

by

Eamon Kavanagh

B.Sc., McMaster University, 2011

A THESIS SUBMITTED IN PARTIAL FULFILLMENT OF
THE REQUIREMENTS FOR THE DEGREE OF

MASTER OF SCIENCE

in

The Faculty of Graduate and Postdoctoral Studies

(Mathematics)

THE UNIVERSITY OF BRITISH COLUMBIA

(Vancouver)

August 2014

Abstract

Ostwald ripening and chemotaxis are two different mechanisms that describe particle motion throughout a domain. Ostwald ripening describes the redistribution of a solid solution due to energy potentials while chemotaxis is a cellular phenomenon where organisms move based on the presence of chemical gradients in their environment. Despite the two systems coming from disparate fields, they are connected by the late-stage dynamics of interfacial motion.

For the Ostwald ripening system we consider the case of N droplets in the asymptotic limit of small radii $r_i \ll 1$. We first derive a system of ODEs that describe the motion of the droplets and then improve this calculation by including higher order terms. Certain properties, such as area preservation and finite time extinction of certain droplets are proved and a numerical example is presented to support the claims.

In the chemotaxis model we look at the asymptotic limit of diffusive forces being small compared to that of chemotactic gradients. We use a boundary-fitted coordinate system to derive an equation for the velocity of an arbitrary interface and analyze a few specific examples. The asymptotic results are also explored and confirmed using the finite element and level set methods.

Our analysis reveals the mechanism of movement to be motion by curvature in Ostwald ripening and a surface diffusion law in chemotaxis. The governing rules of motion may be different in the two systems but the end result is typically characteristically similar- exchange of mass and smoothing in favor of a larger and more stable configuration of drops.

Preface

Chapter 2 and 3 are based on research conducted by Dr. Michael Ward of UBC's mathematics department and Eamon Kavanagh. I was responsible for much of the analysis, verification, and numerical simulations. Chapter 4 is based on work of myself and Dr. Anthony Peirce, also of UBC's mathematics department. I was responsible for coding, numerical simulations, and error analysis.

Table of Contents

List of Tables

List of Figures

Acknowledgements

I would like to thank my supervisors Anthony Peirce and Michael Ward for their help and guidance over the past two years as well as giving me this great project to work on. I would also like to thank the professors who offered courses that I took for their time spent lecturing and mentoring: Neil Balmforth, George Bluman, Chen Greif, Michael Friedlander and Brian Wetton with additional thanks to Ian Mitchell for his help on level set methods. I want to thank Michael Lindstrom and Iain Moyles for answering many questions along the way and providing the advice that comes with years in graduate school. Last but not least I want to express my appreciation to the helpful staff of the Mathematics Department as well as the Institute of Applied Mathematics.

Chapter 1

Introduction

1.1 Ostwald Ripening

Ostwald ripening, colloquially known as 'survival of the fattest', is a coarsening process that describes the change of an inhomogeneous structure over time. Similar particles separate into groups throughout a domain and exchange mass with each other, favoring larger regions over smaller ones. The result is an increase in size and a decrease in the overall number of individual groups. Mass diffuses against concentration gradients in order to reduce interfacial energy (the mean curvature of all interfaces). By the Gibbs-Thomson condition, this reduces the gradient of the chemical potential and thus the driving force for the diffusion (see [2]). Ostwald ripening can be seen in an oil and water emulsion separating over time and typically occurs after a phase transformation such as spinodal decomposition.

Spinodal decomposition is a form of phase separation in which a homogenous solution separates into regions of distinct concentration; that is, uniform within the region. Spinodal decomposition may occur when an alloy composed of only two metals is sufficiently heated and then quenched (rapidly cooled) into an unstable state. After this metastable equilibrium is reached, the stage is set for coarsening and particles diffuse to reach a static equilibrium.

The form of phase separation described above has been modeled by the nonlinear Cahn-Hilliard equation, first proposed in [4]. The ground work for this model comes from an earlier work by John W. Cahn and John E. Hilliard in [5] where a measure for total free energy in a binary medium is derived. From this free energy functional one can derive the chemical potential and apply the diffusion equation to obtain a model of phase separation. Much like how Ostwald ripening occurs after a phase transformation, a Mullins-Sekerka free boundary problem can be derived from the late stages ($t \gg 1$) of the Cahn-Hilliard equation that describes this coarsening process. This is quite remarkable and gives credence to the belief that the Cahn-Hilliard equation is an accurate model for phase separation.

In the literature review below, we present the Cahn-Hilliard equation and

its derivation along with some interesting asymptotic results from [23]. We employ matched asymptotic expansions and multiple time scales to derive the aforementioned Mullins-Sekerka problem that will eventually lead to Ostwald ripening.

1.1.1 Literature Review

We begin with the concentration $u(\mathbf{x}, t)$ of one phase in a binary mixture contained in a domain $\Omega \subseteq \mathbb{R}^n$, and a function F that is a measure of bulk free energy density. Performing a Taylor expansion of this function F, we see

$$\begin{aligned} &F(u, \nabla u, \nabla^2 u, \ldots) \\ &\qquad = F(u) + \sum_i \partial_{u_{x_i}} F \partial_{x_i} u + \sum_{i,j} \alpha_{ij}^1 \partial_{x_i x_j}^2 u + \tfrac{1}{2} \sum_{i,j} \alpha_{ij}^2 \partial_{x_i} u \partial_{x_j} u + \ldots, \end{aligned}$$

where $\alpha_{ij}^{1,2}$ are defined by

$$\alpha_{ij}^1 = \partial F / \partial(\partial^2 u / \partial x_i \partial x_j), \quad \alpha_{ij}^2 = \partial^2 F / \partial(\partial u / \partial x_i) \partial(\partial u / \partial x_j).$$

We assume the solution to be isotropic, which allows us to discard the 'off diagonal' terms $i \neq j$. This means that there is no favored direction; everything diffuses as one would expect. Assuming isotropy also means the free energy needs to be symmetric under reflection and rotation of axes, which allows us to conclude that the polarization vector (second term in the Taylor expansion) must be zero. Thus, we have

$$\begin{aligned} \partial_{u_{x_i}} F &= 0, \\ \alpha_{ii}^1 = \alpha_1 &= [\partial F / \partial \nabla^2 u], \\ \alpha_{ii}^2 = \alpha_2 &= [\partial^2 F / (\partial |\nabla u|)^2]. \end{aligned}$$

Upon integrating over the domain, we obtain

$$\int_\Omega [F(u) + \alpha_1 \nabla^2 u + \alpha_2 |\nabla u|^2 + \ldots] \, dV.$$

Applying Green's first identity to the second term in the integral, where the boundary terms vanish due to imposed Neumann conditions, we have

$$\int_\Omega \alpha_1 \nabla^2 u \, dV = -\int_\Omega \nabla \alpha_1 \cdot \nabla u \, dV.$$

Realizing that $\nabla\alpha_1 = (\partial\alpha_1/\partial u)\nabla u$ and letting $\frac{1}{2}\epsilon^2 = \alpha_2 - (\partial\alpha_1/\partial u)$ with $\epsilon \ll 1$, we arrive at the free energy functional, a measure of free energy of $u(\mathbf{x}, t)$ in Ω, as derived in [5]

$$I[u] = \int_\Omega F(u) + \tfrac{1}{2}\epsilon^2 |\nabla u(\mathbf{x})|^2 \, d\mathbf{x}. \tag{1.1}$$

The second term in the functional is motivated by the thought that higher surface tension will increase the free energy in a system. $F(u)$ is chosen to be a double welled quartic polynomial. This double welled structure is known as the 'Flory-Huggins' free energy density and, with its shape, spinodal decomposition can occur (see [27]).

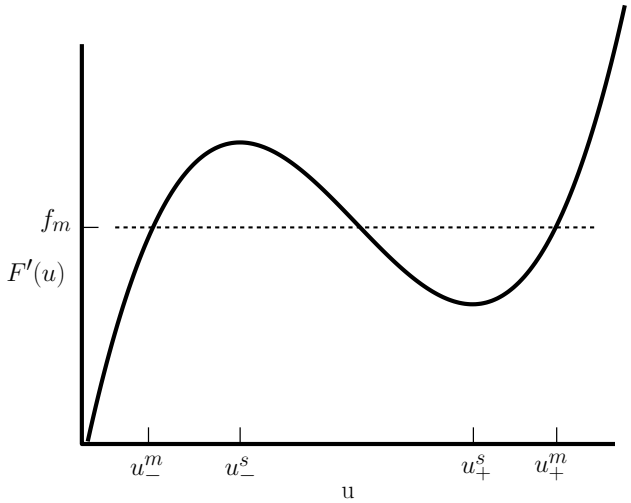

Figure 1.1: $u_m^\pm$ denote max and min concentrations respectively and f_m is the equilibrium free energy level

Now, we take the variational derivative to derive the chemical potential

$$\mu = \frac{\delta I}{\delta u} = \lim_{\delta \to 0} \frac{I[u + \delta v] - I[u]}{\delta}.$$

We calculate,

$$\begin{aligned} I[u + \delta v] &= \int_\Omega F(u + \delta v) + \tfrac{1}{2}\epsilon^2 |\nabla u(x) + \delta v|^2 \, d\mathbf{x} \\ &= \int_\Omega F(u) + F'(u)\delta v + \ldots + \tfrac{1}{2}\epsilon^2 (|\nabla u(x)|^2 + 2|\nabla u \cdot \nabla(\delta v)| + \ldots) \, d\mathbf{x}. \end{aligned}$$

Thus, we have

$$\int_\Omega F'(u)\delta v + \epsilon^2 \nabla u \cdot \nabla \delta v \, d\mathbf{x}.$$

Now, applying Green's first identity with Neumann boundary conditions and with δv being arbitrary, we have

$$\mu = F'(u) - \epsilon^2 \Delta u. \tag{1.2}$$

Finally, we apply the diffusion equation to above to obtain the Cahn-Hilliard equation

$$u_t = \Delta \mu = \Delta(F'(u) - \epsilon^2 \Delta u),$$
$$\mathbf{n} \cdot \nabla \mu = 0, \quad \mathbf{x} \in \partial\Omega; \qquad \mathbf{n} \cdot \nabla u = 0, \quad \mathbf{x} \in \partial\Omega.$$

Energy Decay

Here we prove that $dI[u]/dt \leq 0$, which implies that the energy will decay as $t \to \infty$ and thus the system will eventually reach an equilibrium concentration. Taking a derivative of the free energy functional given in equation (1.1), we see that

$$\frac{dI[u]}{dt} = \int_\Omega \left(\frac{dF(u)}{dt} + \tfrac{1}{2}\epsilon^2 \frac{d}{dt} |\nabla u|^2 \right) d\mathbf{x} = \int_\Omega \left(F'(u) u_t + \epsilon^2 \nabla u \cdot \nabla u_t \right) d\mathbf{x}.$$

Applying Green's first identity, we have

$$\int_\Omega \left(\epsilon^2 \nabla u \cdot \nabla u_t \right) d\mathbf{x} = \int_{\partial\Omega} \left(u_t \frac{\partial u}{\partial n} \right) d\mathbf{x} - \int_\Omega \left(\epsilon^2 u_t \Delta u \right) d\mathbf{x}.$$

Where the boundary term vanishes by the imposed boundary conditions. Thus, we have

$$\frac{dI[u]}{dt} = \int_\Omega u_t(-\epsilon^2 \Delta u + F'(u)) \, d\mathbf{x} = \int_\Omega \Delta\mu(-\epsilon^2 \Delta u + F'(u)) \, d\mathbf{x}.$$

Now, with μ defined in (1.2), we substitute μ into the equation above and apply Green's first identity once again. As before, the boundary terms vanish due to the imposed boundary conditions and we obtain

$$\frac{dI[u]}{dt} = -\int_\Omega |\nabla \mu|^2 \, d\mathbf{x} \leq 0.$$

Thus, we conclude that the energy decays in time and we will eventually reach an equilibrium solution.

After Internal Layer Equilibration

At this point many different directions can be taken with the Cahn-Hilliard equation. [23] first looks at the behavior on a very fast ($T_2 = t/\epsilon^2$) time scale. Instead of following this route we will restrict the analysis to consider the normal t scale and, in this way, derive a limiting system characterizing Ostwald ripening.

First, we define the front Γ, that moves in time and divides Ω into two separate regions Ω_+ and Ω_-. We also assume that Γ does not intersect the boundary of Ω and that u reaches the maximum concentration in Ω_+ and the minimum in Ω_-.

Most of the behavior in which we are interested occurs near Γ. In order to accurately characterize u and μ near this front we define a new variable, z, that measures the stretched normal distance from the front.

$$z = \frac{\phi(\mathbf{x}, t)}{\epsilon},$$

where $\phi(\mathbf{x}, t)$ is the signed distance from Γ to a point $\mathbf{x}$, $\phi > 0$ if $\mathbf{x} \in \Omega_+$, $\phi < 0$ if $\mathbf{x} \in \Omega_-$.

One thing to note is that if a function depends upon $(z, \mathbf{x}, t)$ and $\mathbf{x}$ changes in a direction normal to Γ with z held fixed then the function should remain unchanged, up to terms of $O(\epsilon)$. That is, $w(z, \mathbf{x}, t) = w(z, \mathbf{x} + \delta\nabla\phi(\mathbf{x}, t), t)$ for small real δ.

We also need to define

$$\mathbf{n} = \nabla\phi(\mathbf{x}, t); \qquad \kappa = \nabla \cdot \mathbf{n}; \qquad V = \partial_t\phi(\mathbf{x}, t).$$

Here $\mathbf{n}$ is the unit normal to Γ pointing towards Ω_+, κ is the mean curvature of the interface, positive when the center of curvature is in Ω_- and V is the normal velocity of the front, positive when moving towards Ω_-.

With the new variable definition, $v(\mathbf{x}, t) = w(z, \mathbf{x}, t) = w(\frac{\phi(\mathbf{x},t)}{\epsilon}, \mathbf{x}, t)$, the derivatives change in the following way

$$\begin{aligned} \nabla v &= \nabla_{\mathbf{x}} w + \frac{1}{\epsilon}\mathbf{n}\partial_z w, \\ \Delta v &= \Delta_{\mathbf{x}} w + \frac{1}{\epsilon}\kappa\partial_z w + \frac{1}{\epsilon^2}\partial_{zz} w, \\ \partial_t v &= \partial_t w + \frac{1}{\epsilon}V\partial_z w. \end{aligned} \tag{1.3}$$

There is no $\partial_z \nabla_{\mathbf{x}} w \cdot \nabla \phi$ term in the second equation above because we require that the function be unchanged when z is held fixed and you move in a direction normal to the front. Continuing with the asymptotic expansion, we expand μ and u near the front as

$$\tilde{\mu} = \tilde{\mu}_0 + \epsilon\tilde{\mu}_1 + \epsilon^2\tilde{\mu}_2 + \ldots; \qquad \tilde{u} = \tilde{u}_0 + \epsilon\tilde{u}_1 + \epsilon^2\tilde{u}_2 + \ldots.$$

Expanding terms of the Cahn-Hilliard equation to the lowest order yields

$$\begin{aligned} 0 = \partial_{zz}\tilde{\mu}_0 = \partial_{zz}(F'(\tilde{u}_0) - \partial_{zz}\tilde{u}_0), \\ V\partial_z\tilde{u}_0 = \partial_{zz}\tilde{\mu}_1 + \kappa\partial_z\tilde{\mu}_0. \end{aligned}$$

Integrating the equation for $\tilde{\mu}_0$ we see that

$$F'(\tilde{u}_0) - \partial_{zz}\tilde{u}_0 = a_0 z + a_1,$$

but we assume $\tilde{u}_0$ must be bounded as $z \to \pm\infty$ and thus $a_0 = 0$.

For a_1 we look at far field values of z, $z \gg 0$ or $z \ll 0$. Here, since the phase transformation has ended and we are in a state of quasi-equilibrium, we expect that the values of $\tilde{u}_0$ will be constant in space; that is, $\tilde{u}_0 = u_+^m$ or $\tilde{u}_0 = u_-^m$. Thus, $\partial_{zz}\tilde{u}_0 = 0$ for $z \gg 0$ or $z \ll 0$ and, assuming u is smooth, we determine that $a_1 = F'(\tilde{u}_0(\pm\infty)) = f_m$ (see figure 1.1 for an example of the structure of F'). Thus, the equation to solve is

$$\tilde{\mu}_0 = F'(\tilde{u}_0) - \partial_{zz}\tilde{u}_0 = f_m. \tag{1.4}$$

Without loss of generality, we take $F'(\tilde{u}_0) = \tilde{u}_0^3 - \tilde{u}_0$ and as a result $f_m = 0$, which centers the bulk chemical potential about 0 and has the maximum and minimum concentrations of u normalized to 1 and -1, respectively. The problem becomes

$$\begin{aligned} \tilde{u}_0^3 - \tilde{u}_0 = \partial_{zz}\tilde{u}_0 \\ \lim_{z\to\pm\infty} \tilde{u}_0(z) = \pm 1, \quad \tilde{u}_0(0) = 0. \end{aligned}$$

Now, let $W = \partial_z\tilde{u}_0$, thus $\partial_{zz}\tilde{u}_0 = W_z = WW_{\tilde{u}_0}$. This gives us a separable equation that we can integrate as

$$(\tilde{u}_0^3 - \tilde{u}_0)d\tilde{u}_0 = WdW \longrightarrow \frac{\tilde{u}_0^4}{4} - \frac{\tilde{u}_0^2}{2} + c_0 = \frac{W^2}{2}.$$

By using the fact that $\tilde{u}_0(\pm\infty) = \pm 1$ and that the derivative is zero in the far field as we are in phase equilibrium, we see that $c_0 = 1/2$, which gives us

$$\frac{1}{2}(\tilde{u}_0^2 - 1)^2 = (\partial_z \tilde{u}_0)^2.$$

Choosing the negative square root we obtain another separable equation

$$\frac{\partial \tilde{u}_0}{(1-\tilde{u}_0^2)} = \frac{\partial_z}{\sqrt{2}} \implies \operatorname{arctanh}(\tilde{u}_0) = \frac{z}{\sqrt{2}} + c_1.$$

To match the boundary condition $\tilde{u}_0(0) = 0$ we set $c_1 = 0$. The other two boundary conditions are already satisfied and we obtain an interface that connects the two phases smoothly. Thus, the planar front profile is

$$\tilde{u}_0(z) = \tanh\left(\frac{z}{\sqrt{2}}\right).$$

This can be easily adapted to fit any F of this type. To conclude this section we define the front profile as $U = \tilde{u}_0$ and U satisfies the planar front profile equation given by

$$F'(U) - \partial_{zz} U = f_m \tag{1.5}$$

Late-Stage Dynamics

Next, we provide a formal derivation of the Mullins-Sekerka free boundary problem that gives us the equations used in [2]. We assume the solution is at equilibrium on the $O(1)$ time scale and define a slower time variable, $\tau = \epsilon t$. To continue with the matching, μ_1 and μ_2 are necessary. The higher order expansions of μ are given by

$$\begin{aligned}\mu =& F'(u_0 + \epsilon u_1 + \epsilon^2 u_2 + \ldots) - \epsilon^2 \Delta(u_0 + \ldots) \\ =& F'(u_0) + \epsilon F''(u_0)u_1 + \epsilon^2(F'''(u_0)u_2 + \tfrac{1}{2}F''(u_0)u_1^2 - \Delta u_0) + O(\epsilon^3)\end{aligned}$$

By writing $\mu = \mu_0 + \epsilon\mu_1 + \epsilon\mu_2 + \ldots$ we identify that

$$\mu_0 = F'(u_0), \qquad \mu_1 = F''(u_0)u_1, \qquad \mu_2 = F'''(u_0)u_2 + \tfrac{1}{2}F''(u_0)u_1^2 - \Delta u_0.$$

This gives us these three equations

$$\begin{aligned}0 = \Delta\mu_0 &= \Delta F'(u_0), \\ \partial_\tau u_0 = \Delta\mu_1 &= \Delta F''(u_0)u_1, \\ \partial_\tau u_1 = \Delta\mu_2 &= \Delta(F''(u_0)u_2 + \tfrac{1}{2}F'''(u_0)u_1^2 - \Delta u_0).\end{aligned}$$

These equations, as before, have Neumann boundary conditions and the interfacial matching conditions come from matching to the inner solution. The next step is to proceed with the inner expansion, now on the τ timescale. The derivative with respect to τ for an arbitrary function $v(\mathbf{x}, t) = w(z, \mathbf{x}, \epsilon t)$ is

$$\partial_t v = \epsilon \partial_\tau w + V \partial_z w.$$

As with the outer expansion, we need to develop more information about the inner equations. The change in the spatial derivatives for the inner functions $\tilde{\mu}$ and $\tilde{u}$ are the same as in (1.3). When we substitute these spatial derivative changes with the asymptotic expansion into (1.2) we obtain

$$\tilde{\mu}_0 = F'(\tilde{u}_0) - \partial_{zz}\tilde{u}_0, \tag{1.6a}$$
$$\tilde{\mu}_1 = F''(\tilde{u}_0)\tilde{u}_1 - \partial_{zz}u_1 - \kappa\partial_z\tilde{u}_0, \tag{1.6b}$$
$$\tilde{\mu}_2 = F''(\tilde{u}_0)\tilde{u}_2 - \partial_{zz}\tilde{u}_2 - \kappa\partial_z\tilde{u}_1 + \tfrac{1}{2}F'''(\tilde{u}_0) - \Delta_{\mathbf{x}}\tilde{u}_0. \tag{1.6c}$$

Using this information we expand $\partial_t u = \Delta\mu$ as on the $t = O(1)$ time scale. Since our lowest order term involving time is $O(1)$ and the lowest order term for spatial derivatives is $O(\epsilon^{-2})$, the time derivative term only arises in the third equation. We obtain,

$$0 = \partial_{zz}\tilde{\mu}_0, \tag{1.7a}$$
$$0 = \partial_{zz}\tilde{\mu}_1 + \kappa\partial_z\tilde{\mu}_0, \tag{1.7b}$$
$$V\partial_z\tilde{u}_0 = \partial_{zz}\tilde{\mu}_2 + \kappa\partial_z\tilde{\mu}_1 + \Delta_{\mathbf{x}}\tilde{\mu}_0. \tag{1.7c}$$

The equation for $\tilde{\mu}_0$ has already been solved on the $t = O(1)$ time scale and thus $\tilde{\mu}_0 = f_m$ from (1.4). This is to be expected as to leading order the solution should still be in equilibrium.

For the equation at the next order, we integrate it twice in z and substitute for $\tilde{\mu}_1$ as defined in (1.6b) to arrive at

$$b_0 z + b_1 = \tilde{\mu}_1 = F''(U)\tilde{u}_1 - \partial_{zz}u_1 - \kappa U'(z). \tag{1.8}$$

To determine the constants b_0 and b_1 we need to derive the matching conditions for μ. Roughly speaking, for a point $\mathbf{x}$ on Γ, the value of the chemical potential near this point can be described as $\mathbf{x} + \epsilon z\mathbf{n}$. Thus, to

derive boundary conditions, as $z \to 0^{\pm}$ in the outer expansion and $z \to \pm\infty$ in the inner, the chemical potentials need to agree. We require

$$(\mu_0 + \epsilon\mu_1 + \ldots)(\mathbf{x} + \epsilon z\mathbf{n}, t) \sim (\tilde{\mu}_0 + \epsilon\tilde{\mu}_1 + \ldots)(z, \mathbf{x}, t). \tag{1.9}$$

For the left hand size we take $z \to 0^{\pm}$ and for the right $z \to \pm\infty$. Performing a Taylor expansion (for $z \to 0^{+}$),

$$\mu_0^+ + \epsilon(\mu_1^+ + zD_{\mathbf{n}}\mu_0^+) + \epsilon^2(\mu_2^+ + zD_{\mathbf{m}}\mu_1^+ + \tfrac{1}{2}z^2D_{\mathbf{m}}^2\mu_0^+) + \ldots, \tag{1.10}$$

where $D_{\mathbf{n}}$ is the directional derivative along $\mathbf{n}$. The same argument can be made for $z \to 0^{-}$. With this in hand we can describe the matching conditions for the chemical potential by collecting terms of the same order from (1.9) and (1.10).

$$\mu_0^{\pm}(\mathbf{x}, t) = \tilde{\mu}_0^{\pm}(z, \mathbf{x}, t), \tag{1.11a}$$

$$(\mu_1^{\pm} + zD_{\mathbf{m}}\mu_0^{\pm})(\mathbf{x}, t) = \tilde{\mu}_1^{\pm}(z, \mathbf{x}, t), \tag{1.11b}$$

$$(\mu_2^{\pm} + zD_{\mathbf{m}}\mu_1^{\pm} + \tfrac{1}{2}z^2D_{\mathbf{m}}^2\mu_0^{\pm})(\mathbf{x}, t) = \tilde{\mu}_2^{\pm}(z, \mathbf{x}, t), \tag{1.11c}$$

where for everything on the right hand side we are taking $\lim_{z\to\pm\infty}$.

Now, with these matching conditions in hand, we can solve for b_0 in equation (1.8). Since we know that $\partial_z\tilde{\mu}_1 = b_0(\mathbf{x}, t)$ from (1.8), we can a take partial derivative of the matching condition for $\tilde{\mu}_1$ given in (1.11b) with respect to z to determine b_0. This leads us to

$$\mathbf{n} \cdot \nabla\mu_0^{\pm} = \partial_z\tilde{\mu}_1, \quad \text{as } z \to \pm\infty.$$

Since μ_0 must match $\tilde{\mu}_0$ near the front from (1.11a), and $\tilde{\mu}_0 = f_m$ from (1.4), we know that, near the front, $\nabla\mu_0 = 0$ because f_m is a constant. This implies that the far field behavior of $\partial_z\tilde{\mu}_1 = 0$ from the equation above and thus $b_0 = 0$. To determine $b_1(\mathbf{x}, t)$ in (1.8) we first rearrange the equation slightly and substitute in for b_0, yielding

$$b_1 + \kappa U'(z) = F''(U)\tilde{u}_1 - \partial_{zz}u_1.$$

We now multiply this by U' and integrate from $-\infty$ to ∞. This gives us

$$\int_{-\infty}^{\infty} \left(b_1U' + \kappa U'^2\right)\, dz = \int_{-\infty}^{\infty} \left[(F''(U)U'\tilde{u}_1 - U'\partial_{zz}\tilde{u}_1\right]\, dz. \tag{1.12}$$

Upon integrating the second term on the right hand side of the expression by parts twice, we see that

$$\int_{-\infty}^{\infty} U'\partial_{zz}\tilde{u}_1\,dz = U'\partial_z\tilde{u}_1\Big|_{-\infty}^{\infty} - \partial_z U'\partial_z\tilde{u}_1\Big|_{-\infty}^{\infty} + \int_{-\infty}^{\infty}\partial_{zz}U'\tilde{u}_1\,dz.$$

The boundary terms vanish because U is the equilibrium planar front solution and so the derivatives in the far field are zero. Substituting this information into (1.12) we have

$$\int_{-\infty}^{\infty}\left(b_1U' + \kappa U'^2\right)\,dz = \int_{-\infty}^{\infty}\left[(F''(U)U' \tilde{-} U'''\right]\tilde{u}_1\,dz. \tag{1.13}$$

Now consider taking a partial derivative with respect to z of equation (1.5). This tells us that

$$F''(U)U' - U''' = 0.$$

Combining the above information with (1.13) we determine that

$$b_1\int_{-\infty}^{\infty}U'dz = -\kappa(\mathbf{x},\tau)\int_{-\infty}^{\infty}U'^2\,dz,$$

which yields

$$b_1 = -\kappa(\mathbf{x},\tau)\frac{S}{[U]},$$

with

$$S = \int_{-\infty}^{\infty}U'^2\,dz, \qquad [U] = U(\infty) - U(-\infty).$$

From (1.8) and the fact that $b_0 = 0$ we know that $b_1 = \tilde{\mu}_1$. Using this as the matching condition to the outer equation for the chemical potential, we have arrived at a free boundary Mullins-Sekerka problem that describes the late-stage dynamics of the Cahn-Hilliard equation, and, as we will soon see, Ostwald ripening. The system is formulated as

$$\begin{aligned}
\Delta\mu_1 &= 0, \quad \mathbf{x}\in\Omega_+ \text{ and } \Omega_-,\\
\mu_1 &= -\kappa(\mathbf{x},\tau)\frac{S}{[U]}, \quad \mathbf{x}\in\Gamma,\\
\mathbf{n}\cdot\nabla\mu_1 &= 0, \quad \mathbf{x}\in\partial\Omega.
\end{aligned} \tag{1.14}$$

The physical interpretation is that on this time scale ($t = O(\epsilon^{-1})$) the chemical potential is in equilibrium and we have steady state diffusion. The Gibbs-Thomson condition appears on the interface, relating the mean curvature to the chemical potential. Finally, we derive how the front evolves in time by looking at equation (1.7c). Since $\tilde{\mu}_0$ and $\tilde{\mu}_1$ are constant with respect to $\mathbf{x}$ and z respectively, the equation reduces to

$$V\partial_z \tilde{u}_0 = \partial_{zz}\tilde{\mu}_2.$$

Upon integrating both sides of the equation from $z = -\infty$ to $z = \infty$ we have

$$V = [U]^{-1}\partial_z \tilde{\mu}_2\Big|_{-\infty}^{\infty} \tag{1.15}$$

We can substitute in the matching condition for $\tilde{\mu}_2$ from (1.11c) after taking the derivative of it with respect to z. This tells us that

$$\mathbf{n}\cdot\nabla\mu_1^{\pm}(\mathbf{x},\tau) = \partial_z\tilde{\mu}_2(z,\mathbf{x},\tau) \text{ as } z \to \pm\infty,$$

which, when substituted into (1.15), yields

$$V(\mathbf{x},\tau) = \frac{[\mathbf{n}\cdot\nabla\mu_1(\mathbf{x},\tau)]^{\pm}}{[U]}.$$

Note that a very similar calculation can be done on an $O(1)$ timescale, which shows the front velocity to be zero at this order. In this case V is related to the jump in the normal derivative of μ_0 instead of μ_1. Since we have already shown $\mu_0 = f_m$, it is easy to see that the normal derivative must be zero.

In summary, the late-stage dynamics characterizing the coarsening phenomena for the Cahn-Hilliard equation is given by the limiting system (1.14).

1.2 Chemotaxis

Chemotaxis is a biological phenomenon in which organisms move about their environment due to the presence of a chemical concentration. Bacteria such as *E. coli* move seemingly randomly, switching between periods of *swimming*, characterized by aligned flagella (arm-like appendages) resulting in straight motion, and *tumbling*, where the flagella spread out and the bacteria rotates into a new direction. In the presence of an attractive chemical gradient, *E. coli* will swim in this direction and tumble when realignment with the gradient is necessary. They preference their movement along increasing amounts

of this chemical attractant (see [3]). Sperm cells also exhibit chemotactic behavior, moving towards the oocyte due to a compound released from its outer wall. Chemotaxis need not be attractive; some organisms sense poisonous molecules (such as carbolic acid for E. coli) and direct their movement away.

Aggregation of cells has been seen since the early use of microscopes but it wasn't until 1881 with the work of Theodor Engelmann and later in 1884 with the work of Wilhelm Pfeffer that an accurate description of chemotaxis was made. By the 1930s the significance of chemotaxis was widely accepted. Since then, much progress has been made, advancing the field not only biologically but also mathematically.

The mathematical study of chemotaxis dates back to the 1950s with work by Patlak in [22] and later in the 1970s with the work of Keller and Segel [15]. Although there have been other attempts, the Patlak-Keller-Segel (PKS) model is the prevailing one. This is due to the intuitive nature of the equations, tractability, and clear representation of sought-after phenomenon. The derivation is reasonable and clear; the assumptions made are both biologically and mathematically logical. There is a strong connection between the source of the assumptions and how they manifest in the equations. The general model is

$$\begin{aligned} u_t &= \nabla \cdot (k_1(u,v)\nabla u - k_2(u,v)u\nabla v) + k_3(u,v), \\ v_t &= D_v \Delta v + k_4(u,v) - k_5(u,v)v, \end{aligned}$$

where u is the organism concentration/density in a domain $\Omega \in \mathbb{R}^n$ and v is the concentration of the chemical signal. k_1 represents the diffusivity of the organism modeled by u and k_2 is the chemotactic sensitivity. As the gradient of v increases, advection of u increases. k_3 is a cell kinematic term for u, measuring growth and death. k_4, and k_5 are chemical signal kinematics, representing production and degradation. We see that v obeys a basic diffusion equation with an additional growth/death factor while u is slightly different, involving diffusion and advection.

The original model, seen in [22] and later in [15], referred to as the 'minimal model' in [12], is

$$u_t = \nabla \cdot (D_u \nabla u - \chi_u u \nabla v); \qquad v_t = D_v \Delta v + \mu u - \delta v,$$

with zero-flux boundary conditions imposed on the outer walls of the domain Ω and some specified initial concentration. Diffusivity (D_u, D_v), chemotactic sensitivity (χ_u), and cell kinematic factors (μ, δ) are assumed to be constant. Assuming that chemical kinematics occur on a much larger time scale or

possibly do not occur during aggregation, we can also ignore k_3. This is a reasonable assumption in many cases (see [12]). For the chemical signal, kinematics are taken to be linear. There is an additional condition that the model has, namely mass conservation.

$$\begin{aligned}\frac{\partial}{\partial t}\int_\Omega u\,d\mathbf{x} = \int_\Omega u_t\,d\mathbf{x} &= \int_\Omega \nabla\cdot(D_u\nabla u - \chi_u u\nabla v)\,d\mathbf{x}\\ &= \int_{\partial\Omega}(D_u\nabla u - \chi_u u\nabla v)\cdot\mathbf{n}\,d\mathbf{x} = 0,\end{aligned}$$

due to the zero-flux boundary condition. Thus, we see that mass in conserved as

$$\int_\Omega u(x,t)\,d\mathbf{x} = \int_\Omega u_0(x)\,d\mathbf{x} = M.$$

The model can be nondimensionalized to have a homogeneous steady state such that $(u_s, v_s) = (1, 1)$ and $M = 1$.

During the 1990s and early 2000s a series of papers (see [14]) proved that the minimal model has a major deficiency. In 2D and 3D domains, global existence depends on a threshold level of initial mass. If there is too much mass in the system we see finite time blow-up. The cells in the model aggregate to a spot with infinite density, which is obviously not biologically feasible. Since, for a typical application, the initial mass lies above this threshold, regularizations of the model are necessary. Initial aggregation is only one small part in chemotaxis and thus, there is a need for a model that allows for longer time scales without blow-up. We present a few of these regularizations but focus specifically on the volume-filling case in this paper.

1.2.1 Literature Review

Considering the simplified system of PDEs,

$$\begin{aligned}u_t &= \nabla\cdot(D(u)\nabla u - A(u)B(v)u\nabla v) + f(u),\\ v_t &= \Delta v + g(u)u - v.\end{aligned}$$

Below is a table outlining the choices of functions for each of the regularizations considered.

Model	$D(u)$	$A(u)$	$B(v)$	$f(u)$	$g(u)$
Minimal	D	u	χ	0	1
Nonlinear Diffusion	Du^n	u	χ	0	1
Volume Filling	D	$u\left(1\text{-}\frac{u}{\gamma}\right)$	χ	0	1
Signal Dependent Sensitivity	D	u	$\frac{\chi}{(1+\alpha v)^2}$	0	1
Cell Kinematics	D	u	χ	$ru(1-u)$	1
Saturated Signal Production	D	u	χ	0	$\frac{1}{1+\phi u}$

This list is certainly not exhaustive. There are more covered in [12] and even more that they mention as being left out. These excluded variations have such properties as nonlinear gradient functions, nonlocal terms, or even zero diffusion models.

We will now work through the details of each model individually, explaining the reasoning behind the regularization and the impact it has on the behavior.

The Minimal Model

For completeness and ease of comparison, we present the details of the minimal model as well as the derivation. We consider the movement of each cell as modeled by a biased random walk, where the bias is due to the chemotactic gradient. This allows for an easier transition from microscopic to macroscopic behavior.

Consider an infinite 1D lattice where particles may instantaneously jump a constant distance h to the left or the right. Assuming the particles do not interact directly, we have the following continuous-time discrete space system for the particle density $u(x,t)$ given by

$$\frac{\partial u(x,t)}{\partial t} = T^+_{x-h}u(x-h,t) + T^-_{x+h}u(x+h,t) - (T^+_x + T^-_x)u(x,t).$$

$T^\pm_x$ is a probability function that gives a chance per unit time for a particle at x to make a jump to $x \pm h$. In the model, at each time step, we have possible contributions from the point to the left and the right, $x-h$, and $x+h$, respectively. This is represented by T^+_{x-h} and T^-_{x+h}. There is also loss from the currently position as particles jump away, which is indicated by T^+_x and T^-_x.

As stated before, the chemotactic sensitivity is incorporated through the bias in the random walk, which we see in the T function. We want to bias the

jump with regards to a local spatial gradient of v, which we do by specifying $T_x^{\pm}$ as

$$T_x^{\pm} = a + b(v(x \pm h, t) - v(x, t)),$$

where a and b are positive constants. The probability to jump in a given direction increases if the concentration of the chemical is larger in that direction. Substituting this into the equation and performing a Taylor expansion of the right hand side, we obtain

$$u_t = h^2(au_x - 2buv_x)_x + O(h^4).$$

Now, we scale time by the transformation $t = \lambda\hat{t}$. This results in

$$u_{\hat{t}} = \lambda h^2(au_x - 2buv_x)_x + O(h^4),$$

where we assume that the limits $\lim_{h\to 0,\lambda\to\infty} a\lambda h^2 = D_u$ and $lim_{h\to 0,\lambda\to\infty} 2b\lambda h^2 = \chi_u$, which results in a continuous space and time equation. Dropping the hat for convenience, we arrive at

$$u_t = (D_u u_x - \chi_u u v_x)_x.$$

We assume the equation for v is a standard diffusion equation with linear kinetics. Thus, in higher dimensions we have the following system of PDEs with zero-flux boundary conditions on the outer wall of the domain Ω

$$u_t = \nabla \cdot (D_u \nabla u - \chi_u u \nabla v); \qquad v_t = D_v \Delta v + \mu u - \delta v.$$

As mentioned previously, the minimal model can be nondimensionalized to have mass, M, equal to 1 and the number of parameters reduced. In one dimension, we have global existence of solutions, which was recently proved in [20]. In two dimensions the model has finite time blow-up when the initial mass is over some threshold level, which is why we employ these regularizations. This result can be found in [14].

Nonlinear Diffusion

The nonlinear diffusion model considered is

$$u_t = \nabla \cdot (Du^n \nabla u - \chi u \nabla v),$$

with the equation for v given as before. Thus, the only change is the nonlinear dependence on cell density for the diffusion term. As stated in [12],

this dependence is neglected in cell movement but crops up in ecological applications such as population-induced insect movement. Hillen and Painter suggest that, although most applications assume a constant diffusion coefficient, a nonlinear dependence is much more likely. This specific case, involving u^n, was studied by Kowalczyk in [16] and Eberl in [9] as a model for biofilm growth.

Much like the minimal model, after nondimensionalization the nonlinear diffusion model has a homogeneous steady state of $(u, v) = (1, 1)$. Kowalczyk proved in [16] that this model has global existence of solutions in n dimensions. The Lyapunov function

$$L_{\text{nonlinear}}(u) = \frac{D}{n(n+1)\chi} u^{n+1}$$

is used for this result.

Volume Filling

The effects of volume filling are explored in [11]. Since this model is of particular importance to this paper we will go through the derivation of the volume effects; that is, how and at what stage of the model they crop up. Higher concentrations of cells should inhibit the ability for other cells to move into a given region, creating a hard cap on the density in a given area. This is modeled by a function $q(u)$ that gives the probability of finding space based on the local density u. We want q to be a positive and decreasing function. One such choice is $q(u) = 1 - u/\gamma$, $\gamma > 1$, with u having a maximum density of γ. Now, the jump function T becomes

$$T_x^{\pm} = q(u(x \pm h))(a + b(v(x \pm h) - v(x))).$$

Following the same steps as before, we arrive at

$$u_t = \nabla \cdot (D(q - uq_u)\nabla u - \chi u q(u)\nabla v); \qquad v_t = D_v \Delta v + \mu u - \delta v.$$

With $q(u)$ given as $q(u) = 1 - u/\gamma$, the equation for u reduces to

$$u_t = \nabla \cdot \left(D\nabla u - \chi u \left(1 - \frac{u}{\gamma}\right) \nabla v \right).$$

The volume filling approach is intuitive and easy to implement. Global existence is achieved, as expected, and was proved in [10, 30] using the Lyapunov function

$$L_{\text{volume}}(u) = \frac{D}{\chi}\left(u\log(u) + \gamma\left(1-\frac{u}{\gamma}\right)\log\left(1-\frac{u}{\gamma}\right)\right).$$

Signal-dependent Sensitivity

The signal-dependent sensitivity model, also referred to as the receptor model, is

$$u_t = \nabla\cdot\left(D\nabla u - \frac{\chi u}{(1+\alpha v)^2}\nabla v\right),$$

with v given as before (diffusion & linear kinetics).

The model is motivated by *in vivo* experimentation and observation. Chemotactic response is controlled first by signal detection, through binding of the chemical to exterior receptors, followed by transduction, where a change takes place in the internal receptor component. This not only causes a change in movement but may also affect receptor production and degradation. We want to build these effects into the model and thus add a signal-dependent sensitivity function, specifically, the receptor form

$$B(v) = \frac{\chi}{(1+\alpha v)^2}.$$

At high concentrations of v we see that $B(v)$ decreases, indicating that, in a sense, the receptors on a cell are full and can no longer impact movement. This is only one such model for signal-dependent sensitivity and there are others that employ slightly different assumptions. Global existence of solutions for this model was proved only very recently in [29].

Cell Kinematics

As stated previously, it is occasionally reasonable to ignore cell growth and death. *Dictyostelium discoideum*, for instance, halts cell proliferation during aggregation stages. In other cases the movement takes place on a much faster time scale than growth, also allowing us to ignore those additional terms. This is not always the case and with most bacteria these time scales match up. Using a standard logistic growth models, we derive a cell kinematics model given by

$$u_t = \nabla\cdot(D\nabla u - \chi u\nabla v) + ru(1-u).$$

Global existence of solutions in the cell kinematic model in n dimensions is proved in[30].

Saturated Signal Production

The basis for saturated signal production comes from what was mentioned previously about receptor binding and saturation effects. Since, biologically, a receptor binding to a site on the cell has other affects not limited to movement but also influences signal production, the model is changed accordingly. A saturated signal production model tries to correct the overly simplistic assumption of linear kinetics through the term

$$g(u) = \frac{1}{1+\phi u},$$

which decays as $u \to \infty$. Thus, the production of chemical saturates the environment and slows to a halt when cell density increases. The resulting model is

$$u_t = \nabla \cdot (D\nabla u - \chi u \nabla v); \qquad v_t = \Delta v + \frac{u}{1+\phi u} - v.$$

Global existence of solutions in n dimensions was proved in [13]. Thus, we have global existence for all models considered with the exception of the minimal model.

Stability

The survey by Hillen and Painter ([12]) gives a brief rundown of one dimensional linear analysis, which we summarize here. We assume the model in question has a spatially homogeneous steady state solution, $(\bar{u}, \bar{v})$ and linearize around this solution, which gives us

$$U_t = D(\bar{u})U_{xx} - A(\bar{u})B(\bar{v})V_{xx} + f'(\bar{u})U,$$
$$V_t = V_{xx} + (g(\bar{u}) + \bar{u}g'(\bar{u}))U - V.$$

We now define $\bar{A} = A(\bar{u})$, $\bar{B} = B(\bar{v})$, $\bar{f} = f(\bar{u})$, $\bar{g} = g(\bar{u})$. We take U and V to be the typical small perturbation function to derive the stability matrix whose eigenvalues tell us the stability of the linear homogeneous solution.

$$M = \begin{pmatrix} -k^2\bar{D} + \bar{f}' & k^2\bar{A}\bar{B} \\ \bar{g} + \bar{u}\bar{g}' & -k^2 - 1 \end{pmatrix}$$

On a closed interval $[0, L]$ with Neumann boundary conditions we have $k = n\pi/L$, $n = 0, 1, 2, \ldots$. If the eigenvalues have positive real part then the homogeneous solution is unstable and we expect pattern formation due to the global existence of solutions for each model in one dimension. This gives

us the following necessary conditions for instability in each of the models considered

Model	Necessary Conditions	Unstable Modes k
Minimal	$\chi > D$	$k^2 < \frac{\chi}{D} - 1$
Nonlinear Diffusion	$\chi > D$	$k^2 < \frac{\chi}{D} - 1$
Volume Filling	$\chi\left(1 - \frac{1}{\gamma}\right) > D$	$k^2 < \frac{\chi\left(1-\frac{1}{\gamma}\right)}{D} - 1$
Signal Dependent Sensitivity	$\chi > D(1+\alpha)^2$	$k^2 < \frac{\chi}{D(1+\alpha)^2} - 1$
Cell Kinematics	$\chi > (\sqrt{D} + \sqrt{r})^2$	$k^2 \in (k_1, k_2)$
Saturated Signal Production	$\chi > D(1+\phi)^2$	$k^2 < \frac{\chi}{D(1+\phi)^2} - 1$

where $k_{1,2} = \frac{\chi - D - r}{2D} \pm \frac{1}{2D}\sqrt{(D + r - \chi)^2 - 4rD}$. We see that in all models considered the spatially homogeneous solution has a region of instability and patterns may develop.

Numerical Results

In this section we present numerical results from [12] for the models considered and additional results from [11] for the volume-filling model. This is to show the many different solutions that can arise. We provide extra information on the volume-filling case to give evidence of coarsening as well as comment on the parameter values that bring about these long transients.

In figure 1.2 we see the myriad solutions that not only arise from the different way the model was regularized but also the different parameter values inherent in each of these regularizations. The asterisk indicates, as in [11], a "plateau" solution. We see that aggregation, when it transpires, can occur in many different ways although qualitatively the results behave similarly (grouping around a high concentration of the chemical signal). Figure 1.3 is similar to 1.2 but depicts the solution over longer time scales. Finally, figures 1.4 through 1.6 show coarsening effects for select regularizations.

This concludes the literature review and introduction. Next, we move on to a more in depth look at Ostwald ripening where new results are presented.

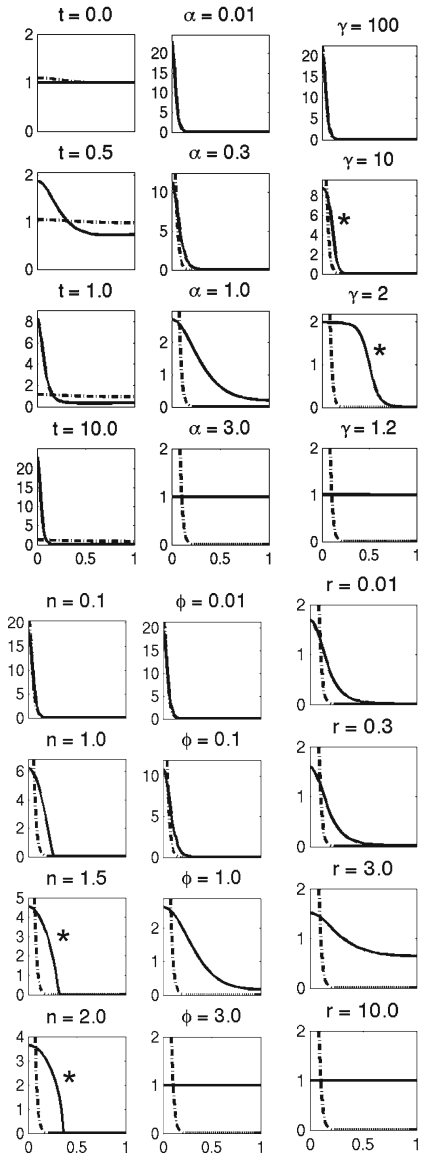

Figure 1.2: 1D simulations for the models considered. Minimal model is given at different times where as others have varying relevant parameters. The solid line is the adapted model where as the dot-dash line is the minimal model steady state solution. In order, the models are: minimal, signal-dependent sensitivity, volume-filling, non-linear diffusion, saturating signal production, and cell kinetic. $D = .1$, $\chi = 5$. ICs: $u(x,0) = 1$, $v(x,0) = 1 + .1\exp(-10x^2)$.

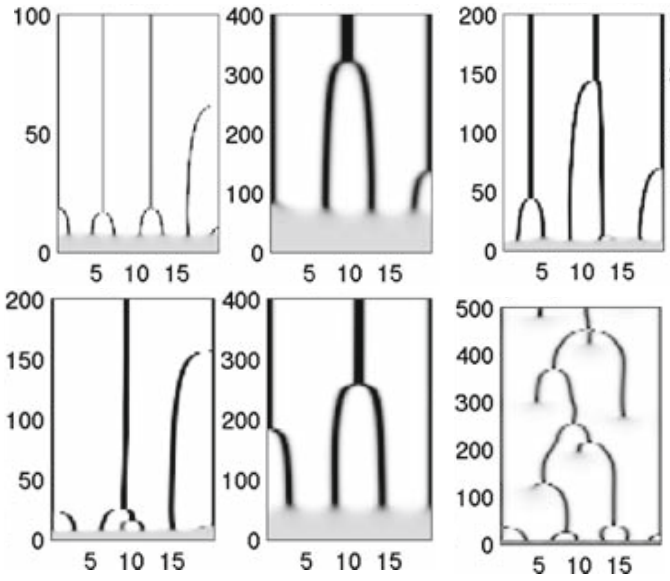

Figure 1.3: One dimensional numerical simulations for the models considered, now on a larger domain. Models appear in the same order as the previous figure. D is given to be .1 and $\chi = 2$. Initial conditions are set at $u(x,0) = 1$, $v(x,0) = 1 + r(x)$ where $r(x)$ is a random spatial perturbation of the steady state, $.01 \leq r(x) \leq .01$. We see that in most cases a coarsening process occurs and what initially started as a multi-peak structure evolves into fewer and fewer regions of concentration. This is not the case in the cell kinematics regularization as we see a continual emergence of cells and decay of peaks.

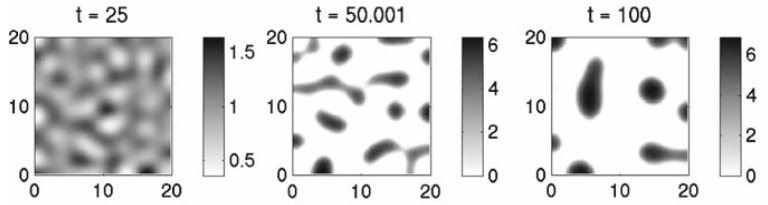

Figure 1.4: Here is an example of a 2D simulation. This is a time evolution of a combination of a few regularizations, namely signal-dependent sensitivity ($\alpha = .4$), volume-filling ($\gamma = 10$), non-linear diffusion ($n = 1$) and saturating chemical production ($\phi = 1$). $D = .1$, $\chi = 5$, $\Omega = [0,20] \times [0,20]$. ICs: $u(x,y,0) = 1$, $v(x,y,0) = 1 + r(x,y)$, where $r(x,y)$ is the 2D analog from the previous figure. We once again see a coarsening process as time goes on.

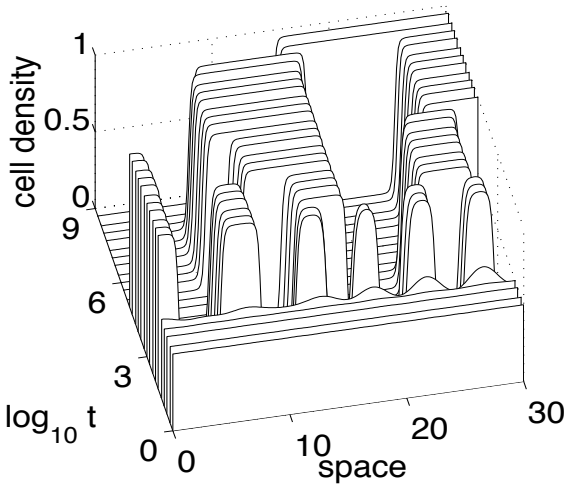

Figure 1.5: A 1D time evolution picture that shows coarsening occurring on a log time scale for the volume-filling model. In this case, initial cell density is set at .5 with $D = .25$ and $\chi = 4$.

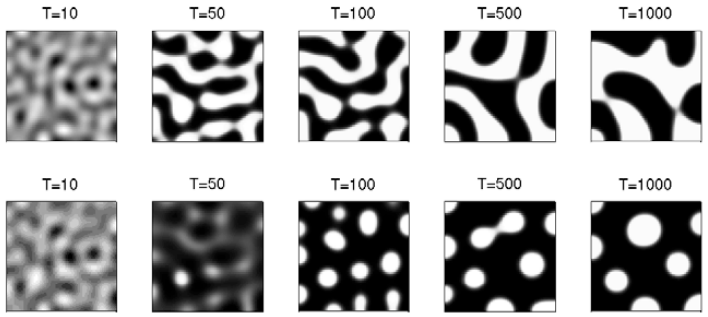

Figure 1.6: Coarsening of the volume filling model. The top row has initial concentration of $u = .5$ and the bottom has $u = .25$. As above, $D = .25$, $\chi = 4$. Here, the domain, $\Omega = [0, 25] \times [0, 25]$. In this picture black is low cell density where white is high cell density.

Chapter 2

Ostwald Ripening

We begin this chapter with a deeper look at Ostwald ripening. From the introduction, we left off with the free boundary Mullins-Sekerka problem seen in (1.14). The problem has been rewritten slightly as

$$\begin{gathered} \Delta u = 0, \quad \mathbf{x} \in \Omega \setminus \Gamma, \\ u = -\kappa, \quad \mathbf{x} \in \Gamma; \qquad \frac{\partial u}{\partial n} = 0, \quad \mathbf{x} \in \partial\Omega, \\ V = -\left[\frac{\partial u}{\partial n}\right], \quad \mathbf{x} \in \Gamma. \end{gathered} \tag{2.1}$$

Here, the variable has been changed to u and has been scaled so that only κ, the mean curvature, shows up on the interface.

As mentioned in the introduction, the next step is to draw the connection between this and the equations that govern Ostwald ripening. There are many ways to do this, one of which can be seen in [2]. Instead, we will present a matched asymptotic approach to arrive at a system of ODEs that describe the motion of each drop.

2.1 Mullins-Sekerka to Ostwald Ripening Dynamics

We start by considering an arbitrary domain $\Omega \subset \mathbb{R}^2$ with a collection of N small circular droplets inside the domain whose boundaries are described by $\Gamma_i = |\mathbf{x} - \mathbf{x}_i| = r_i$ for $i = 1, 2, \ldots, N$, where r_i is the radius of the droplet and $\mathbf{x}_i$ the center. The interface between the two regions, Γ, is given as $\Gamma = \bigcup \Gamma_i$. Since we assume the droplets are small, $r_i = \epsilon\rho_i$ for $\epsilon \ll 1$ and $\rho_i = O(1)$. The droplets are expected to move in time so r_i and ρ_i depend upon t. Since the interfacial velocity V is negative for a shrinking drop by convection,

$$V = -\frac{dr_i}{dt} = -\epsilon\frac{d\rho_i}{dt},$$

for a given i. We also know the mean curvature, κ, for a circular drop, is given by

$$\kappa = \frac{1}{r_i} = \frac{1}{\epsilon\rho_i}.$$

Inside each drop we know that $u_- = 1/r_i(0)$, a constant, which means that $\partial_n u_- = 0$ on Γ_i. This tells us

$$\left[\frac{\partial u}{\partial n}\right] = \frac{\partial u}{\partial n}\Big|_+ - 0 = \frac{\partial u}{\partial r}\Big|_{r=r_i} = \frac{1}{\epsilon}\frac{\partial u}{\partial \rho}\Big|_{\rho=\rho_i}.$$

We know from (2.1) that the jump in the normal derivative given above is also equal to the velocity V. Therefore,

$$\epsilon^2 \frac{d\rho_i}{dt} = \frac{\partial u}{\partial \rho}\Big|_{\rho=\rho_i}.$$

Collecting this information, the problem that we need to solve can be rewritten as

$$\begin{aligned} \Delta u = 0, \quad \mathbf{x} \in \Omega \setminus \Gamma, \\ u = \frac{1}{\epsilon\rho_i}, \quad \mathbf{x} \in \Gamma_i; \qquad \frac{\partial u}{\partial n} = 0, \quad \mathbf{x} \in \partial\Omega, \end{aligned}$$

with the droplet dynamics satisfying

$$\epsilon^2 \frac{d\rho_i}{dt} = \frac{\partial u}{\partial \rho}\Big|_{\rho=\rho_i}.$$

Determining u means we obtain a system of ODEs that describe the motion of each drop throughout the domain. We can scale u by $1/\epsilon$ to simplify the problem and remove the ϵ that appears on the boundary of each interface. Note that this also causes an additional power of ϵ to appear in our system of ODEs.

Proceeding with the asymptotic analysis, we expand u as

$$u = u_0 + \nu u_1 + \nu^2 u_2 + \dots,$$

where u_0 is readily seen as an unknown constant that is determined as a solvability condition in later expansion and ν is the order of the subsequent terms, also to be determined. For u_1, the problem to solve is

$$\begin{aligned} \Delta u_1 = 0, \quad \mathbf{x} \in \Omega \setminus \{\mathbf{x}_1, \dots, \mathbf{x}_N\}, \\ \frac{\partial u_1}{\partial n} = 0, \quad \mathbf{x} \in \partial\Omega; \qquad u_1 \sim \ ?, \quad \text{as } \mathbf{x} \to \mathbf{x}_j, \text{ for } j = 1, \dots, N. \end{aligned} \tag{2.2}$$

To figure out this singularity condition as $\mathbf{x} \to \mathbf{x}_j$, we move to an inner expansion. We define $\mathbf{y} = \epsilon^{-1}(\mathbf{x} - \mathbf{x}_j)$ near the j^{th} droplet and U be the inner u function. Now, we have

$$U = U_0 + \nu U_1 + \dots$$

As with all matched asymptotic expansions, we require the outer solution and inner solution agree as $\mathbf{x} \to \mathbf{x}_j$ and as $|\mathbf{y}| \to \infty$ respectively. So we must have $U_0 \to u_0$ as $|\mathbf{y}| \to \infty$. The first two inner equations to solve are

$$\begin{aligned} \Delta_{\mathbf{y}} U_0 &= 0, \quad \mathbf{y} \notin \Gamma_j, \\ U_0 = \frac{1}{\rho_j}, \quad \mathbf{y} \in \Gamma_j; &\qquad U_0 \sim u_0, \quad \text{as } |\mathbf{y}| \to \infty. \end{aligned} \tag{2.3}$$

$$\begin{aligned} \Delta_{\mathbf{y}} U_1 &= 0, \quad \mathbf{y} \notin \Gamma_j, \\ U_1 = 0, \quad \mathbf{y} \in \Gamma_j; &\qquad U_1 \sim \ ?, \quad \text{as } |\mathbf{y}| \to \infty. \end{aligned} \tag{2.4}$$

Both equations can be solved by switching to polar coordinates and looking for a radially symmetric solution. The corresponding solutions are

$$U_0 = \frac{1}{\rho_j} + B_{0,j}(\log(\rho) - \log(\rho_j)), \tag{2.5a}$$

$$U_1 = B_{1,j}(\log(\rho) - \log(\rho_j)), \tag{2.5b}$$

for constants $B_{0,j}$ and $B_{1,j}$. To determine $B_{0,j}$ and $B_{1,j}$, we look to the matching condition for the inner and outer solution. Near the j^{th} droplet, we must have (as $\mathbf{x} \to \mathbf{x}_j$ and as $|\mathbf{y}| \to \infty$)

$$u_0 + \nu u_1 + \nu^2 u_2 \sim U_0 + \nu U_1 + \dots$$

Substituting in for U_0 and U_1 from (2.5) and switching to a common variable, we see that

$$\begin{aligned} u_0 + \nu u_1 + \nu^2 u_2 \sim \frac{1}{\rho_j} &+ B_{0,j}(\log(|\mathbf{x} - \mathbf{x}_j|) - \log(\epsilon) - \log(\rho_j)) \\ &+ \nu B_{1,j}(\log(|\mathbf{x} - \mathbf{x}_j|) - \log(\epsilon) - \log(\rho_j)) + \dots \end{aligned}$$

In order to keep the order of the right hand side and left hand side consistent, the $\log(\epsilon)$ term must vanish. This tells us that $B_{i,j} = C_{ij}/\log(\epsilon)$ for some arbitrary constant C_{ij}, where j corresponds to the droplet in question. This also specifies $\nu = -1/\log(\epsilon)$. Rearranging terms, we now have

$$u_0 + \nu u_1 \sim \frac{1}{\rho_j} + C_{0j} + \nu[C_{0j}(\log(|\mathbf{x} - \mathbf{x}_j|) - \log(\rho_j)) + C_{1j}] + O(\nu^2).$$

Since $u_0 = 1/\rho_j + C_{0j}$, we see that $C_{0j} = u_0 - 1/\rho_j$ which tells us the singularity condition for u_1, specifically, $u_1 \sim (u_0 - 1/\rho_j)\log(|\mathbf{x} - \mathbf{x}_j|)$ as $\mathbf{x} \to \mathbf{x}_j$, for $j = 1, \ldots, N$ since there are no other terms to match on $O(\nu)$. We can substitute this into equation (2.2) and rewrite it as

$$\Delta u_1 = 2\pi \sum_{j=1}^{N} \left(u_0 - \frac{1}{\rho_j} \right) \delta(\mathbf{x} - \mathbf{x}_j), \quad \mathbf{x} \in \Omega,$$
$$\frac{\partial u_1}{\partial n} = 0, \quad \mathbf{x} \in \partial\Omega.$$

Here, u_0 is still undetermined. We use the divergence theorem to reveal that

$$u_0 N = \sum_{j=1}^{N} \frac{1}{\rho_j},$$

and thus

$$u_0 = \frac{\sum_{j=1}^{N} \frac{1}{\rho_j}}{N} = \frac{1}{\rho_{\text{harm}}},$$

where ρ_{harm} is the harmonic mean. This also tells us that $C_{0j} = 1/\rho_{\text{harm}} - 1/\rho_j$.

At this point we can conclude with a leading order expansion for the dynamics of each droplet and the resulting system of ODEs. We substitute $B_{0,j} = -\nu C_{0j}$ into (2.5a) and take a derivative with respect to ρ to determine that

$$U_0 = \nu \left[\frac{1}{\rho_{\text{harm}}} - \frac{1}{\rho_j} \right] \frac{1}{\rho},$$

and since, to leading order, $u \sim U_0$ as $\mathbf{x} \to \mathbf{x}_j$ ($\rho \to \rho_j$), we have

$$\frac{d\rho_j}{dt} = \frac{\nu}{\epsilon^3} \frac{\partial u}{\partial \rho}\Big|_{\rho=\rho_j} \approx \frac{\nu}{\epsilon^3} \left[\frac{1}{\rho_{\text{harm}}} - \frac{1}{\rho_j} \right] \frac{1}{\rho_j}, \quad j = 1, \ldots, N.$$

Principal Result 2.1: *Consider the 2-D free boundary Mullins-Sekerka problem given below.*

$$\Delta u = 0, \quad \mathbf{x} \in \Omega \setminus \Gamma,$$
$$u = -\kappa, \quad \mathbf{x} \in \Gamma; \qquad \frac{\partial u}{\partial n} = 0, \quad \mathbf{x} \in \partial\Omega,$$
$$V = -\left[\frac{\partial u}{\partial n}\right], \quad \mathbf{x} \in \Gamma.$$

where u is the chemical potential, κ the curvature and V is the interfacial velocity. In the case where Γ is the boundary of a collection of small circles (radius $\sim O(\epsilon)$, $\epsilon \ll 1$), the following system of ODEs describes, to leading order, the coarsening phenomenon present.

$$\frac{d\rho_j}{dt} = \frac{\nu}{\epsilon^3}\frac{\partial u}{\partial \rho}\Big|_{\rho=\rho_j} \approx \frac{\nu}{\epsilon^3}\left[\frac{1}{\rho_{\text{harm}}} - \frac{1}{\rho_j}\right]\frac{1}{\rho_j}, \quad j = 1, \ldots, N,$$

where $\nu = -1/\log(\epsilon)$ and ρ_{harm} is the harmonic mean.

2.2 Properties of the System

Here we will derive a few properties of the system before moving on to a higher order expansion. These properties are (i) the system is area preserving, (ii) the perimeter of droplets is non-increasing and (iii) the smallest droplet will vanish in finite time.

2.2.1 Area Preserving

Consider the area of a given droplet, $\pi\rho_i^2$, and total area of the system $\pi\sum_{i=1}^N \rho_i^2$, the sum of all the individual areas. We proceed by taking a derivative with respect to time of the total area.

$$\frac{d}{dt}\sum_{i=1}^N \rho_i^2 = 2\sum_{i=1}^N \rho_i\rho_i' = 2\sum_{i=1}^N \rho_i\left(\frac{1}{\rho_{\text{harm}}} - \frac{1}{\rho_i}\right)\frac{1}{\rho_i}\frac{\nu}{\epsilon^3}$$
$$= \frac{2\nu}{\epsilon^3}\left(\sum_{i=1}^N \frac{1}{\rho_{\text{harm}}} - \sum_{i=1}^N \frac{1}{\rho_i}\right) = \frac{2\nu}{\epsilon^3}\left(\frac{N}{\rho_{\text{harm}}} - \sum_{i=1}^N \frac{1}{\rho_i}\right)$$
$$= \frac{2\nu}{\epsilon^3}\left(\frac{N}{\frac{N}{\sum_{i=1}^N \frac{1}{\rho_i}}} - \sum_{i=1}^N \frac{1}{\rho_i}\right) = 0.$$

As a result the total area of the system is unchanged and the droplets exchange mass with each other without any loss. The initial mass is the same as the mass at any future time.

2.2.2 Perimeter Reducing

Consider the perimeter of a given droplet, $2\pi\rho_i$. The total perimeter of the system will be the sum of all the individual perimeters. We take a derivative with respect to time of the total perimeter to determine that

$$\frac{d}{dt}\sum_{i=1}^{N}\rho_i = \frac{\nu}{\epsilon^3}\sum_{i=1}^{N}\left(\frac{1}{\rho_i\rho_{\text{harm}}} - \frac{1}{\rho_i^2}\right) = \frac{\nu}{\epsilon^3}\left[\left(\sum_{i=1}^{N}\frac{1}{\rho_i}\right)\frac{1}{\rho_{\text{harm}}} - \sum_{i=1}^{N}\frac{1}{\rho_i^2}\right]$$
$$= \frac{\nu}{\epsilon^3}\left[\frac{1}{N}\left(\sum_{i=1}^{N}\frac{1}{\rho_i}\right)^2 - \sum_{i=1}^{N}\frac{1}{\rho_i^2}\right].$$

Since ν/ϵ^3 is positive it suffices to show that $\sum_{i=1}^{N}\alpha_i^2 \geq (\sum_{i=1}^{N}\alpha_i)^2/N$. This result means the derivative is negative signifying that the perimeter decreases. We begin with

$$0 \leq \sum_{i=1}^{N}\sum_{j=1}^{N}(\alpha_i - \alpha_j)^2 = \sum_{i=1}^{N}\sum_{j=1}^{N}(\alpha_i^2 + \alpha_j^2 - 2\alpha_i\alpha_j) = 2N\sum_{i=1}^{N}\alpha_i^2 - 2\left(\sum_{i=1}^{N}\alpha_i\right)^2,$$

and thus

$$N\sum_{i=1}^{N}\alpha_i^2 \geq \left(\sum_{i=1}^{N}\alpha_i\right)^2.$$

The perimeter therefore decreases in time and the system moves to a configuration with a smaller total perimeter.

2.2.3 Finite Time Extinction

Here we wish to prove that, for the particles in the system, all but the largest go extinct in finite time. We are assuming that the timescale has been adjusted to remove ν/ϵ^3 on the right hand side of the ODE equation. To do this, we assume $\rho_1(0) \leq \rho_2(0) \leq \ldots \leq \rho_N(0)$ and show that for the smallest particle, ρ_1, there exists a time T_1 such that $\rho_1(T_1) = 0$ and

$$\frac{\rho_1(0)^3}{3} \leq T_1 \leq \frac{N\rho_1(0)^3\rho_N(0)}{\rho_N(0)-\rho_1(0)}.$$

This is sufficient because the calculation can then be repeated for the next smallest particle. Consider the system of ODEs derived in principal result 2.1

$$\frac{d\rho_1}{dt} = \frac{1}{\rho_1}\left[\frac{1}{\rho_{\text{harm}}} - \frac{1}{\rho_1}\right] \geq -\frac{1}{\rho_1^2}, \tag{2.6}$$

where the inequality arises from discarding the first term on the right. Now, we have

$$\rho_1^2\frac{d\rho}{dt} \geq -1.$$

If we separate the equation and integrate, we wind up with

$$\rho_1(t)^3 \geq -3t + \rho_1(0)^3 \geq 0, \quad t \leq \frac{1}{3}\rho_1(0)^3.$$

Thus ρ_1 is greater than zero for all t less than the value shown above and thus the extinction time must satisfy $T_1 \geq \rho_1(0)^3/3$. For the upper bound, we again look to the system of ODEs. First, consider

$$\frac{1}{\rho_{\text{harm}}} - \frac{1}{\rho_1} = \frac{1}{N}\left(\frac{1}{\rho_2} - \frac{1}{\rho_1} + \ldots + \frac{1}{\rho_N} - \frac{1}{\rho_1}\right) \leq \frac{1}{N}\left(\frac{1}{\rho_N} - \frac{1}{\rho_1}\right). \tag{2.7}$$

From (2.6) we can see that

$$\rho_1^2\frac{d\rho_1}{dt} = \rho_1\left[\frac{1}{\rho_{\text{harm}}} - \frac{1}{\rho_1}\right].$$

Combining this and (2.7) we see that

$$\rho_1^2\frac{d\rho}{dt} \leq \frac{1}{N}\left(\frac{\rho_1-\rho_N}{\rho_N}\right) \leq \frac{1}{N}\left(\frac{\rho_1(0)-\rho_N(0)}{\rho_N(0)}\right).$$

The last inequality arises because $1/\rho_N \leq 1/\rho_{\text{harm}} \leq 1/\rho_1$ which means $\rho_N' \geq 0$ and $\rho_1' \leq 1$. This means the difference between ρ_1 and ρ_N will grow in time and is smallest when $t = 0$.

We can integrate the above equation as with the lower bound to show that

$$\rho_1(t)^3 \leq \frac{t}{N}\left(\frac{\rho_1(0)-\rho_N(0)}{\rho_N(0)}\right)+\rho_1(0)^3 \leq 0, \quad t \geq \frac{N\rho_1(0)^3\rho_N(0)}{\rho_N(0)-\rho_1(0)}.$$

This shows that p_1 is less than zero (extinct) for t greater than the value given above. We conclude with

$$\frac{\rho_1(0)^3}{3} \leq T_1 \leq \frac{N\rho_1(0)^3\rho_N(0)}{\rho_N(0)-\rho_1(0)}.$$

2.3 Summing the Logarithmic Terms

In this section we go back to our leading order approximation for the droplet evolution and make further progress, calculating the asymptotic solution for all terms of $O(\nu^k)$ for any k. We begin by taking another look at the inner expansion for u. We can rewrite U, this inner expansion, as

$$U = \frac{1}{\rho_j} + \nu B_j(\nu) U_1 + \epsilon U_2 + \dots, \tag{2.8}$$

for functions $B_j(\nu)$, $j = 1, 2, \dots, N$ to be found. The equation U_1 satisfies is the same as in (2.4) and thus has the same form: $U_1 = \log(\rho) - \log(\rho_j)$. $B_j(\nu)$ is taking the place of $B_{0,j}$ and $B_{1,j}$ from equation (2.5). Notice that we have separated logarithmic dependence from U_0 in (2.5a) and rearranged it to lie within U_1 and $B_j(\nu)$.

The idea is that all terms of logarithmic order can be captured by one function for each droplet. Since this captures the terms of *all* logarithmic orders it will result in a more accurate solution. Switching to the outer coordinate, we have

$$U = \frac{1}{\rho_j} + \nu B_j(\nu)\left[\log|\mathbf{x}-\mathbf{x}_j| + \frac{1}{\nu} - \log(\rho_j)\right] + \dots \tag{2.9}$$

The matching works very similarly to the leading order case but we now group u_0 and u_1 as one function, u_H. The equation u_H satisfies is

$$\begin{gathered}
\Delta u_H = 0, \quad \mathbf{x} \in \Omega \setminus \{\mathbf{x}_1, \dots, \mathbf{x}_N\}, \\
\frac{\partial u_H}{\partial n} = 0, \quad \mathbf{x} \in \partial\Omega, \\
u_H \sim \frac{1}{\rho_j} + B_j(\nu) + \nu B_j(\nu)[\log|\mathbf{x}-\mathbf{x}_j| - \log(\rho_j)], \quad \text{as } \mathbf{x} \to \mathbf{x}_j, \text{ for } j = 1, \dots, N.
\end{gathered}$$

This can be solved by making use of the Neumann Green's function $G(\mathbf{x};\mathbf{x}_j)$ which satisfies

$$\Delta G = \frac{1}{|\Omega|} - \delta(\mathbf{x}-\mathbf{x}_j), \quad \mathbf{x}\in\Omega,$$
$$\frac{\partial G}{\partial n} = 0, \quad \mathbf{x}\in\partial\Omega; \qquad \int_\Omega G\,d\mathbf{x} = 0,$$
$$G(\mathbf{x};\mathbf{x}_j) \sim -\frac{1}{2\pi}\log|\mathbf{x}-\mathbf{x}_j| + R_{jj} + o(1), \quad \text{as } \mathbf{x}\to\mathbf{x}_j,$$

where R_{jj} is the regular (non-singular) part of the j^{th} Neumann Green's function and depends upon the domain Ω. Thus, u_H can be written as

$$u_H = -2\pi\sum_{j=1}^{N} B_j(\nu)G(\mathbf{x};\mathbf{x}_j) + u_0. \tag{2.10}$$

As before, u_0 is an arbitrary constant to be found. This system has $N+1$ unknowns ($B_j(\nu)$ and u_0) but only N equations. To resolve this issue we impose the area preserving condition

$$\sum_{j=1}^{N} B_j(\nu) = 0$$

To determine the rest of the unknowns we expand (2.10) as $\mathbf{x}\to\mathbf{x}_j$, giving us

$$u_H \sim \nu B_j(\nu)\log|\mathbf{x}-\mathbf{x}_j| - 2\pi\left[B_j(\nu)R_{jj} + \nu\sum_{i\neq j} B_i(\nu)G_{ji}\right] + u_0,$$

where G_{ji} is the i^{th} Green's function evaluated at $\mathbf{x}_j$. Now, we match this with the singularity behavior determined from the inner solution in equation (2.9). After canceling the $\log|\mathbf{x}-\mathbf{x}_j|$ term in (2.9) and above, we wind up with

$$-2\pi\left[B_j(\nu)R_{jj} + \nu\sum_{i\neq j} B_i(\nu)G_{ji}\right] + u_0 = \frac{1}{\rho_j}B_j(\nu) - \nu B_j(\nu)\log(\rho_j),$$

for $j = 1, 2, \ldots, N$.

We can rewrite this as a linear algebraic system for the unknowns $B_j(\nu)$ and u_0.

$$-2\pi\nu\mathcal{G}\mathbf{B} + u_0\mathbf{e} = \boldsymbol{\rho_0} + \mathbf{B} - \nu\mathcal{P}\mathbf{B}, \tag{2.11}$$

where $\mathcal{G}$, $\mathbf{e}$, $\boldsymbol{\rho_0}$ $\mathbf{B}$ and $\mathcal{P}$ are given as

$$\mathcal{G} = \begin{pmatrix} R_{11} & & G_{ij} \\ & \ddots & \\ G_{ji} & & R_{nn} \end{pmatrix}; \qquad \mathcal{P} = \begin{pmatrix} \log(\rho_1) & & 0 \\ & \ddots & \\ 0 & & \log(\rho_N) \end{pmatrix},$$

$$\mathbf{e} = \begin{pmatrix} 1 \\ \vdots \\ 1 \end{pmatrix}; \qquad \boldsymbol{\rho_0} = \begin{pmatrix} \frac{1}{\rho_1} \\ \vdots \\ \frac{1}{\rho_N} \end{pmatrix}; \qquad \mathbf{B} = \begin{pmatrix} B_1(\nu) \\ \vdots \\ B_N(\nu) \end{pmatrix}.$$

If we multiply (2.11) on the left by $\mathbf{e}^T$, we realize that by the area preserving condition on $B_j(\nu)$, $\mathbf{e}^T\mathbf{B} = 0$. We are left with

$$-2\pi\nu\mathbf{e}^T\mathcal{G}\mathbf{B} + Nu_0 = \mathbf{e}^T\boldsymbol{\rho_0} - \nu\mathbf{e}^T\mathcal{P}\mathbf{B},$$

and therefore,

$$u_0 = \frac{1}{N}\left[2\pi\nu\mathbf{e}^T\mathcal{G}\mathbf{B} + \mathbf{e}^T\boldsymbol{\rho_0} - \nu\mathbf{e}^T\mathcal{P}\mathbf{B}\right].$$

We can now return to (2.11) and substitute in for u_0. Since u_0 is a constant, we can swap which side of $\mathbf{e}$ it appears on. Thus,

$$-2\pi\nu\mathcal{G}\mathbf{B} + 2\pi\nu\mathbf{E}\mathcal{G}\mathbf{B} + \mathbf{E}\boldsymbol{\rho_0} - \nu\mathbf{E}\mathcal{P}\mathbf{B} = \boldsymbol{\rho_0} + \mathbf{B} - \nu\mathcal{P}\mathbf{B}, \tag{2.12}$$

where $\mathbf{E}$ is given by

$$\mathbf{E} = \frac{1}{N}\begin{pmatrix} 1 & \dots & 1 \\ \vdots & \ddots & \vdots \\ 1 & \dots & 1 \end{pmatrix}.$$

Finally, we can rearrange (2.12) to give us the following result:

$$[\mathbf{I} + \nu(\mathbf{I} - \mathbf{E})(2\pi\mathcal{G} - \mathcal{P})]\mathbf{B} = (\mathbf{E} - \mathbf{I})\boldsymbol{\rho_0}.$$

Recall that the components of $\mathbf{B}$ are $B_j(\nu)$. Therefore, when this system is solved, we will determine the system of ODEs that describes the motion of

each droplets. We substitute $B_j(\nu)$ and U_1 into (2.8) and take a derivative with respect to ρ, giving us

$$\frac{d\rho_j}{dt} = \frac{\nu}{\epsilon^3}\frac{\partial u}{\partial \rho}\Big|_{\rho=\rho_j} \approx \frac{\nu}{\epsilon^3}\frac{B_j(\nu)}{\rho_j}, \quad j = 1, \ldots, N.$$

Principal Result 2.2: *Consider the 2-D free boundary Mullins-Sekerka problem given below.*

$$\Delta u = 0, \quad \mathbf{x} \in \Omega \setminus \Gamma,$$
$$u = -\kappa, \quad \mathbf{x} \in \Gamma; \qquad \frac{\partial u}{\partial n} = 0, \quad \mathbf{x} \in \partial\Omega,$$
$$V = -\left[\frac{\partial u}{\partial n}\right], \quad \mathbf{x} \in \Gamma.$$

where u is the chemical potential, κ the curvature and V is the interfacial velocity. In the case where Γ is the boundary of a collection of small circles (radius $\sim O(\epsilon)$, $\epsilon \ll 1$), the following system of ODEs describes, to logarithmic order, the coarsening phenomenon present.

$$\frac{d\rho_j}{dt} = \frac{\nu}{\epsilon^3}\frac{\partial u}{\partial \rho}\Big|_{\rho=\rho_j} \approx \frac{\nu}{\epsilon^3}\frac{B_j(\nu)}{\rho_j}, \quad j = 1, \ldots, N,$$

where $\nu = -1/\log(\epsilon)$ and $B_j(\nu)$ comes from the solution to the linear algebraic system given in (2.12).

As stated before, this will be more accurate than the previous example as it contains higher order correction terms; in particular, it contains all of the terms of $O(\nu^k)$.

2.4 Two Droplet Example

In this section we look at a specific example of the system above with only two droplets. This serves as a check to ensure that everything behaves as expected.

Let $\Omega \subset \mathbf{R}^2$ be a circle of radius 1 centered at the origin. That is, $\Omega = \{\mathbf{x} || \mathbf{x}| \leq 1\}$. Let $\epsilon = .05$, $r_1(0) = .025$, $r_2(0) = .05$ which gives $\rho_1(0) = 1/2$ and $\rho_2(0) = 1$. The droplets will be centered at $\mathbf{x}_1 = (-1/2, 0)$ and $\mathbf{x}_2 = (2/3, 0)$, along the x-axis.

In order to solve the algebraic system from the previous section we need to first solve for the Green's function that arises for this domain and boundary condition. Once again, the problem to solve is:

$$\Delta G = \frac{1}{|\Omega|} - \delta(\mathbf{x}-\mathbf{x}_j), \quad \mathbf{x}\in\Omega$$
$$\frac{\partial G}{\partial n} = 0, \quad \mathbf{x}\in\partial\Omega; \qquad \int_\Omega G\,d\mathbf{x} = 0,$$
$$G(\mathbf{x};\mathbf{x}_j) \sim -\frac{1}{2\pi}\log|\mathbf{x}-\mathbf{x}_j| + R_{jj} + o(1) \text{ as } \mathbf{x}\to\mathbf{x}_j.$$

The domain was chosen in this example so that the Green's function is well-known. It is

$$G(\mathbf{x},\mathbf{x}_j) = \frac{1}{2\pi}\left[-\log(|\mathbf{x}-\mathbf{x}_j|) - \log\left(\left|\mathbf{x}|\mathbf{x}_j| - \frac{\mathbf{x}_j}{|\mathbf{x}_j|}\right|\right) + \frac{1}{2}(|\mathbf{x}|^2+|\mathbf{x}_j|^2) - \frac{3}{4}\right],$$

with regular part

$$R(\mathbf{x},\mathbf{x}_j) = \frac{1}{2\pi}\left[-\log\left(\left|\mathbf{x}|\mathbf{x}_j| - \frac{\mathbf{x}_j}{|\mathbf{x}_j|}\right|\right) + \frac{1}{2}(|\mathbf{x}|^2+|\mathbf{x}_j|^2) - \frac{3}{4}\right].$$

Plugging in the given parameters, we determine that

$$R_{11} \approx -.0338; \qquad R_{22} \approx .04492; \qquad G_{12} = G_{21} \approx -.1344.$$

Now we must go through the steps of solving the 2×2 algebraic system. We know that

$$\mathbf{I}-\mathbf{E} = \frac{1}{2}\begin{pmatrix} 1 & -1 \\ -1 & 1\end{pmatrix}; \qquad 2\pi\mathcal{G}-\mathcal{P} = \begin{pmatrix} 2\pi R_{11}-\log(\rho_1) & 2\pi G_{12} \\ 2\pi G_{21} & 2\pi R_{22}-\log(\rho_2)\end{pmatrix}.$$

Thus, we solve

$$\mathcal{A}\mathbf{B} = \rho_0,$$

where

$$A = \begin{pmatrix} 1+\nu\pi(R_{11}-G_{21}) - \frac{\nu}{2}\log(\rho_1) & \nu\pi(G_{12}-R_{22}) + \frac{\nu}{2}\log(\rho_2) \\ \nu\pi(G_{21}-R_{11}) + \frac{\nu}{2}\log(\rho_1) & 1+\nu\pi(R_{22}-G_{12}) - \frac{\nu}{2}\log(\rho_2)\end{pmatrix},$$
$$\mathbf{B} = \begin{pmatrix} B_1(\nu) \\ B_2(\nu)\end{pmatrix}; \qquad \rho_0 = \frac{1}{2}\begin{pmatrix} \frac{1}{\rho_2}-\frac{1}{\rho_1} \\ \frac{1}{\rho_1}-\frac{1}{\rho_2}\end{pmatrix}.$$

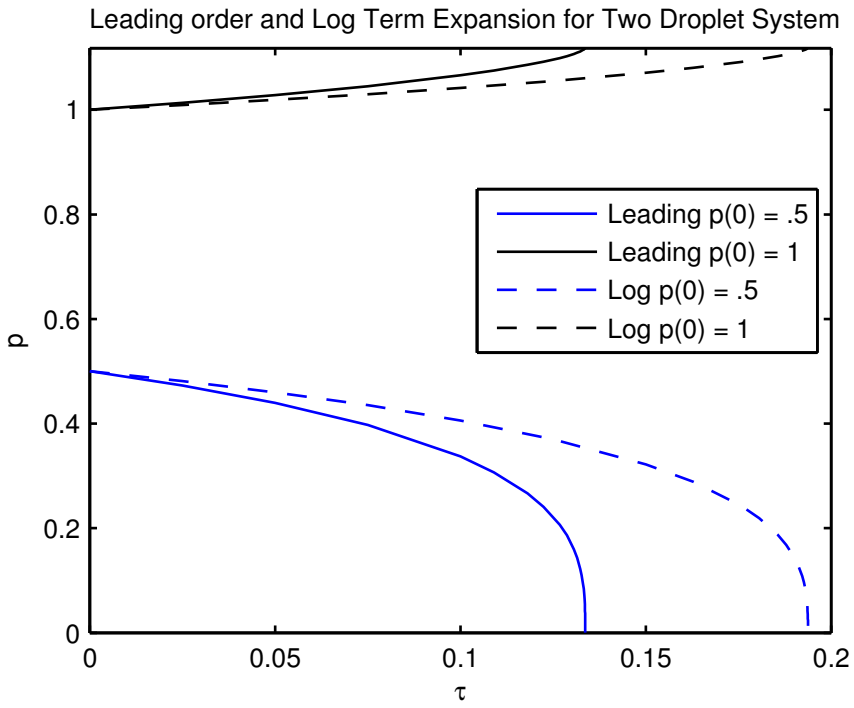

Figure 2.1: Here is a plot of the solutions to the system of ODEs that come from both the leading order expansion as well as the one that includes all of the logarithmic terms. You can clearly see in both cases that the system is area preserving and the smallest drop extinguishes in finite time.

Since the system is 2×2 it is trivial to invert. We use MATLAB's ODE23s to solve the resulting system of ODEs. The first step was to scale t so that the RHS of the system is $O(1)$. We let $t = \tau\epsilon^3/\nu$, a slow timescale. As you can see from figure 2.1, the larger drop grows at the expense of the smaller drop and we see the area preservation property as well as finite time extinction.

Chapter 3

The Chemotaxis Model

Now we return to our volume-filling chemotaxis model as mentioned in the introduction. As we will see, the chemotaxis model has very similar behavior to that of Ostwald ripening, with surface diffusion replacing motion by curvature but still maintaining a coarsening effects. This is the link between the two different systems- the mechanism for exchange of mass may be different but the phenomena is qualitatively similar.

The system will be nondimensionalized and then studied in a general two-dimensional domain with the use of a boundary-fitted coordinate framework. After deriving the velocity equation that governs the interfacial motion we will look at a few specific cases to verify intuition and motivate numerical studies.

3.1 Nondimensionalization

With the model in hand we can begin nondimensionalization to simplify our equations and highlight key parameters. The full model is

$$u_t = \nabla \cdot \left(D_u \nabla u - \chi u \left(1 - \frac{u}{\gamma} \right) \nabla v \right), \quad \mathbf{x} \in \Omega \tag{3.1a}$$

$$v_t = D_v \Delta v + \alpha u - \beta v, \quad \mathbf{x} \in \Omega \tag{3.1b}$$

$$\frac{\partial u}{\partial n} = 0, \quad \mathbf{x} \in \partial\Omega.; \qquad \frac{\partial v}{\partial n} = 0, \quad \mathbf{x} \in \partial\Omega. \tag{3.1c}$$

We make the following variable changes

$$\hat{\mathbf{x}} = \frac{\mathbf{x}}{L}; \qquad \hat{t} = \frac{t}{T}; \qquad \hat{u} = \frac{u}{u^*}.$$

Dividing by χ in equation (3.1a) and β in equation (3.1b), we have

$$\frac{u^*\hat{u}_{\hat{t}}}{\chi T} = \frac{1}{L^2}\nabla_{\hat{\mathbf{x}}}\cdot\left(\frac{D_u u^*}{\chi}\nabla_{\hat{\mathbf{x}}}\hat{u} - u^*\hat{u}\left(1-\frac{u^*}{\gamma}\hat{u}\right)\nabla_{\hat{\mathbf{x}}}v\right),$$
$$\frac{v_{\hat{t}}}{\beta T} = \frac{D_v}{\beta L^2}\Delta_{\hat{\mathbf{x}}}v + \frac{\alpha}{\beta}u - v.$$

We choose $u^* = \gamma$, $T = \gamma L^2/\chi$ and define

$$D_1 = \frac{D_u}{\chi}; \qquad D_2 = \frac{D_v}{\beta L^2}; \qquad \tau = \frac{\chi}{\gamma\beta L^2}; \qquad \sigma = \frac{\alpha}{\beta}.$$

The hats over the variables are dropped for convenience and we assume that $D_1 \ll 1$ as the diffusion strength, D_u, is typically much smaller than the chemotactic sensitivity, χ. We rename D_1 as ϵ and remove the subscript from D_2, relabeling it as D. The nondimensionalized system is

$$\begin{aligned} u_t &= \nabla\cdot(\epsilon u - u(1-u)\nabla v), \\ \tau v_t &= D\Delta v + \sigma - v, \\ \frac{\partial u}{\partial n} = 0, \quad \mathbf{x}\in\partial\Omega.; &\qquad \frac{\partial v}{\partial n} = 0, \quad \mathbf{x}\in\partial\Omega. \end{aligned} \tag{3.2}$$

3.2 Boundary Fitted Coordinate Expansion

Motivated by numerical results and other similar situations where this approach has been fruitful, we switch to a boundary fitted coordinate system. The idea is to describe points in space by their distance from an interface wall instead of standard cartesian coordinates. The derivation of the coordinate system can be seen in appendix A.

We begin the calculation by unraveling the nondimensionalized chemotaxis model (3.2) into this boundary fitted coordinate framework. The equations become

$$\begin{aligned} u_t = \epsilon&\left[u_{\eta\eta} - \frac{\kappa}{1-\kappa\eta}u_\eta + \frac{1}{1-\kappa\eta}\partial s\left(\frac{u_s}{1-\kappa\eta}\right)\right] \\ &-f(u)\left[v_{\eta\eta} - \frac{\kappa}{1-\kappa\eta}v_\eta + \frac{1}{1-\kappa\eta}\partial s\left(\frac{v_s}{1-\kappa\eta}\right)\right] \\ &- f'(u)\left[\frac{u_s v_s}{(1-\kappa\eta)^2} + u_\eta v_\eta\right], \end{aligned}$$

Figure 3.1: A depiction of the boundary fitted coordinate system. Ω is the outer domain and can be partitioned into two regions, Ω_- ($\eta > 0$) and Ω_+ ($\eta < 0$) with Γ representing the interface between them. Note the inward normal and sign convention for η.

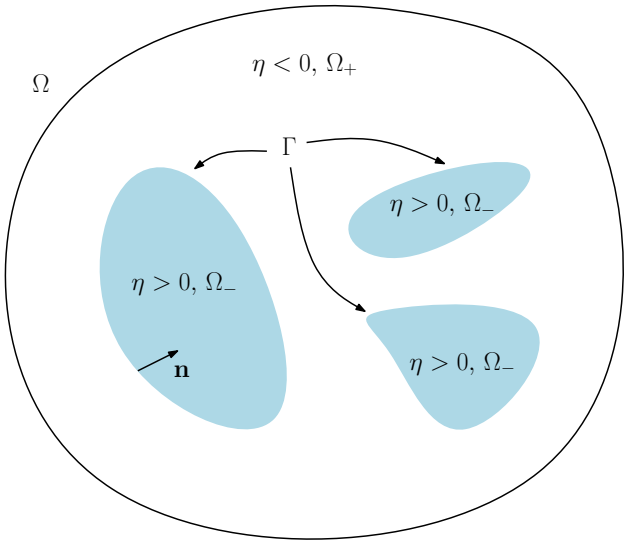

$$\tau v_t = D\left[v_{\eta\eta} - \frac{\kappa}{1-\kappa\eta}v_\eta + \frac{1}{1-\kappa\eta}\partial s\left(\frac{v_s}{1-\kappa\eta}\right)\right] + \sigma u - v,$$

where $f(u) = u(1-u)$. We solve these two PDEs in some domain Ω with Neumann boundary conditions on the outer wall. We define Ω_- to be regions where u has value 1 and $\Omega_+ = \Omega \setminus \Omega_-$. Γ, known as the front or interface, is the boundary of Ω_-.

Now we expand near the front, using the inner variable $\hat{\eta} = \eta/\epsilon$. We obtain

$$\tau V_t = D\left[\frac{1}{\epsilon^2}V_{\hat{\eta}\hat{\eta}} - \frac{1}{\epsilon}\left(\frac{\kappa}{1-\kappa\hat{\eta}\epsilon}\right)V_{\hat{\eta}} + \frac{1}{1-\kappa\hat{\eta}\epsilon}\partial s\left(\frac{V_s}{1-\kappa\hat{\eta}\epsilon}\right)\right] + \sigma u - V.$$

Expanding V as $V = V_0 + \epsilon V_1 + \epsilon^2 V_2 + \ldots$, we determine that for $t = O(1)$,

$$\tau\partial_t V_0 = D\Bigg[\frac{1}{\epsilon^2}\partial_{\hat\eta\hat\eta}V_0 + \frac{1}{\epsilon}\partial_{\hat\eta\hat\eta}V_1 + \partial_{\hat\eta\hat\eta}V_2 - \frac{\kappa}{\epsilon}\partial_{\hat\eta}V_0 - \kappa\partial_{\hat\eta}V_1 \\ - \kappa^2\hat\eta\partial_{\hat\eta}V_0 + \partial_{ss}V_0\Bigg] + \sigma u - V_0 + \dots$$

We can see from above that the leading order equation is

$$\partial_{\hat\eta\hat\eta}V_0 = 0,$$

which has solution

$$V_0 = A_0(s)\hat\eta + B_0(s). \tag{3.3}$$

Since v is bounded, V_0 cannot grow linearly as $\hat\eta \to \pm\infty$ and thus $A_0(s) \equiv 0$. Thus, we set $V_0 = V_0(s)$. This also tells us that $\partial_{\hat\eta}V_0 = 0$ which gives the following first correction equation

$$\partial_{\hat\eta\hat\eta}V_1 = 0,$$

with solution

$$V_1 = A_1(s) + B_1(s). \tag{3.4}$$

where in this case we cannot make any conclusions about the growth of $\hat\eta$ yet.

Now we apply the same treatment to the inner equation for U. Expanding U as $U = U_0 + \epsilon U_1 + \dots$, we arrive at the following equation

$$\partial_t U_0 = \epsilon\Bigg[\frac{1}{\epsilon^2}\partial_{\hat\eta\hat\eta}U_0 + \frac{1}{\epsilon}\partial_{\hat\eta\hat\eta}U_1 - \frac{\kappa}{\epsilon}\partial_{\hat\eta}U_0 + \partial_{ss}U_0\Bigg] \\ -f(U_0)\Bigg[\frac{1}{\epsilon^2}\partial_{\hat\eta\hat\eta}V_0 + \frac{1}{\epsilon}\partial_{\hat\eta\hat\eta}V_1 + \partial_{\hat\eta\hat\eta}V_2 - \frac{\kappa}{\epsilon}\partial_{\hat\eta}V_0 - \kappa\partial_{\hat\eta}V_1 - \kappa^2\hat\eta\partial_{\hat\eta}V_0 + \partial_{ss}V_0\Bigg] \\ - f'(U_0 + \epsilon U_1)\left[\partial_s U_0\partial_s V_0 + \frac{1}{\epsilon^2}V_{\hat\eta}U_{\hat\eta}\right] + \dots \tag{3.5}$$

The $\frac{1}{\epsilon^2}f'(U_0 + \epsilon U_1)V_{\hat\eta}U_{\hat\eta}$ that is left unexpanded is of particular importance and produces many terms; we shall focus on this now. Note that $\partial_{\hat\eta}V_0 = 0$ and as a result can be eliminated from the equation. We calculate,

$$\frac{1}{\epsilon^2}f'(U_0+\epsilon U_1)V_{\hat{\eta}}U_{\hat{\eta}} \approx \frac{1}{\epsilon}f'(U_0)\partial_{\hat{\eta}}U_0\partial_{\hat{\eta}}V_1 + f'(U_0)\partial_{\hat{\eta}}U_1\partial_{\hat{\eta}}V_1 + f''(U_0)U_1\partial_{\hat{\eta}}U_0\partial_{\hat{\eta}}V_1 + f'(U_0)\partial_{\hat{\eta}}U_0\partial_{\hat{\eta}}V_2.$$

Since we know that $\partial_{\hat{\eta}\hat{\eta}}V_0 = \partial_{\hat{\eta}\hat{\eta}}V_1 = 0$ they can be eliminated from equation (3.5). Additionally, we can replace instances of $\partial_{\hat{\eta}}V$ with $A_1(s)$. Substituting this information and the above equation into (3.5), the full expansion becomes

$$\begin{aligned}\partial_t U_0 = \epsilon\left[\frac{1}{\epsilon^2}\partial_{\hat{\eta}\hat{\eta}}U_0 + \frac{1}{\epsilon}\partial_{\hat{\eta}\hat{\eta}}U_1 - \frac{\kappa}{\epsilon}\partial_{\hat{\eta}}U_0 + \partial_{ss}U_0\right] - f(U_0)\left[\partial_{\hat{\eta}\hat{\eta}}V_2 - \kappa A_1(s) + \partial_{ss}V_0\right] \\ -f'(U_0)\left[\partial_s U_0\partial_s V_0 + \frac{1}{\epsilon}\partial_{\hat{\eta}}U_0A_1(s) + \partial_{\hat{\eta}}U_1A_1(s) + \partial_{\hat{\eta}}U_0\partial_{\hat{\eta}}V_2\right] \\ -f''(U_0)U_1\partial_{\hat{\eta}}U_0A_1(s) + \ldots\end{aligned} \tag{3.6}$$

Our goal is to derive an equation for the motion of the front, that is, an equation that $\eta'(t)$ satisfies. Supposing that the front changes slowly in time, $\eta = \eta(T)$, where $T = \epsilon^p t$. The change to u_t becomes

$$u_t = u_{\hat{\eta}}\epsilon^{p-1}\eta'(T). \tag{3.7}$$

We let $\dot{\eta} = \eta'(T)$ be the normal velocity to Γ where $\dot{\eta} >$ if Γ is expanding. p is chosen to be 1 to match the slow evolution assumption and first correction term.

Since the front evolves slowly, the leading order equation does not change in time and is

$$\partial_{\hat{\eta}\hat{\eta}}U_0 - f'(U_0)\partial_{\hat{\eta}}U_0A_1(s) = 0,$$

which can be written as

$$[\partial_{\hat{\eta}}U_0 - f(U_0)A_1(s)]_{\hat{\eta}} = 0.$$

After integrating once, we have a term depending on s on the right hand side. Since we will have to integrate once more and can't have growth as $\hat{\eta} \to \infty$, this term must be zero. We now have a 1-D profile equation parametrized by s.

$$\begin{gathered}\partial_{\hat{\eta}}U_0 - f(U_0)A_1(s) = 0, \\ U_0 \longrightarrow 0 \text{ as } \hat{\eta} \to -\infty; \qquad U_0 \longrightarrow 1 \text{ as } \hat{\eta} \to +\infty.\end{gathered} \tag{3.8}$$

To identify $A_1(s)$ we consider the matching condition between the inner and outer expansion for V. Returning to (3.3) and (3.4), the two-term inner expansion for V is

$$V = A_0(s) + \epsilon[A_1(s)\hat{\eta} + B_1(s)] + \dots \tag{3.9}$$

In the outer region (to leading order), we have that $u \sim 1$ in Ω_- and $u \sim 0$ in Ω_+, which tells us that the outer problem for v is

$$\begin{aligned} v_t &= D\Delta v - v + \sigma \begin{cases} 1 : \mathbf{x} \in \Omega_- \\ 0 : \mathbf{x} \in \Omega_+ \end{cases}, \\ \frac{\partial v}{\partial n} &= 0, \quad \mathbf{x} \in \partial\Omega. \end{aligned} \tag{3.10}$$

Now, if the initial condition for v is such that $v|\Omega| = \sigma|\Omega_-|$, where $|\Omega|$ is the area of Ω, then we expect that v is near its steady-state and will evolve slowly in time. Hence, $v(\mathbf{x}, 0) = \sigma|\Omega_-|/|\Omega|$ for v satisfying (3.10).

If we expand the outer equation for v as $\mathbf{x} \to \mathbf{x}_0(s)$ (as $\eta \to 0$), where $\mathbf{x}_0(s)$ is a point on the interface Γ, approaching from the $\pm$ direction, we have (by Taylor's theorem)

$$v = v\big|_\Gamma + \nabla v\big|_\Gamma \cdot (\mathbf{x} - \mathbf{x}_0) + \dots$$

Recall from the boundary fitted coordinate system that

$$\nabla v = \frac{v_s}{1 - \kappa\eta}\mathbf{t} + v_\eta \mathbf{n}; \qquad \mathbf{x} = \mathbf{x}_0(s) + \eta\mathbf{n}(s).$$

Thus, we derive that

$$v = v\big|_\Gamma + \eta v_\eta\big|_{\eta=0} + \dots$$

as $\mathbf{x} \to \mathbf{x}_0$. Recalling that $\hat{\eta} = \eta/\epsilon$ and noting (3.9), we have that

$$v\big|_\Gamma + \eta v_\eta\big|_{\eta=0} + \dots \sim A_0(s) + \epsilon[A_1(s)\frac{\eta}{\epsilon} + B_1(s)] + \dots$$

We conclude that

$$A_0(s) = v\big|_\Gamma; \qquad A_1(s) = v_\eta\big|_{\eta=0} = \nabla v \cdot \mathbf{n}\big|_\Gamma.$$

To summarize, in the outer region on the long timescale inherent to the evolution of the front where $v_t = \epsilon v_T$, v solves

$$D\Delta v - v = -\sigma \begin{cases} 1 : \mathbf{x} \in \Omega_- \\ 0 : \mathbf{x} \in \Omega_+ \end{cases},$$
$$\frac{\partial v}{\partial n} = 0, \quad \mathbf{x} \in \partial\Omega,$$

and with a given Γ, $A_0(s) = v\big|_\Gamma$ and $A_1(s) = \nabla v \cdot \mathbf{n}\big|_\Gamma$.

Returning to the 1-D profile equation for U_0 (3.8), we can write the exact solution as

$$U_0 = \frac{U_0(0)}{U_0(0) + (1 - U_0(0))e^{-\hat{\eta}A_1(s)}},$$

where $U_0(0)$ is some arbitrary value of U_0 on Γ. If $A_1(s) > 0$ then as $\hat{\eta} \to \infty$, which is inside of Γ, $U_0 \to 1$. Likewise, as we move outside of Γ ($\hat{\eta} \to -\infty$), $U_0 \to 0$.

Conjecture 3.1: *Consider the outer problem (3.10) for v. The solution of (3.10) is such that*

$$A_1(s) = \nabla v \cdot \mathbf{n}\big|_\Gamma > 0.$$

For now we just assume this to be the case. Under this assumption we may set $U_0(0) = 1/2$, the mid-value, which gives a precise definition of Γ.

Now we return to equation (3.6). From (3.7) we have

$$\begin{aligned} \partial_{\hat{\eta}} U_0 \dot{\eta} = \partial_{\hat{\eta}\hat{\eta}} U_1 - \kappa \partial_{\hat{\eta}} U_0 - f(U_0)\partial_{\hat{\eta}\hat{\eta}} V_2 + \kappa f(U_0) A_1(s) \\ - f(U_0)\partial_{ss} V_0 - f'(U_0)\partial_s U_0 \partial_s V_0 - f'(U_0)\partial_{\hat{\eta}} U_0 \partial_{\hat{\eta}} V_2 \\ - f'(U_0)\partial_{\hat{\eta}} U_1 A_1(s) - f''(U_0) U_1 \partial_{\hat{\eta}} U_0 A_1(s). \end{aligned} \tag{3.11}$$

From the leading order equation for U given in (3.8), we know that $\partial_{\hat{\eta}} U_0 = f(U_0)A_1(s)$ so we can cancel those terms in the above equation. We now define the operator L, such that

$$L\phi = \phi_{\hat{\eta}\hat{\eta}} - f'(U_0)A_1(s)\phi_{\hat{\eta}} - f''(U_0)A_1(s)\partial_{\hat{\eta}} U_0 \phi. \tag{3.12}$$

Thus, (3.11) becomes

$$\partial_{\hat{\eta}} U_0 \dot{\eta} = LU_1 - f(U_0)\partial_{\hat{\eta}\hat{\eta}} V_2 - f(U_0)\partial_{ss} V_0 - f'(U_0)\partial_s U_0 \partial_s V_0 - f'(U_0)\partial_{\hat{\eta}} U_0 \partial_{\hat{\eta}} V_2.$$

This can be written this more elegantly as

$$\partial_{\hat{\eta}} U_0 \dot{\eta} = LU_1 - \left(f(U_0)\partial_{\hat{\eta}} V_2\right)_{\hat{\eta}} - \left(\frac{\partial_{\hat{\eta}} U_0 \partial_s V_0}{A_1(s)}\right)_s. \tag{3.13}$$

We want to eliminate the terms contained in L so we need to determine the adjoint operator L^*. We look for L^* such that $(L\phi, \psi) = (\phi, L^*\psi)$ After rewriting (3.12), we have

$$(L\phi, \psi) = \int_{-\infty}^{\infty} \left[\phi_{\hat{\eta}\hat{\eta}} - \left(f'(U_0)A_1(s)\phi\right)_{\hat{\eta}}\right] \psi \, d\hat{\eta}.$$

Upon integrating the first term in the integral by parts twice and the second term once, with the boundary terms vanish due to imposed boundary conditions, we obtain

$$(\phi, L^*\psi) = \int_{-\infty}^{\infty} \left[\psi_{\hat{\eta}\hat{\eta}} + f'(U_0)A_1(s)\psi_{\hat{\eta}}\right] \phi \, d\hat{\eta},$$

and therefore,

$$L^*\psi = \psi_{\hat{\eta}\hat{\eta}} + f'(U_0)A_1(s)\psi_{\hat{\eta}}.$$

Lemma 3.1: *Suppose that*

$$L\phi = \phi_{\hat{\eta}\hat{\eta}} - f'(U_0)A_1(s)\phi_{\hat{\eta}} - f''(U_0)A_1(s)\partial_{\hat{\eta}} U_0 \phi,$$

on $-\infty < \hat{\eta} < \infty$*, with* $\phi \to 0$ *as* $\hat{\eta} \to \pm\infty$*. Then for* ψ *bounded as* $\hat{\eta} \to \pm\infty$*, we have*

$$\int_{-\infty}^{\infty} \psi L\phi \, d\hat{\eta} = \int_{-\infty}^{\infty} \phi L^*\psi \, d\hat{\eta},$$

as the boundary terms cancel. Here,

$$L^*\psi = \psi'' - A_1 f'(U_0).$$

The function in the kernel of L^* is just a constant function. Without loss of generality, we say the kernel is 1. Thus, using this solvability condition, we multiply everything in (3.13) by 1 and integrate from $-\infty$ to ∞ with respect to $\hat{\eta}$. This eliminates the terms in L (due to the boundary conditions and adjoint operator kernel) and we are left with

$$\int_{-\infty}^{\infty} \partial_{\hat{\eta}} U_0 \dot{\eta} \, d\hat{\eta} = -\int_{-\infty}^{\infty} \left[\left(f(U_0)\partial_{\hat{\eta}} V_2\right)_{\hat{\eta}} + \left(\frac{\partial_{\hat{\eta}} U_0 \partial_s V_0}{A_1(s)}\right)_s\right] d\hat{\eta}.$$

We can immediately integrate the left hand side and apply the fact that $U_0 \to 1$ as $\hat{\eta} \to \infty$ and $U_0 \to 0$ as $\hat{\eta} \to -\infty$, leaving us with $\dot{\eta}$. Note that $\dot{\eta}$ does not depend upon $\hat{\eta}$ and can be factored out of the integral. Since V_0 and $A_1(s)$ only depend on s, we can switch the order of the derivatives in the second term of the right hand side and integrate $\partial_{\hat{\eta}} U_0$ as we did on the left hand side. This leaves us with

$$\dot{\eta} = -\int_{-\infty}^{\infty} \left(f(U_0)\partial_{\hat{\eta}} V_2\right)_{\hat{\eta}} \, d\hat{\eta} - \left(\frac{\partial_s V_0}{A_1(s)}\right)_s .$$

The final integral becomes

$$\int_{-\infty}^{\infty} \left(f(U_0)\partial_{\hat{\eta}} V_2\right)_{\hat{\eta}} \, d\hat{\eta} = f(U_0)\partial_{\hat{\eta}} V_2 \Big|_{-\infty}^{\infty}.$$

Recall that $f(U_0) = U_0(1-U_0)$ and that $U_0 \to 1$ or $U_0 \to 0$ as $\hat{\eta} \to \pm\infty$, respectively. Thus, the integral vanishes and we are left with our key result,

$$\dot{\eta} = -\left(\frac{\partial_s V_0}{A_1(s)}\right)_s .$$

Principal Result 3.1: *Let Γ be a simple closed smooth curve and let $T = \epsilon t$ with $T = O(1)$. Consider the outer solution v defined by the quasi-steady problem*

$$D\Delta v - v = -\sigma \begin{cases} 1 : \mathbf{x} \in \Omega_- \\ 0 : \mathbf{x} \in \Omega_+ \end{cases},$$
$$\frac{\partial v}{\partial n} = 0, \quad \mathbf{x} \in \partial\Omega,$$

and Γ evolves on the slow timescale ϵt. The normal velocity $\dot{\eta}(T)$ to Γ on the long timescale T satisfies the surface diffusion law

$$\dot{\eta} = -\left(\frac{\partial_s V_0}{A_1(s)}\right)_s , \tag{3.14}$$

where s is the arc length of Γ, $V_0 = A_0 = v\big|_\Gamma$ and $A_1 = \nabla v \cdot \mathbf{n}\big|_\Gamma$. Note that $\dot{\eta} > 0$ if the interface is expanding.

3.3 Specific Domain Choices

In order to analyze principal result 3.1 and verify some intuition about the behavior of the system, we take a closer look at a few specific examples.

The first example is the case of two concentric circles, where the domain is the unit disk ($\Omega = \{\mathbf{x}||\mathbf{x}| \leq 1\}$) and Γ, the interface that separates Ω_+ and Ω_-, is a circle. Next, we analyze the effects of a small perturbation to this circular interface, where $\Gamma = r_0 + \delta h(\theta)$, $h(\theta)$ periodic, for $\delta \ll 1$. Finally, we examine the case of many circular interfaces and how they interact with each other as well as a brief look at the effects of small perturbations to these many circular interfaces. In all of these examples we highlight how the velocity from principal result 3.1 changes.

3.3.1 Concentric Circles

In our first example, we assume the initial amount of mass in the system is small and choose the outer domain to be the unit disk; that is, $\Omega = \{\mathbf{x} : |\mathbf{x}| \leq 1\}$. We also assume that the initial aggregation phase for u has already occurred and we are in a metastable state of two concentric circles. We have $u = 1$ for $\mathbf{x} \in \Omega_-$ and $u = 0$ for $\mathbf{x} \in \Omega_+$, where $\Omega_- = \{\mathbf{x} : |\mathbf{x}| \leq \delta\}$, $\Omega_+ = \{\mathbf{x} : |\mathbf{x}| > \delta\}$, and $\Gamma = \{\mathbf{x} : |\mathbf{x}| = \delta\}$, for some constant δ.

Consider M, the initial mass of u. Since u is uniform within Ω_+ and Ω_-, we have

$$M = \int_\Omega u \, d\mathbf{x} = \int_{\Omega_-} 1 \, d\mathbf{x} = \pi r^2 = \pi \delta^2,$$

and therefore,

$$\delta = \sqrt{\frac{M}{\pi}},$$

which means $\delta = O(\sqrt{M})$. Since we assume M is small ($M \ll 1$), we must also have $\delta \ll 1$.

We suspect that in this case, due to the radial symmetry of the domain, the solution will be radially symmetric and therefore not depend upon s, the arc length of Γ. Since the solution will be independent of s, the velocity from principal result 3.1 and (3.14) will be zero and we are actually in the case of a stable equilibrium, not a metastable one.

The reduced problem we have to solve is

$$\begin{aligned} D\Delta v - v &= -\sigma \begin{cases} 1 & : 0 \leq |\mathbf{x}| \leq \delta \\ 0 & : \delta < |\mathbf{x}| \leq 1 \end{cases}, \\ \frac{\partial v}{\partial n} &= 0, \quad |\mathbf{x}| = 1. \end{aligned} \tag{3.15}$$

Expanding v in terms of δ as $v = v_0 + \mu(\delta)v_1 + \dots$ and substituting in, we have the following leading order equation.

$$D\Delta v_0 - v_0 = 0, \quad |\mathbf{x}| \leq 1,$$
$$\frac{\partial v_0}{\partial n} = 0, \quad |\mathbf{x}| = 1,$$

which has solution $v_0 = 0$. The $O(\mu(\delta))$ equation is

$$D\Delta v_1 - v_1 = 0, \quad |\mathbf{x}| \leq 1, \mathbf{x} \neq 0,$$
$$\frac{\partial v_1}{\partial n} = 0, \quad |\mathbf{x}| = 1; \qquad v_1 \sim \ ?, \quad \text{as } \mathbf{x} \to 0,$$

where the singular behavior of v_1 as $\mathbf{x} \to 0$ is determined by matching to the inner expansion around 0. Now, consider the inner variable $\mathbf{y} = \mathbf{x}/\delta$ and the inner v function V. Using this change of variables for equation (3.15), our inner equation to solve becomes

$$D\frac{\Delta V}{\delta^2} - V = -\sigma \begin{cases} 1 & : |\mathbf{y}| \leq 1 \\ 0 & : |\mathbf{y}| > 1 \end{cases}.$$

We now scale V as $V = \delta^2 W$ and expand W as

$$W = \log(\delta)W_0 + W_1 + \dots \tag{3.16}$$

The choice of the $\log(\delta)$ term will be made clear shortly. Substituting in this scaling and expansion, we wind up solving the following O($\log(\delta)$) equation for W_0,

$$\Delta W_0 = 0,$$
$$W_0 \text{ bounded as } \mathbf{y} \to \infty,$$

which implies that $W_0 = C_0$, a constant that will be determined by matching to the outer solution. The O(1) equation is

$$\Delta W_1 = -\frac{\sigma}{D} \begin{cases} 1 & : |\mathbf{y}| \leq 1 \\ 0 & : |\mathbf{y}| > 1 \end{cases}$$

This equation can be solved by switching to polar coordinates and using the fact that the solution must be radially symmetric. With $\rho = |\mathbf{y}|$ we have

$$\partial_{\rho\rho} W_1 + \frac{1}{\rho}\partial_\rho W_1 = -\frac{\sigma}{D} \begin{cases} 1 & : \rho \leq 1 \\ 0 & : \rho > 1 \end{cases},$$

with W_1 well-behaved as $\rho \to 0$. Solving in each region separately, we have

$$W_1 = \begin{cases} -\frac{\sigma}{D}\left(\frac{1}{4}\rho^2 + A_0\right) & : \rho \leq 1 \\ B_0 \log(\rho) + C_1 & : \rho > 1 \end{cases}$$

We impose continuity and differentiability at $\rho = 1$ to patch together the two solutions together and solve for the unknown constants. The solution is

$$W_1 = \begin{cases} -\frac{\sigma}{D}\left(\frac{1}{4}\rho^2 - \frac{C_1}{\sigma} - \frac{1}{4}\right) & : \rho \leq 1 \\ -\frac{1}{2}\frac{\sigma}{D}\log(\rho) + C_1 & : \rho > 1 \end{cases}.$$

where C_1 is undetermined and comes from matching to higher order terms in the outer expansion. To proceed with matching the inner and outer solutions and determining C_0 and C_1, we examine the behavior of W as $\rho \to \infty$. Adding together W_0 and W_1 and switching to the outer radial coordinate, $r = \rho/\delta$, we see that

$$W \sim \log(\delta)C_0 - \frac{\sigma}{2D}\log(r) + \frac{\sigma}{2D}\log(\delta) + C_1 + \dots$$

As $\rho \to \infty$, W has an unmatchable $\log(\delta)$ term. This explains why we expanded W as in (3.16) and forces $C_0 = -\sigma/2D$ to cancel this term. As a result, for $\rho > 1$, W becomes

$$W = -\frac{\sigma}{2D}\log(\delta) - \frac{\sigma}{2D}\log(\rho) + C_1 + \dots$$

Since $V = \delta^2 W$, for $|\mathbf{y}| \leq 1$ ($\rho \leq 1$), we have

$$V = \delta^2\left[-\frac{\sigma}{2D}\log(\delta) - \frac{\sigma}{D}\left(\frac{1}{4}|\mathbf{y}|^2 - \frac{C_1 D}{\sigma} - \frac{1}{4}\right) + \dots\right], \tag{3.17}$$

and for $|\mathbf{y}| > 1$ ($\rho > 1$), we have

$$V = \delta^2\left[-\frac{\sigma}{2D}\log(\delta) - \frac{\sigma}{2D}\log(|\mathbf{y}|) + C_1 + \dots\right]. \tag{3.18}$$

Now, as $\mathbf{y} \to \infty$, we must have the inner and outer solutions match. Switching to the outer variable in (3.18), we have

$$\mu(\delta)v_1 + \dots \sim \delta^2\left[-\frac{\sigma}{2D}\log(|\mathbf{x}|) + C_1 + \dots\right],$$

which means $\mu(\delta) = \delta^2$ and determines the problem v_1 satisfies as

$$D\Delta v_1 - v_1 = 0, \quad |\mathbf{x}| \leq 1, \mathbf{x} \neq 0,$$
$$\frac{\partial v_1}{\partial n} = 0, \quad |\mathbf{x}| = 1; \qquad v_1 \sim -\frac{\sigma}{2D}\log(|\mathbf{x}|) + C_1, \quad \text{as } \mathbf{x} \to 0.$$

This equation can be solved by once again switching to polar coordinates and leveraging the radial symmetry of the domain. The problem becomes

$$\partial_{rr} v_1 + \frac{1}{r}\partial_r v_1 - \lambda^2 v_1 = 0, \quad r < 1,$$
$$\partial_r v_1 = 0, \quad r = 1; \qquad v_1 \sim -\frac{\sigma}{2D}\log(r) + C_1, \quad r \to 0,$$

where $\lambda = 1/\sqrt{D}$. This ODE has solution

$$v_1 = \frac{\sigma}{2D} K_0(r\lambda) + \frac{\sigma K_1(1)}{2I_1(1)} I_0(r\lambda),$$

where I_0 and K_0 are modified Bessel functions of the first and second kind respectively. As $r \to 0$, using [1] for the asymptotic expansions of $K_0(r)$, v_1 becomes

$$v_1 \sim \frac{\sigma}{2D}(-\log(r\lambda) + \log(2) - \gamma) + \frac{\sigma K_1(1)}{2DI_1(1)} = -\frac{\sigma}{2D} + C_1,$$

where γ is the Euler-Mascheroni constant. We can see that C_1 must be

$$C_1 = \frac{\sigma}{2D}\left(\log(2) - \gamma + \frac{K_1(1)}{I_1(1)}\right). \tag{3.19}$$

Finally, since $v = \delta^2 v_1 + \ldots$, the solution to equation (3.15) is

$$v = \delta^2\left(\frac{\sigma}{2D} K_0(|\mathbf{x}|\lambda) + \frac{\sigma K_1(1)}{2DI_1(1)} I_0(|\mathbf{x}|\lambda)\right) + \ldots \tag{3.20}$$

As suspected, due to the symmetry of the domain the solution v, to $O(\delta^2)$, has no dependence on θ and thus is independent of s. This means the derivatives with respect to s in (3.14) will be 0 and there is no movement.

As a check, we verify our asymptotic results numerically. For this choice of domain Ω and interface Γ, the solution can be found exactly by expressing equation (3.15) in polar coordinates, using radial symmetry, and imposing continuity and differentiability on the interface. The solution is

$$v = \begin{cases} \sigma + AI_0(|\mathbf{x}|\lambda) & : |\mathbf{x}| \leq \delta \\ BI_0(|\mathbf{x}|\lambda) + CK_0(|\mathbf{x}|\lambda) & : \delta < |\mathbf{x}| \leq 1 \end{cases}, \tag{3.21}$$

with A, B, and C given as

$$A = C\left[\frac{(K_0(\delta)-\sigma)I_1(1)+K_1(1)I_0(\delta)}{I_1(1)I_0(\delta)}\right],$$
$$B = C\frac{K_1(1)}{I_1(1)}; \qquad C = \frac{I_1(\delta)\sigma}{\mathcal{W}(K_0(\delta), I_0(\delta))},$$

where $\mathcal{W}(a,b) = ab' - ba'$ is the Wronskian.

The two figures below compare the asymptotic and exact solution. We chose $\sigma = 1$ and $D = 1$. Figure 3.2 compares (3.21) to (3.20) for $0 < r \leq 1$. In figure 3.3, we compare the exact solution (3.21) and the inner asymptotic solution given in (3.17) at $r = 0$ for changing values of δ. In figure 3.3 we plot against $1 - \delta$.

Figure 3.2: Asymptotic solution plotted with the exact solution for $0 < r \leq 1$. Here, $\delta = .05$. We can see that for everywhere except very close to $r = 0$, they are in almost complete agreement.

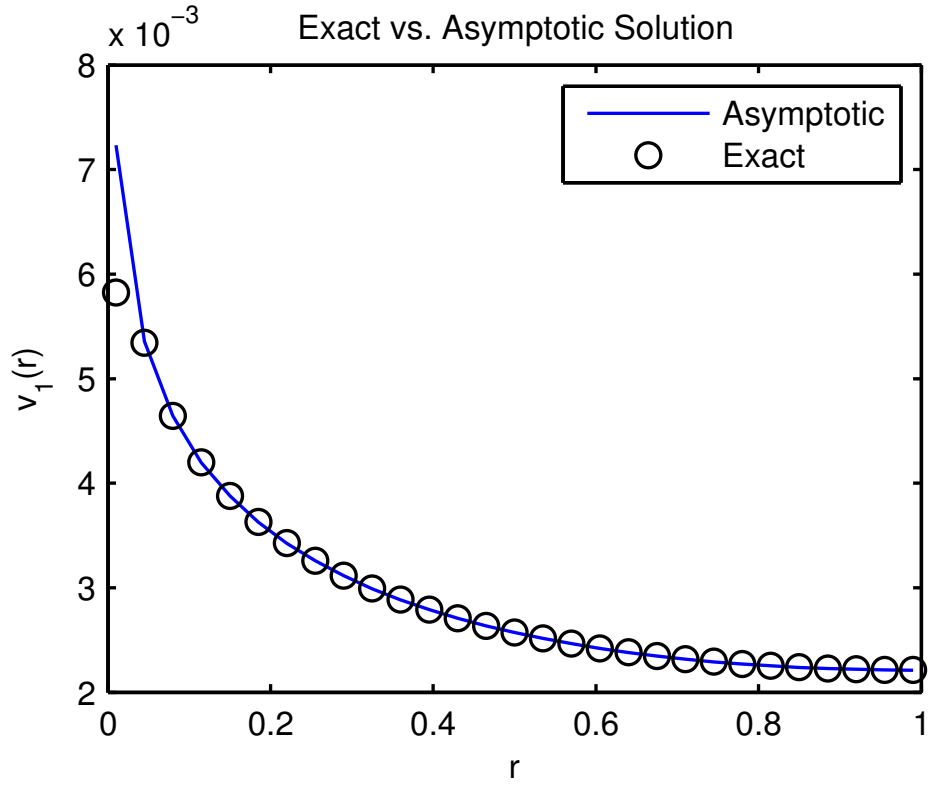

3.3.2 Circular Domain with Perturbed Circular Interface

In this example we look at the case where the interface is a near annulus. Once again, Ω is the unit disk and Γ at time $t = 0$ is the curve

$$r = r_0 + \delta h(\theta), \quad \text{with } h(\theta) + 2\pi) = h(\theta),$$

for $0 < r_0 \leq 1$ and $0 < \delta \ll 1$.

The question to ask is how does Γ evolve for near-circular initial interfaces. Since we don't assume the interfaces themselves are small, we don't have an inner variable but instead two comparably sized solutions in which we impose continuity and differentiability where they meet. The problem to

Figure 3.3: Asymptotic solution plotted with the exact solution for $r = 0$. Here, δ ranges from .5 to .01. As $\delta \to 0$, the approximation becomes more accurate but is surprisingly accurate for fairly large values of δ.

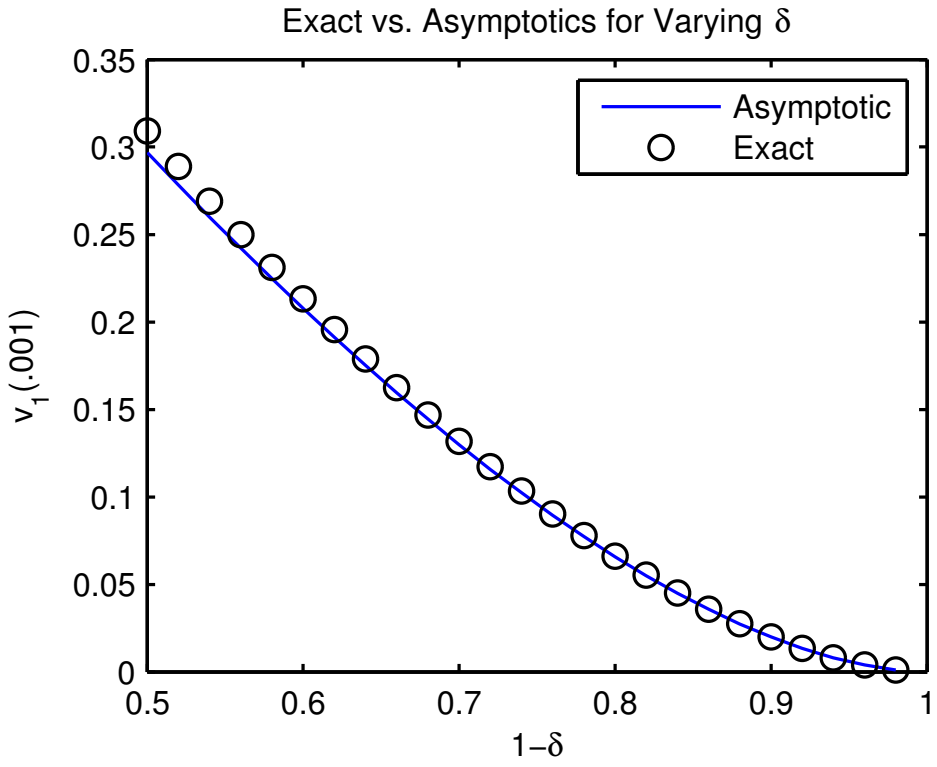

solve is

$$
\begin{gathered}
D\Delta v^+ - v^+ = 0, \quad r_0 + \delta h(\theta) < r \leq 1, \\
D\Delta v^- - v^- = -\sigma, \quad 0 < r \leq r_0 + \delta h(\theta), \\
v, \frac{\partial v}{\partial n} \text{ continuous across } r = r_0 + \delta h(\theta); \qquad v \text{ regular as } r \to 0, \\
v_r = 0, \quad r = 1,
\end{gathered}
$$

where v^+ indicates the solution in the outer region and v^- is the solution in the inner region.

The first thing we will do is unravel the inward normal for this interface. In polar coordinates, the gradient and level surface, $\phi = 0$, are

$$\nabla v = v_r r + \frac{1}{r} v_\theta \theta; \qquad \phi = r - (r_0 + \delta h(\theta)).$$

As a result,

$$\frac{\partial v}{\partial n} = -\nabla v \cdot \frac{\nabla \phi}{\|\nabla \phi\|} = -\frac{v_r \phi_r + \frac{1}{r^2} v_\theta \phi_\theta}{\sqrt{\phi_r^2 + \frac{\phi_\theta^2}{r^2}}}.$$

At this point we can substitute in $\phi_r = 1$, $\phi_\theta = -\delta h'(\theta)$, and $r = r_0 + \delta h(\theta)$ is $\phi = 0$ to derive

$$\frac{\partial v}{\partial n} = -\frac{v_r - \omega v_\theta}{\sqrt{1 + \delta h'(\theta)\omega}}, \tag{3.22}$$

with ω given as

$$\omega = \frac{\delta h'(\theta)}{(r_0 + \delta h(\theta))^2}.$$

Now we will do a perturbation calculation by starting with

$$\begin{gathered} \Delta v^+ - \frac{1}{D} v^+ = 0, \quad r_0 + \delta h(\theta) < r \leq 1, \\ v_r^+ = 0, \quad r = 1, \end{gathered} \tag{3.23}$$

$$\begin{gathered} \Delta v^- - \frac{1}{D} v^- = 0, \quad 0 < r \leq r_0 + \delta h(\theta), \\ v^- \text{ non-singular as } r \to 0, \end{gathered} \tag{3.24}$$

and we have the transmission and continuity conditions on $r = r_0 + \delta h(\theta)$

$$v^+ = v^-; \qquad \frac{\partial v^+}{\partial n} = \frac{\partial v^-}{\partial n}, \tag{3.25}$$

with the normal derivative defined as in (3.22). The goal is to calculate $A_0(\theta) = v^+\big|_\Gamma$, $A_1(\theta) = \partial_n v^+\big|_\Gamma$ with $\Gamma = r_0 + \delta h(\theta)$ for the velocity in equation (3.14).

The inner and outer equations are expanded in polar coordinates as

$$v^+ = v_0^+ + \delta v_1^+ + \delta^2 v_2^+ + \ldots; \qquad v^- = v_0^- + \delta v_1^- + \delta^2 v_2^- + \ldots,$$

and we use

$$v^+(r_0 + \delta h(\theta), \theta) = v^+(r_0) + \delta h(\theta) v_r^+(r_0) + \frac{\delta^2 h(\theta)^2}{2} v_{rr}^+(r_0) + \ldots,$$

to gives us our radially symmetric leading order problem

$$\begin{gathered}
\Delta v_0^+ - \frac{1}{D} v_0^+ = 0, \quad r_0 < r \leq 1; \qquad \Delta v_0^- - \frac{1}{D} v_0^- = -\frac{\sigma}{D}, \quad 0 < r \leq r_0, \\
v_0^+ = v_0^-, \quad r = r_0; \qquad \partial_r v_0^+ = \partial_r v_0^-, \quad r = r_0, \\
v_0^- \text{ non-singular as } r \to 0; \qquad \partial_r v_0^+ = 0, \quad r = 1.
\end{gathered}$$

This is precisely the problem specified in (3.15), which was solved exactly in section 3.3.1. Written compactly, the solution is

$$\begin{aligned}
v_0^+(r) &= C_0 \frac{K_0(\lambda r) + \frac{K_1(\lambda)}{I_1(\lambda)} I_0(\lambda r)}{K_0(\lambda r_0) + \frac{K_1(\lambda)}{I_1(\lambda)} I_0(\lambda r_0)}, \quad r_0 < r < 1, \\
v_0^-(r) &= \sigma + (C_0 - \sigma) \frac{I_0(\lambda r)}{I_0(\lambda r_0)}, \quad 0 < r < r_0,
\end{aligned} \tag{3.26}$$

where $\lambda = 1/\sqrt{D}$, K_0 and I_0 are once again modified Bessel Functions and C_0 comes from enforcing differentiability at $r = r_0$. To determine C_0, we will define τ_1 and τ_2 as

$$\tau_1(r) = K_0(\lambda r) + \frac{K_1(\lambda)}{I_1(\lambda)} I_0(\lambda r); \qquad \tau_2(r) = I_0(\lambda r), \tag{3.27}$$

which gives us

$$v_0^+(r) = C_0 \frac{\tau_1(r)}{\tau_1(r_0)}; \qquad v_0^-(r) = \sigma + (C_0 - \sigma) \frac{\tau_2(r)}{\tau_2(r_0)}.$$

Imposing differentiability on $r = r_0$, we calculate that

$$C_0 \left(\frac{\tau_1'(r_0)}{\tau_1(r_0)} - \frac{\tau_2'(r_0)}{\tau_2(r_0)} \right) = -\sigma \frac{\tau_2'(r_0)}{\tau_2(r_0)}.$$

If we multiply both sides of the above equation by $\tau_1(r_0)\tau_2(r_0)$ we obtain

$$C_0 \mathcal{W}(\tau_2, \tau_1) = -\sigma \tau_2'(r_0) \tau_1(r_0),$$

where $\mathcal{W}(\tau_2, \tau_1)$ is the Wronskian of τ_2 and τ_1. It is not hard to work out that $\mathcal{W}(\tau_2, \tau_1) = \mathcal{W}(I_0(\lambda r), K_0(\lambda r))$ and, since $\mathcal{W}(I_0(z), K_0(z)) = -1/z$ by Abel's identity, we determine that

$$C_0 = r_0 \sigma \tau_2'(r_0)\tau_1(r_0), \tag{3.28}$$

with τ_1 and τ_2 given in (3.27).

This tells us that the leading order approximation of A_0 is

$$A_0 = v_0^+\big|_{\partial\Gamma} + O(\delta) = C_0, \tag{3.29}$$

and we calculate $\partial_r v_0^-(r_0)$ to determine A_1 as

$$A_1 = \partial_r v_0^+(r_0) = -\partial_r v_0^-(r_0) = \lambda(\sigma - C_0)\frac{I_0'(\lambda r_0)}{I_0(\lambda r_0)} + O(\delta), \tag{3.30}$$

with C_0 defined as in (3.28).

Notice that A_1 is independent of θ and as a result, independent of arc length s along Γ. Thus, A_1 can be used in the denominator of the surface diffusion law in equation (3.14). We must show that $A_1 > 0$ to ensure we have the correct sign of the velocity. Note that this was conjectured in section 3.1, conjecture 3.1; with this specific case we can make asymptotic and numerical progress. Substituting C_0 from (3.28) into (3.31) we are left with

$$A_1 = \lambda\sigma(1 - r_0\tau_2'(r_0)\tau_1(r_0))\frac{I_0'(\lambda r_0)}{I_0(\lambda r_0)}. \tag{3.31}$$

Since $I_0(z)$ and $I_0'(z) > 0\ \forall z$, we only need to focus on the terms in the parenthesis above. Now, consider β given by

$$\beta(r_0) = r_0\tau_2'(r_0)\tau_1(r_0). \tag{3.32}$$

Determining the sign of A_1 reduces to showing that $\beta < 1$ for $0 < r_0 < 1$.

First we consider the case when $r_0 \to 0$. Here, $\tau_1(r_0) = O(-\log(r_0))$ and $\tau_2'(r_0) = O(r_0)$ due to the fact that, as $z \to 0$, we have

$$K_0(z) \sim -[\log(\tfrac{z}{2}) + \gamma_e]\left(1 + \frac{z^2}{4} + \dots\right); \qquad I_0(z) \sim 1 + \frac{z^2}{4} + \dots,$$

which implies $\beta = O(r_0^2(-\log(r_0)))$ and thus $\beta \to 0$ as $r_0 \to 0$. Now, when $r_0 = 1$, we have

$$\beta(1) = \lambda[K_0(\lambda)I_0'(\lambda) - K_0'(\lambda)I_0(\lambda)] = -\lambda\mathcal{W}(I_0, K_0) = 1,$$

by Abel's identity.

What is left to prove is that β is monotone increasing for $0 < r_0 < 1$. For now all we can do is conjecture that this is the case and provide numerical evidence for a few values of λ in figure 3.4.

Figure 3.4: A plot of β as given in (3.32) showing monotonicity for a few values of λ.

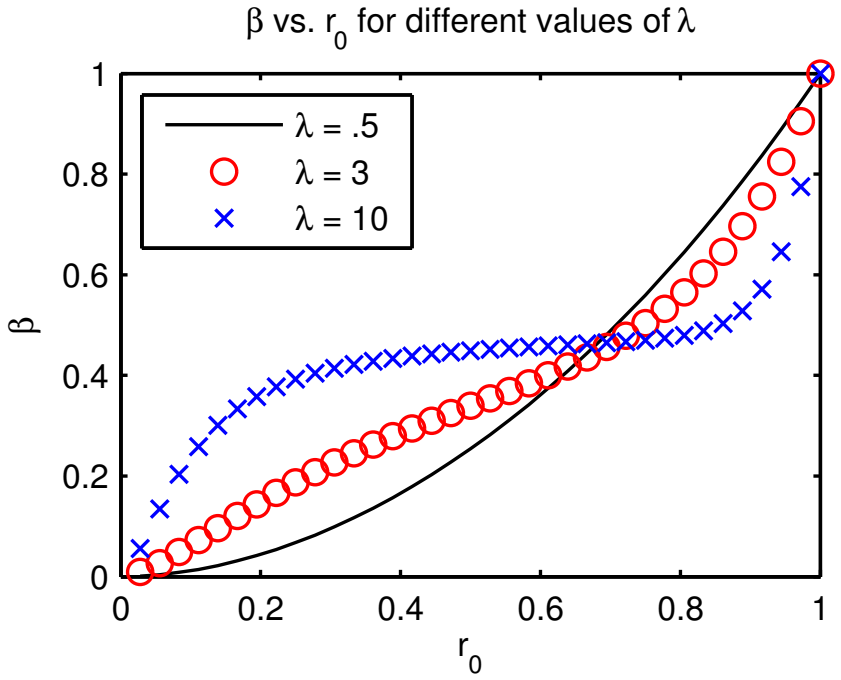

We now make progress to determine the $O(\delta)$ and $O(\delta^2)$ contributions. First we take a closer look at our transmission and continuity conditions (3.25). Recall

$$v^+(r_0 + \delta h(\theta), \theta) = v^+\big|_0 + \delta h(\theta) v_r^+\big|_0 + \frac{\delta^2 h(\theta)^2}{2} v_{rr}^+\big|_0 + \dots$$

where $f\big|_0 = f(r_0, \theta)$. We expand v^+ as

$$v^+ = v_0^+ + \delta v_1^+ + \delta^2 v_2^+ + \dots$$

Combining these two equations we arrive at

$$v^+(r_0+\delta h,\theta) = v_0^+\big|_0+\delta(v_1^+\big|_0+h\partial_r v_0^+\big|_0)+\delta^2(v_2^+\big|_0+h\partial_r v_1^+\big|_0+\frac{h^2}{2}\partial_{rr}v_0^+\big|_0)+\dots$$

From this equation we can determine the $O(\delta)$ and $O(\delta^2)$ continuity condition. They are

$$O(\delta): \quad v_1^+\big|_0 - v_1^-\big|_0 = h(\partial_r v_0^-\big|_0 - \partial_r v_0^+\big|_0) = 0, \tag{3.33a}$$

$$O(\delta^2): \quad v_2^+\big|_0 - v_2^-\big|_0 = h(\partial_r v_1^-\big|_0 - \partial_r v_1^+\big|_0) + \frac{h^2}{2}(\partial_{rr} v_0^-\big|_0 - \partial_{rr} v_0^+\big|_0), \tag{3.33b}$$

where the $O(\delta)$ equation is simplified in that way since we already know $\partial_r v_0^+\big|_0 = \partial_r v_0^-\big|_0$ from the leading order equation. Next we examine the second condition in (3.25) using (3.22). Since the denominator in (3.22) is independent of v it plays no role in the transmission condition and thus we can ignore it and label

$$\mathcal{D} = \sqrt{1 + \frac{\delta h'}{r_0+\delta h}^2}.$$

We can also expand $1/(r_0+\delta h)^2$ as

$$\frac{1}{(r_0+\delta h)^2} \sim \frac{1}{r_0^2}\left(1+\frac{\delta h}{r_0}\right)^{-2} \sim \frac{1}{r_0^2}\left(1-\frac{2\delta h}{r_0}+\dots\right).$$

Using the above, (3.22) gives

$$\frac{\partial v}{\partial n} = -\frac{1}{\mathcal{D}}\left[v_r^+(r_0+\delta h,\theta) - \frac{\delta h'}{r_0^2}\left(1-\frac{2\delta h}{r_0}+\dots\right)v_\theta^+(r_0+\delta h,\theta)\right], \tag{3.34}$$

where v_θ^+ (a partial derivative, not total derivative) can be expanded as

$$v_\theta^+ = v_\theta^+(r_0,\theta) + \delta h v_{\theta r}^+(r_0,\theta) + \dots$$

We can now substitute this and the fact that v_0^+ is radially symmetric in to (3.34) while also expanding v^+ as $v^+ = v_0^+ + \delta v_1^+ + \delta^2 v_2^+ + \dots$ to derive

$$\frac{\partial v}{\partial n} = -\frac{1}{\mathcal{D}}\Big[\partial_r v_0^+\big|_0 + \delta(\partial_r v_1^+\big|_0 + h\partial_{rr} v_0^+\big|_0) + \delta^2\left(\partial_r v_2^+\big|_0 + h\partial_{rr} v_1^+\big|_0 + \frac{h^2}{2}\partial_{rrr} v_0^+\big|_0 - \frac{h'}{r_0^2}\partial_\theta v_1^+\big|_0\right)\Big].$$

With the transmission condition given as $v_n^+ = v_n^-$, we can see that, to leading order, $\partial_r v_0^+\big|_0 = \partial_r v_0^-\big|_0$ (as expected). The $O(\delta)$ transmission equation is

$$\partial_r v_1^+\big|_0 - \partial_r v_1^-\big|_0 = h(\partial_{rr} v_0^-\big|_0 - \partial_{rr} v_0^+\big|_0), \tag{3.35}$$

and $O(\delta^2)$ gives

$$\begin{aligned}\partial_r v_2^+\big|_0 - \partial_r v_2^-\big|_0 = h(\partial_{rr} v_1^-\big|_0 - \partial_{rr} v_1^+\big|_0) + \frac{h^2}{2}(\partial_{rrr} v_0^-\big|_0 - \partial_{rrr} v_0^+\big|_0) \\ + \frac{h'}{r_0^2}(\partial_\theta v_1^+\big|_0 - \partial_\theta v_1^-\big|_0).\end{aligned} \tag{3.36}$$

We combine (3.23), (3.24), (3.33a), and (3.35) to obtain the $O(\delta)$ problem

$$\begin{gathered}\Delta v_1^+ - \frac{1}{D} v_1^+ = 0, \quad r_0 < r \le 1; \qquad \Delta v_1^- - \frac{1}{D} v_1^- = 0, \quad 0 < r \le r_0, \\ \partial_r v_1^+ = 0, \quad r = 1; \qquad v_1^- \text{ non-singular as } r \to 0, \\ v_1^+\big|_0 = v_1^-\big|_0; \qquad \partial_r v_1^+\big|_0 - \partial_r v_1^-\big|_0 = h(\partial_{rr} v_0^-\big|_0 - \partial_{rr} v_0^+\big|_0).\end{gathered}$$

The $O(\delta^2)$ problem can be found by combining (3.23), (3.24), (3.33b), and (3.36) to give us

$$\begin{gathered}\Delta v_2^+ - \frac{1}{D} v_2^+ = 0, \quad r_0 < r \le 1; \qquad \Delta v_2^- - \frac{1}{D} v_2^- = 0, \quad 0 < r \le r_0, \\ \partial_r v_2^+ = 0, \quad r = 1; \qquad v_2^- \text{ non-singular as } r \to 0, \\ v_2^+\big|_0 - v_2^-\big|_0 = -\frac{h^2}{2}(\partial_{rr} v_0^-\big|_0 - \partial_{rr} v_0^+\big|_0),\end{gathered}$$

with transmission condition

$$\begin{aligned}\partial_r v_2^+\big|_0 - \partial_r v_2^-\big|_0 = h(\partial_{rr} v_1^-\big|_0 - \partial_{rr} v_1^+\big|_0) + \frac{h^2}{2}(\partial_{rrr} v_0^-\big|_0 - \partial_{rrr} v_0^+\big|_0) \\ + \frac{h'}{r_0^2}(\partial_\theta v_1^+\big|_0 - \partial_\theta v_1^-\big|_0).\end{aligned}$$

The main goal is to find terms of A_0 that include θ and breaks the radial symmetry. We have

$$A_0(\theta) = v^+\big|_{\partial\Gamma} = v_0^+(r_0) + \delta(\partial_r v_0^+(r_0) + v_1^+(r_0,\theta)) + O(\delta^2). \tag{3.37}$$

which upon taking a derivative with respect to θ gives

$$A_0'(\theta) = \delta(\partial_r v_0^+(r_0)h'(\theta) + \partial_\theta v_1^+(r_0,\theta)) + \dots$$

This shows that our goal is to calculate $\partial_\theta v_1^+(r_0,\theta)$ and despite developing the equations for the $O(\delta^2)$ correction term, it may, in principle, not be necessary.

We return our focus to the $O(\delta)$ equation, which can be rewritten as

$$\begin{gathered}
\Delta v_1^+ - \lambda^2 v_1^+ = 0, \quad r_0 < r \le 1; \qquad \Delta v_1^- - \frac{1}{D} v_1^- = 0, \quad 0 < r \le r_0, \\
\partial_r v_1^+ = 0, \quad r = 1; \qquad v_1^- \text{ non-singular, as } r \to 0, \\
v_1^+\big|_0 = v_1^-\big|_0; \qquad \partial_r v_1^+\big|_0 - \partial_r v_1^-\big|_0 = h\gamma_0,
\end{gathered} \tag{3.38}$$

with $\gamma_0 = \partial_{rr} v_0^-(r_0) - \partial_{rr} v_0^+(r_0)$. In order to solve this PDE we first assume that $h(\theta)$ has a complex Fourier series expansion; that is,

$$h(\theta) = \sum_{n=-\infty}^{\infty} h_n e^{in\theta}; \qquad h_n = \frac{1}{2\pi}\int_0^{2\pi} h(\theta) e^{-in\theta}\, d\theta.$$

Since the problem (3.38) is linear and the only inhomogeneous term is from the jump in the right hand side, we can write the solution as

$$v_1 = \gamma_0 \sum_{n=-\infty}^{\infty} h_n F_n e^{in\theta}, \tag{3.39}$$

where F_n solves

$$\begin{gathered}
F_n'' + \frac{1}{r}F_n' - \frac{n^2}{r^2}F_n - \frac{1}{D}F_n = 0, \quad 0 < r \le 1; \qquad F_n'(1) = 0, \\
F_n \text{ non-singular as } r \to 0; \qquad F_n'(r_0^+) - F_n'(r_0^-) = 1, \quad r = r_0.
\end{gathered}$$

F_n is very similar in form to the solution for v_0 given in (3.26) and once again involves modified Bessel functions. The solution is

$$F_n = \begin{cases} \hat{\tau}_n \frac{K_n(\lambda r) - \frac{K_n'(\lambda)}{I_n'(\lambda)} I_n(\lambda r)}{K_n(\lambda r_0) - \frac{K_n'(\lambda)}{I_n'(\lambda)} I_n(\lambda r_0)} & r_0 < r \leq 1 \\ \hat{\tau}_n \frac{I_n(\lambda r)}{I_n(\lambda r_0)} & 0 < r \leq r_0 \end{cases},$$

where $\hat{\tau}_n = \hat{\tau}_n(r_0)$ is determined by imposing $F_n'(r_0^+) - F_n'(r_0^-) = 1$. To impose this condition, let us first define $\tau_1(r,n)$ and $\tau_2(r,n)$ in an analogous fashion to τ_1 and τ_2 from (3.27). We have

$$\tau_1(r,n) = K_n(\lambda r) - \frac{K_n'(\lambda)}{I_n'(\lambda)} I_n(\lambda r); \qquad \tau_2(r,n) = I_n(\lambda r).$$

The derivative jump condition for F_n is then

$$F_n'(r_0^+) - F_n'(r_0^-) = \hat{\tau}_n \left(\frac{\tau_1'(r_0,n)}{\tau_1(r_0,n)} - \frac{\tau_2'(r_0,n)}{\tau_2(r_0,n)} \right) = 1.$$

Multiplying both sides by $\tau_1(r_0,n)$ and $\tau_2(r_0,n)$, we obtain

$$\hat{\tau}_n \mathcal{W}(\tau_2(r_0,n), \tau_1(r_0,n)) = \tau_1(r_0,n)\tau_2(r_0,n).$$

Once again, it is not hard to see that $\mathcal{W}(\tau_2(r_0,n), \tau_1(r_0,n)) = \mathcal{W}(I_n(\lambda r_0), K_0(\lambda r_0))$ and thus again using Abel's identity we have

$$\hat{\tau}_n = -r_0 \tau_1(r_0,n)\tau_2(r_0,n), \tag{3.40}$$

which fully determines the solution for v_1 in (3.39). With this information in hand we can now analyze how a perturbation to a circle evolves in time.

Recall the velocity equation

$$\dot{\eta} = -\left(\frac{\partial_s A_0}{A_1} \right)_s, \tag{3.41}$$

and since A_1 is independent of s, we can write this as

$$\dot{\eta} \sim -\frac{1}{A_1} \partial_{ss} A_0 + O(\delta).$$

To translate the arc length derivatives in polar coordinates we use the fact that

$$\frac{ds}{d\theta} = \sqrt{(r_0 + \delta h)^2 + \delta^2 h'^2} \sim r_0 + \delta h + O(\delta^2).$$

Thus,

$$\partial_\theta A_0 = \partial_s A_0 \frac{ds}{d\theta}; \qquad \partial_{\theta\theta} A_0 = \partial_{ss} A_0 \left(\frac{ds}{d\theta}\right)^2 + \partial_s A_0 \frac{d^2 s}{d\theta^2}.$$

But, since $ds/d\theta \sim r_0 + \delta h$, we have that $d^2 s/d\theta^2 \sim O(\delta)$. This gives us

$$\partial_{\theta\theta} A_0 = \partial_{ss} A_0 r_0^2 + O(\delta)\partial_s A_0.$$

This can be substituted into (3.41) along with the expression for $A_0(\theta)$ given in (3.37) to obtain

$$\dot{\eta} \sim -\frac{\delta}{A_1 r_0^2}\left(\partial_r v_0^+(r_0)h''(\theta) + \partial_{\theta\theta} v_1^+(r_0,\theta)\right).$$

Recalling that on this order $A_1 = -\partial_r v_0^-(r_0)$ and that $v_0^+(r_0) = v_0^-(r_0)$. Using this, we can simply the above expression to be

$$\dot{\eta} \sim \frac{\delta}{r_0^2} h''(\theta) - \frac{\delta}{A_1 r_0^2}\partial_{\theta\theta} v_1^+(r_0,\theta).$$

Substituting in v_1 from (3.39) and the fact that $F_n(r_0) = \hat{\tau}_n$, we now have

$$\dot{\eta} \sim -\frac{\delta}{r_0^2}\sum_{n=-\infty}^{\infty} n^2 h_n e^{in\theta} + \frac{\delta\gamma_0}{A_1 r_0^2}\sum_{n=-\infty}^{\infty} n^2 h_n \hat{\tau}_n e^{in\theta} = \frac{\delta}{r_0^2}\sum_{n=\infty}^{\infty}\left(\frac{\hat{\tau}_n\gamma_0}{A_1} - 1\right) n^2 h_n e^{in\theta},$$

where $\gamma_0 = \partial_{rr} v_0^-(r_0) - \partial_{rr} v_0^+(r_0)$. This can easily be calculated from the ODE that v_0 satisfies. This ODE is

$$\partial_{rr} v_0^- + \frac{1}{r}\partial_r v_0^- - \frac{1}{D} v_0^- = -\frac{\sigma}{D},$$
$$\partial_{rr} v_0^+ + \frac{1}{r}\partial_r v_0^+ - \frac{1}{D} v_0^+ = 0.$$

Taking the limit as $r \to r_0^+$ and $r \to r_0^-$ and then subtracting the v_0^+ equation from the v_0^- one (noting the use of continuity and differentiability), we arrive at

$$\gamma_0 = \partial_{rr} v_0^- - \partial_{rr} v_0^+ = -\frac{\sigma}{D}.$$

After substituting in A_1 from (3.31) and γ_0 from above, the velocity becomes

$$\dot{\eta} \sim -\frac{\delta}{r_0^2}\sum_{n=-\infty}^{\infty}\left(\frac{\lambda\hat{\tau}_n I_0(\lambda r_0)}{(1-\beta)I_0'(\lambda r_0)} + 1\right) n^2 h_n e^{in\theta}.$$

Note that the velocity is independent of σ. We can substitute in for $\hat{\tau}_n$ from (3.40) to isolate terms that depend upon n. The velocity becomes

$$\dot{\eta} \sim -\frac{\delta}{r_0^2} \sum_{n=-\infty}^{\infty} \left(1 - \frac{\lambda r_0 I_0(\lambda r_0) C_n}{(1-\beta) I_0'(\lambda r_0)}\right) n^2 h_n e^{in\theta},$$

with C_n given by

$$C_n = I_n(\lambda r_0) K_n(\lambda r_0) - \frac{K_n'(\lambda)}{I_n'(\lambda)} I_n(\lambda r_0)^2.$$

We remark that β is simply

$$\beta(r_0) = r_0 \lambda I_0'(\lambda r_0) \left[K_0(\lambda r_0) - \frac{K_0'(\lambda)}{I_0'(\lambda)} I_0(\lambda r_0)\right]$$

and that we showed numerical evidence that $0 < \beta < 1 \ \forall\, r_0$ in $0 < r_0 < 1$, $\forall\, \lambda > 0$.

To analyze how a perturbed initial interface evolves in time we look to a specific example with $h(\theta) = \cos(n\theta)$ for some choice of n. Thus, we have that $h_{\pm n} = 1/2$ and all other terms are zero. The only terms that remain are

$$\dot{\eta} \sim -\frac{\delta}{r_0^2} \left(1 - \frac{\lambda r_0 I_0(\lambda r_0)}{(1-\beta) I_0'(\lambda r_0)} C_n\right) n^2 \cos(n\theta). \tag{3.42}$$

Notice that the negative sign in front is trying to make $\dot{\eta} < 0$ when $\cos(k\theta) > 0$, which means a bulge will flattens out. The second term, due to the C_n, has an unknown sign which we will now investigate further. To do this we consider a few limiting cases.

Case 1: Suppose $\lambda \to \infty$, i.e. $D \to 0$ and $r_0 \gg D$. The following identities can be found in [1]. As $z \to \infty$, we have

$$\begin{aligned}
I_n(z) &\sim \frac{e^z}{\sqrt{2\pi z}} \left(1 - \frac{4n^2-1}{8z}\right); \qquad K_n(z) \sim \sqrt{\frac{\pi}{2z}} e^{-z} \left(1 + \frac{4n^2-1}{8z}\right), \\
I_n'(z) &\sim \frac{e^z}{\sqrt{2\pi z}} \left(1 - \frac{4n^2+3}{8z}\right); \qquad K_n'(z) \sim \sqrt{\frac{\pi}{2z}} e^{-z} \left(1 + \frac{4n^2+3}{8z}\right), \\
I_n(z) K_n(z) &\sim \frac{1}{2z} \left(1 - \frac{4n^2-1}{8z^2}\right),
\end{aligned} \tag{3.43}$$

which tells us that

$$\frac{K_n'(z)}{I_n'(z)} \sim -\pi e^{-2z}\left(\frac{8z+4n^2+3}{8z-4n^2-3}\right) \sim -\pi e^{-2z}\left(1+\frac{4n^2+3}{4z}\right),$$

and thus

$$\begin{aligned}\frac{K_n'(\lambda)}{I_n'(\lambda)} I_n(\lambda r_0)^2 &\sim -\pi e^{-2\lambda}\left(1+\frac{4n^2+3}{4\lambda}\right)\frac{e^{2\lambda}}{2\pi\lambda}\left(1-\frac{4n^2-1}{8\lambda}\right)^2 \\ &\sim -\frac{1}{2\lambda r_0} e^{-2\lambda(1-r_0)}\left(1+O(\tfrac{1}{\lambda})\right).\end{aligned} \tag{3.44}$$

We can combine (3.43) and (3.44) together to determine C_n as

$$C_n \sim \frac{1}{2\lambda r_0}\left(1-\frac{4n^2-1}{8\lambda^2 r_0^2}\right) + O\left(\frac{e^{-2\lambda(1-r_0)}}{\lambda}\right).$$

The second term is exponential small which means it can safely be ignored. The conclusion is that

$$C_n \sim \frac{1}{2\lambda r_0}\left(1+O\left(\tfrac{1}{\lambda^2}\right)\right), \quad \text{as } \lambda \to \infty.$$

What remains is to estimate β and $I_0'(\lambda r_0)/I_0(\lambda r_0)$.

$$\begin{aligned}\beta(r_0) &= r_0\lambda\left[I_0'(\lambda r_0)K_0(\lambda r_0) - \frac{K_0'(\lambda)}{I_0'(\lambda)} I_0(\lambda r_0) I_0'(\lambda r_0)\right] \\ &\sim r_0\lambda\left[\frac{e^{\lambda r_0}}{\sqrt{2\pi\lambda r_0}}\sqrt{\frac{\pi}{2\lambda r_0}} e^{-\lambda r_0}\left(1-\frac{3}{8\lambda r_0}\right)\left(1-\frac{1}{8\lambda r_0}\right) + O\left(\frac{e^{-2\lambda(1-r_0)}}{\lambda}\right)\right] \\ &\sim r_0\lambda\left[\frac{1}{2\lambda r_0}\left(1-\frac{1}{2\lambda r_0}\right) + O\left(\frac{e^{-2\lambda(1-r_0)}}{\lambda}\right)\right] \sim \frac{1}{2}\left[1-\frac{1}{2\lambda r_0}\right], \quad \text{as } \lambda \to \infty.\end{aligned}$$

For $I_0(\lambda r_0)/I_0'(\lambda r_0)$ we have

$$\frac{I_0(\lambda r_0)}{I_0'(\lambda r_0)} \sim \frac{\frac{e^{\lambda r_0}}{\sqrt{2\pi\lambda r_0}}\left(1+\frac{1}{8\lambda r_0}\right)}{\frac{e^{\lambda r_0}}{\sqrt{2\pi\lambda r_0}}\left(1-\frac{3}{8\lambda r_0}\right)} \sim \frac{\left(1+\frac{1}{8\lambda r_0}\right)}{\left(1-\frac{3}{8\lambda r_0}\right)} \sim 1+\frac{1}{2\lambda r_0},$$

which leads us to our end result for this case

$$\frac{\lambda r_0 I_0(\lambda r_0)}{(1-\beta)I_0'(\lambda r_0)}C_n \sim \frac{\lambda r_0}{\left[1-\frac{1}{2}\left(1-\frac{1}{2\lambda r_0}\right)\right]}\left(1+\frac{1}{2\lambda r_0}\right)\left(\frac{1}{2\lambda r_0}\right)\left(1+O\left(\tfrac{1}{\lambda^2}\right)\right)$$
$$\sim \frac{\left(1+\frac{1}{2\lambda r_0}\right)}{2\left(\frac{1}{2}+\frac{1}{4\lambda r_0}\right)}\left(1+O\left(\tfrac{1}{\lambda^2}\right)\right) \sim 1+O\left(\tfrac{1}{\lambda^2}\right),$$

and therefore

$$1-\frac{\lambda r_0 I_0(\lambda r_0)}{(1-\beta)I_0'(\lambda r_0)}C_n \sim O\left(\tfrac{1}{\lambda^2}\right),$$

as $\lambda \to \infty$.

As $\lambda \to \infty$ we see that the velocity $\dot{\eta} \ll 1$ but the sign of the $O(1/\lambda^2)$ term has yet to be determined. What is clear is that if there is any instability it will be very weak.

Case 2: Suppose n is fixed and $\lambda \to 0$ which corresponds to large diffusive forces. For $n \geq 1$ and $z \to 0$ we have the following identities

$$I_n(z) \sim \frac{1}{n!}\left(\frac{z}{2}\right)^n; \qquad K_n(z) \sim \frac{(n-1)!}{2}\left(\frac{z}{2}\right)^{-n},$$
$$I_n'(z) \sim \frac{1}{2(n-1)!}\left(\frac{z}{2}\right)^{n-1}; \qquad K_n'(z) \sim -\frac{n!}{4}\left(\frac{z}{2}\right)^{-(n+1)},$$

which tells us

$$I_n(\lambda)K_n(\lambda) \sim \frac{1}{2n}.$$

Now,

$$\frac{K_n'(\lambda)}{I_n'(\lambda)}I_n(\lambda r_0)^2 \sim -\frac{\frac{n!}{4}\left(\frac{\lambda}{2}\right)^{-(n+1)}}{\frac{1}{2(n-1)!}\left(\frac{\lambda}{2}\right)^{n-1}}\frac{1}{(n!)^2}\left(\frac{\lambda r_0}{2}\right)^{2n} \sim -\frac{r_0^{2n}}{2n}$$

and thus for $\lambda \to 0$ we have $C_n > 0$ and

$$C_n \sim \frac{1}{2n}(1-r_0^{2n}).$$

To finish off this case we again need to estimate β and $I_0(\lambda r_0)/I_0'(\lambda r_0)$ as $\lambda \to 0$. For the Bessel functions we have

$$\frac{I_0(\lambda)}{I_0'(\lambda)} \sim \frac{2}{\lambda},$$

and for β

$$\begin{aligned}\beta(r_0) &= r_0\lambda\left[I_0'(\lambda r_0)K_0(\lambda r_0) - \frac{K_0'(\lambda)}{I_0'(\lambda)}I_0(\lambda r_0)I_0'(\lambda r_0)\right] \\ &\sim r_0\lambda\left[\frac{\lambda r_0}{2}O(\log(\lambda)) - \frac{\frac{1}{\lambda}}{\frac{\lambda}{2}}\frac{\lambda r_0}{2}\right] \\ &\sim r_0\lambda\left[O(\lambda\log(\lambda)) + \frac{r_0}{\lambda}\right] \sim r_0^2.\end{aligned}$$

From this we can conclude that

$$\frac{\lambda r_0 I_0(\lambda r_0)}{(1-\beta)I_0'(\lambda r_0)}C_n \sim \frac{\lambda r_0}{1-r_0}\left(\frac{2}{\lambda r_0}\right)\left(\frac{1-r_0^{2n}}{2n}\right) \sim \frac{1-r_0^{2n}}{n(1-r_0^2)}.$$

Therefore for (3.42) in this limit, we obtain

$$\dot{\eta} \sim -\frac{\delta}{r_0}\left(1 - \frac{1-r_0^{2n}}{n(1-r_0^2)}\right)n^2\cos(n\theta). \tag{3.45}$$

We conclude that as $D \to \infty$, perturbations will stabilize. To see this, we define

$$f(k) = n - \frac{1-k^n}{(1-k)},$$

where $k = r_0^2$. Since $0 < r_0 < 1$, the second term in $f(k)$ can be represented as

$$\frac{1-k^n}{(1-k)} = (1 + k + \ldots + k^{n-1}).$$

Now, consider $f(0) = n - (1 + 0 + \ldots + 0) > 0$ if $n > 1$. We also have that $f(1) = n-(1+\ldots+1) = n-n = 0$. Now, since $f'(k)$ is monotone decreasing on $0 < k < 1$, we have that $f(k)$ cannot have a zero in $0 < k < 1$. This means the velocity in (3.45) is negative when $cos(n\theta) > 0$, i.e. a perturbation returns to a circle.

Case 3: Now, we consider the case where $r_0 \ll 1$ but $\lambda = O(1)$. We have

$$\beta(r_0) = r_0\lambda\left[I_0'(\lambda r_0)K_0(\lambda r_0) - \frac{K_0'(\lambda)}{I_0'(\lambda)}I_0(\lambda r_0)I_0'(\lambda r_0)\right].$$

Now, as $r_0 \to 0$, we have

$$B(r_0) \sim r_0\lambda[O(r_0\log(r_0)) + O(r_0)] \to 0, \quad \text{as } r_0 \to 0.$$

Thus,

$$\frac{\lambda r_0 I_0(\lambda r_0)}{(1-\beta)I_0'(\lambda r_0)}C_n \sim \frac{2\lambda r_0}{\lambda r_0}C_n \sim 2C_n, \quad \text{as } r_0 \to 0,$$

since $I_0(\lambda r_0) \sim 1$ and $I_0'(\lambda r_0) \sim \lambda r_0$ in this limit. What is left is to compute C_n. For $n \geq 1$, as $r_0 \to 0$, we have

$$I_n(\lambda r_0)K_n(\lambda r_0) \sim \frac{1}{2n}.$$

Also,

$$\frac{K_n'(\lambda)}{I_n'(\lambda)}I_n(\lambda r_0)^2 = O(r_0^n), \quad \text{as } r_0 \to 0.$$

Thus,

$$\frac{\lambda r_0 I_0(\lambda r_0)}{(1-\beta)I_0'(\lambda r_0)}C_n \sim \frac{1}{n}.$$

We conclude that for $r_0 \ll 1$, that

$$\dot{\eta} \sim -\frac{\delta}{r_0^2}\left(1 - \frac{1}{n}\right)n^2\cos(n\theta). \tag{3.46}$$

Assuming that $r_0 \gg O(\delta)$, with $r = r_0 + \delta\cos(n\theta)$, this law suggests that a bulge flattens out with velocity proportional to $O(\delta/r_0^2)$,

Case 4: Finally, we consider the case where λ and r_0 are fixed and let $n \to \infty$. We want to establish is the interface is stable to a 'high frequency' perturbation $\cos(n\theta)$ for $n \gg 1$.

The only term that requires estimation is C_n. Recall that C_n is given as

$$C_n = I_n(\lambda r_0)K_n(\lambda r_0) - \frac{K_n'(\lambda)}{I_n'(\lambda)}I_n(\lambda r_0)^2$$

For $n \to \infty$ we use

$$I_n(z) \sim \frac{1}{\sqrt{2\pi n}}\left(\frac{ez}{2n}\right)^n; \qquad K_n(z) \sim \sqrt{\frac{\pi}{2\pi n}}\left(\frac{ez}{2n}\right)^{-n},$$

and therefore,

$$I_n(z)K_n(z) \sim \frac{1}{2n}, \quad \text{as } n \to \infty.$$

For the derivative terms we have

$$I_n'(z) \sim \frac{n}{\sqrt{2\pi n}} \left(\frac{ez}{2n}\right)^{n-1} \frac{e}{2n} = \frac{N}{z\sqrt{2\pi n}} \left(\frac{ez}{2n}\right)^{n},$$
$$K_n'(z) \sim -n\sqrt{\frac{\pi}{2\pi n}} \left(\frac{ez}{2n}\right)^{-(n+1)} \frac{e}{2n} = -\frac{n}{z}\sqrt{\frac{\pi}{2\pi n}} \left(\frac{ez}{2n}\right)^{-n}.$$

This gives us

$$\frac{K_n'(\lambda)}{I_n'(\lambda)} \sim -\pi \left(\frac{e\lambda}{2n}\right)^{-2n},$$

so

$$\frac{K_n'(\lambda)}{I_n'(\lambda)} I_n(\lambda r_0)^2 \sim -\frac{1}{2n} \left(\frac{e\lambda}{2n}\right)^{-2n} \left(\frac{e\lambda r_0}{2n}\right)^{2n} \sim -\frac{r_0^{2n}}{2n}.$$

Combining these results we can see that for $n \gg 1$, we have

$$C_n \sim \frac{1 - r_0^{2n}}{2n},$$

but since $0 < r_0 < 1$, we have $C_n \sim O(1/n)$. In the asymptotic limit of $n \gg 1$, we conclude that

$$\dot{\eta} \sim -\frac{\delta}{r_0^2} \left(1 - \frac{\lambda r_0 I_0(\lambda r_0)}{(1-\beta) I_0'(\lambda r_0)} \frac{1}{2n}\right) n^2 \cos(n\theta). \tag{3.47}$$

Since

$$\dot{\eta} \sim -\frac{\delta}{r_0^2} \left(1 - O\left(\frac{1}{n}\right)\right) n^2 \cos(n\theta),$$

it follows that a bulge flattened out rather quickly.

Remark 3.3.2.1: Consider $\mathcal{G}_n(r_0, \lambda)$ given by

$$\mathcal{G}_n(r_0, \lambda) = 1 - \frac{\lambda r_0}{1 - \beta(r_0)} \frac{I_0(\lambda r_0)}{I_0'(\lambda r_0)} C_n.$$

Note that $\mathcal{G}_n(r_0, \lambda)$ is the term with an undetermined sign that appears in (3.42). In figure 3.5, we plot $\mathcal{G}_n(r_0, \lambda)$ versus r_0 for a few values of λ and n. For each pair of λ and n, $\mathcal{G}_n$ crosses the r_0-axis for a certain critical value of r_0. We believe that this sign change is not an instability but comes

from boundary effects. The Neumann boundary conditions on the outer wall create a mirroring effect, attracting the perturbed drop to its image outside the domain.

3.3.3 Many Circular Interfaces

We now consider the case where Γ is initially a collection of N disjoint disks of radii δr_i, $i = 1, \ldots, N$ so that

$$\Omega_\delta = \bigcup_{i=1}^{N} \Omega_{\delta_i}; \qquad \Omega_{\delta_i} = \{\mathbf{x} : \ |\mathbf{x} - \mathbf{x}_i| \leq \delta r_i\}.$$

We then must solve

$$\begin{aligned} D\Delta v - v &= -\sigma \begin{cases} 1 : \mathbf{x} \in \Omega_\delta \\ 0 : \mathbf{x} \in \Omega \setminus \Omega_\delta \end{cases}, \\ \frac{\partial v}{\partial n} &= 0, \quad \mathbf{x} \in \partial\Omega. \end{aligned} \tag{3.48}$$

We will assume that $\delta \ll 1$. In our original analysis we used $\epsilon \ll 1$, so here we need to assume $\epsilon \ll \delta \ll 1$ so that the profile for u across a cross-section of one drop is as in figure 3.6.

Now from our previous analysis we know that the normal velocity of $\partial\Omega_{\delta_j}$ (the boundary of the j^{th} droplet) is

$$\dot{\eta}_j = -\left(\frac{\partial_{s_j} V_0}{A_j(s_j)}\right)_{s_j}, \quad \mathbf{x} \in \partial\Omega_{\delta_j}, \tag{3.49}$$

where s_j is the arc length of the boundary of the j^{th} drop and $A_j(s_j)$ is given as

$$A_j(s_j) = \nabla v \cdot \mathbf{n}\big|_{\partial\Omega_{\delta_j}},$$

and

$$V_0 = v\big|_{\partial\Omega_{\delta_j}}.$$

For a circular drop of radius δr_j, we have $s_j = \delta r_j \theta$, where θ is a local polar coordinate.

We will use strong localized perturbation theory to calculate a high-order approximation for v. We begin by looking at the inner region near the j^{th} drop, where we let

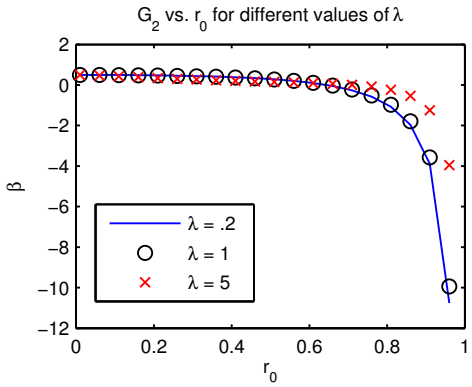

(a) $\mathcal{G}_2$ for $\lambda = .2, 1, 5$

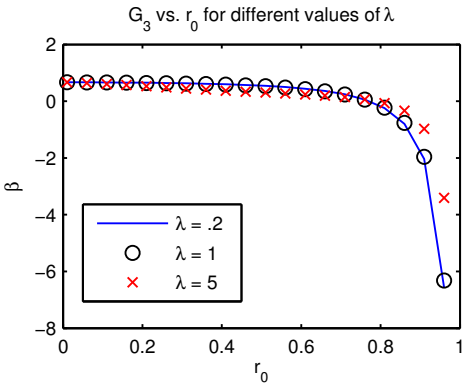

(b) $\mathcal{G}_3$ for $\lambda = .2, 1, 5$

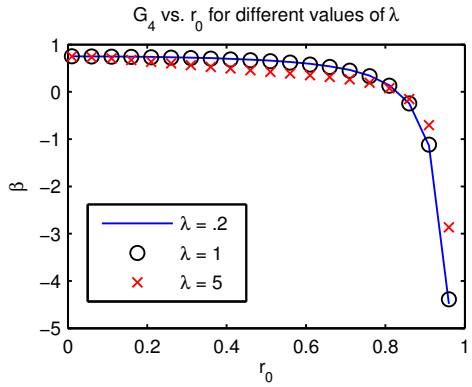

(c) $\mathcal{G}_4$ for $\lambda = .2, 1, 5$

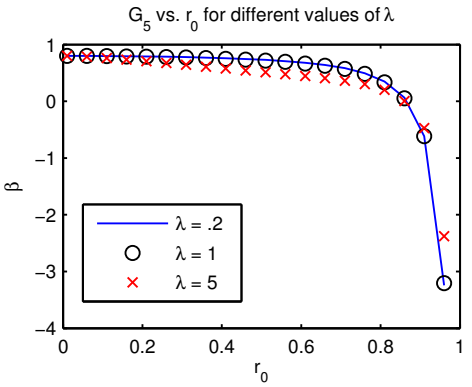

(d) $\mathcal{G}_5$ for $\lambda = .2, 1, 5$

Figure 3.5: $\mathcal{G}_n(r_0, \lambda)$ for $n = 2, 3, 4, 5$, $\lambda = .2, 1, 5$ on $0 < r_0 < .95$. In each plot it is clear that there is a critical r_0 value such that $\mathcal{G}_n < 0$ and thus $\dot{\eta} > 0$ when $\cos(n\theta) > 0$, signifying growth of the perturbation and an instability.

Figure 3.6: Profile for u across a cross-section of one drop centered at x_i, where the drop is of size $O(\delta)$.

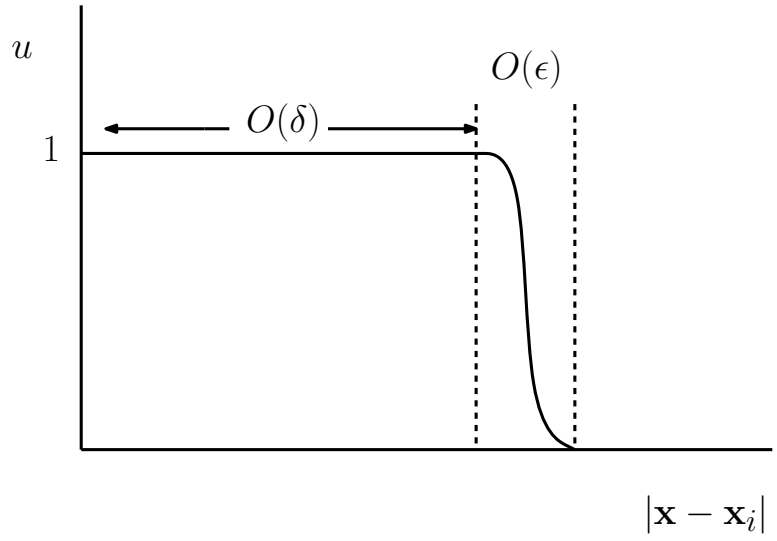

$$V(\mathbf{y}) = v(\mathbf{x}_j + \delta\mathbf{y}), \quad \mathbf{y} = \frac{\mathbf{x} - \mathbf{x}_j}{\delta},$$

Then,

$$\frac{D}{\delta^2}\Delta_{\mathbf{y}} V_j - V_j = -\sigma \begin{cases} 1 : |\mathbf{y}| \le r_j \\ 0 : |\mathbf{y}| > r_j \end{cases}.$$

This suggests that we expand V_j as

$$V_j = \delta^2 \log(\delta) W_{0,j} + \delta^2 W_{1,j} + \dots$$

We substitute to obtain that $W_{0,j}$ is a constant and that

$$\Delta_{\mathbf{y}} W_{1,j} = -\frac{\sigma}{D} \begin{cases} 1 : |\mathbf{y}| \le r_j \\ 0 : |\mathbf{y}| > r_j \end{cases}. \tag{3.50}$$

To solve this equation we look for a radially symmetric solution and obtain, upon imposing $W_{1,j}$ is C^1 across $\rho = |\mathbf{y}| = r_j$, that

$$W_{1,j} = \begin{cases} -\frac{\sigma}{4D}\rho^2 + C_j + \frac{\sigma}{4D} r_j^2 & : \rho \le r_j \\ k_j \log\left(\frac{\rho}{r_j}\right) + C_j & : \rho > r_j \end{cases}, \tag{3.51}$$

where $k_j = -\sigma r_j^2/2D$ and C_j is an arbitrary constant to be found from matching to the outer solution. Note that k_j is found by imposing differentiability across $\rho = r_j$.

Remark 3.3.3.1: Suppose that (3.50) was such that Ω_{δ_j} was an arbitrary closed region. Then we could not solve as in (3.51) but we could still calculate k_j and show it is constant. Let $\Omega_j = \Omega_{\delta_j}/\delta$ so that Ω_j has area that is $O(1)$. The analogous $W_{1,j}$ equation is

$$\Delta_{\mathbf{y}} W_{1,j} = -\frac{\sigma}{D} \begin{cases} 1 : |\mathbf{y}| \in \Omega_j \\ 0 : |\mathbf{y}| \notin \Omega_j \end{cases}.$$

Now, as $|\mathbf{y}| \to \infty$ it still follows that $W_{1,j} \sim k_j \log(|\mathbf{y}|)$ for some constant k_j to be determined. Using the fact that $W_{1,j}$ is C^1 we have from the divergence theorem that

$$\lim_{R\to\infty} \int_{B_R} \Delta W_{1,j}\, d\mathbf{y} = 2\pi \lim_{R\to\infty} R \frac{\partial W_{1,j}}{\partial |\mathbf{y}|}\bigg|_{|\mathbf{y}|=R} = 2\pi k_j,$$

where $B_R = \{\mathbf{y} : |\mathbf{y}| \le R\}$ with R large enough to contain Ω_j. However, since $\Delta W_{1,j} = -\sigma/D$ inside Ω_j, we also have

$$\lim_{R\to\infty} \int_{B_R} \Delta W_{1,j}\, d\mathbf{y} = -\frac{\sigma}{D}|\Omega_j| = 2\pi k_j,$$

and thus,

$$k_j = -\frac{\sigma |\Omega_j|}{2\pi D},$$

where $|\Omega_j|$ is the area of Ω_j. Notice that if $|\Omega_j| = \pi r^2$ as for a circle, then $k_j = -\sigma r_j^2/2D$ as derived for equation (3.51). We conclude that the solution to

$$\Delta_{\mathbf{y}} W_{1,j} = -\frac{\sigma}{D} \begin{cases} 1 : |\mathbf{y}| \in \Omega_j \\ 0 : |\mathbf{y}| \notin \Omega_j \end{cases}, \tag{3.52}$$

has the far field behavior as $|\mathbf{y}| \to \infty$ given by

$$W_{1,j} \sim k_j \log(|\mathbf{y}|) + C_j + o(1), \quad \text{as } \mathbf{y} \to \infty.$$

Here, C_j is an arbitrary constant. We observe that since a constant solves (3.52) then C_j is a constant that is undetermined from the inner problem and will be found by matching to the outer solution.

Returning to the circular drop case, recall that the inner expansion is given as

$$V_j = \delta^2 \log(\delta) W_{0,j} + \delta^2 W_{1,j} + \dots$$

In terms of the outer variable $\rho = |\mathbf{x} - \mathbf{x}_j|/\delta$, the far field behavior for the inner expansion is

$$V_j \sim \delta^2 \log(\delta) W_{0,j} + \delta^2 [k_j \log(|\mathbf{x} - \mathbf{x}_j|) - k_j \log(\delta) - k_j \log(r_j) + C_j] + \dots$$

Rearranging the above equation,

$$V_j \sim \delta^2 \log(\delta)[W_{0,j} - k_j] + \delta^2 [k_j \log(|\mathbf{x} - \mathbf{x}_j|) - k_j \log(r_j) + C_j] + \dots, \quad (3.53)$$

with $k_j = -\sigma r_j^2/2D$.

Here, we see that $W_{0,j}$ must be

$$W_{0,j} = k_j, \quad j = 1, \dots, N.$$

If $W_{0,j}$ was not chosen in this way, the outer solution, a second-order elliptic PDE, would be forced to satisfy a point constraint ($v = \delta^2 \log(\delta) v^*$, $v^*(\mathbf{x}_j) = W_{0,j} - k_j$), which is ill-posed.

It follows that in the outer region we must expand the outer solution as

$$v = \delta^2 v_1 + \dots$$

Upon substituting this expansion into (3.48), we obtain that v_1 solves

$$\begin{gathered} \Delta v_1 - \lambda^2 v_1 = 0, \quad \mathbf{x} \in \Omega \setminus \{\mathbf{x}_1, \dots, \mathbf{x}_N\}, \\ \frac{\partial v_1}{\partial n} = 0, \quad \mathbf{x} \in \partial\Omega, \\ v_1 \sim k_j \log(|\mathbf{x} - \mathbf{x}_j)| - k_j \log(r_j) + C_j, \quad \text{as } \mathbf{x} \to \mathbf{x}_j, \quad \text{for } j = 1, \dots, N. \end{gathered} \quad (3.54)$$

As before, $\lambda = 1/\sqrt{D}$.

To solve (3.54), we introduce the reduced-wave Green's function $G_\lambda(\mathbf{x}; \mathbf{x}_j)$, which satisfies,

$$\Delta G_\lambda - \lambda^2 G_\lambda = -\delta(\mathbf{x} - \mathbf{x}_j), \quad \mathbf{x} \in \Omega; \qquad \frac{\partial G_\lambda}{\partial n} = 0, \quad \mathbf{x} \in \partial\Omega.$$

We can decompose $G_\lambda(\mathbf{x};\mathbf{x}_j)$ globally in Ω as

$$G_\lambda(\mathbf{x};\mathbf{x}_j) = -\frac{1}{2\pi}\log(|\mathbf{x}-\mathbf{x}_j|) + R_\lambda(\mathbf{x};\mathbf{x}_j), \tag{3.55}$$

for some globally defined C^1 function $R_\lambda(\mathbf{x};\mathbf{x}_j)$. As $\mathbf{x}\to\mathbf{x}_j$, we have,

$$R_\lambda(\mathbf{x};\mathbf{x}_j) \sim R_{\lambda j} + \nabla R_\lambda\big|_{\mathbf{x}_j}\cdot(\mathbf{x}-\mathbf{x}_j) + O(|\mathbf{x}-\mathbf{x}_j|^2\log(|\mathbf{x}-\mathbf{x}_j|)),$$

where $R_{\lambda j} = R_\lambda(\mathbf{x}_j;\mathbf{x}_j)$ is the regular part of the reduced-wave Green's function in (3.55). Additionally,

$$\nabla R_\lambda\big|_{\mathbf{x}_j} = \nabla R_\lambda(\mathbf{x};\mathbf{x}_j)\big|_{\mathbf{x}=\mathbf{x}_j}.$$

We can now write v_1 globally in Ω by introducing singular Dirac forces as

$$\Delta v_1 - \lambda^2 v_1 = 2\pi\sum_{i=1}^{N} k_i\delta(\mathbf{x}-\mathbf{x}_j), \quad \mathbf{x}\in\Omega; \qquad \frac{\partial v_1}{\partial n} = 0, \quad \mathbf{x}\in\partial\Omega.$$

The solution to this PDE can be represented as the superposition

$$v_1 = -2\pi\sum_{i=1}^{N} k_i G_\lambda(\mathbf{x};\mathbf{x}_j).$$

Now we expand as $\mathbf{x}\to\mathbf{x}_j$ to obtain

$$v_1 \sim -2\pi k_j\bigg[-\frac{1}{2\pi}\log(|\mathbf{x}-\mathbf{x}_j|) + R_{\lambda j} + \nabla R_\lambda\big|_{\mathbf{x}_j}\cdot(\mathbf{x}-\mathbf{x}_j)\bigg] - 2\pi\sum_{i\neq j}^{N} k_i\left[G_{\lambda ji} + \nabla G_\lambda\big|_{\mathbf{x}_j}\cdot(\mathbf{x}-\mathbf{x}_j)\right],$$

which can be rearranged into

$$v_1 \sim k_j\log(|\mathbf{x}-\mathbf{x}_j|) - 2\pi\bigg[k_j R_{\lambda j} + \sum_{i\neq j}^{N} k_i G_{\lambda ji} + k_j\nabla R_\lambda\big|_{\mathbf{x}_j}\cdot(\mathbf{x}-\mathbf{x}_j) + \sum_{i\neq j}^{N} k_i\nabla G_\lambda\big|_{\mathbf{x}_j}\cdot(\mathbf{x}-\mathbf{x}_j)\bigg].$$

This long expression can be written more compactly as

$$v_1 \sim k_j \log(|\mathbf{x} - \mathbf{x}_j|) - 2\pi \left[k_j R_{\lambda j} + \sum_{i \neq j}^{N} G_{\lambda ji} \right] + \mathbf{a}_j \cdot (\mathbf{x} - \mathbf{x}_j), \tag{3.56}$$

as $\mathbf{x} \to \mathbf{x}_j$ and with $v \sim \delta^2 v_1$. In this equation, $\mathbf{a}_j$ is a vector-quantity defined by

$$\mathbf{a}_j = -2\pi \left(k_j \nabla R_\lambda \big|_{\mathbf{x}_j} + \sum_{i \neq j}^{N} k_i \nabla G_\lambda \big|_{\mathbf{x}_j} \right). \tag{3.57}$$

Ignoring $\mathbf{a}_j \cdot (\mathbf{x} - \mathbf{x}_j)$ in (3.56) for the moment and matching (3.56) with the required behavior in (3.53), we obtain that

$$C_j - k_j \log(r_j) = -2\pi \left[k_j R_{\lambda j} + \sum_{i \neq j}^{N} k_i G_{\lambda ji} \right], \quad \text{for } j = 1, \ldots, N,$$

which yields

$$C_j = k_j \log(r_j) - 2\pi \left[k_j R_{\lambda j} + \sum_{i \neq j}^{N} k_i G_{\lambda ji} \right].$$

This can be written in matrix form as

$$(\mathcal{P} - 2\pi \mathcal{G}_\lambda)\mathbf{k} = \mathbf{C}, \tag{3.58}$$

where

$$\mathcal{P} = \begin{pmatrix} \log(\rho_1) & & 0 \\ & \ddots & \\ 0 & & \log(\rho_N) \end{pmatrix}; \qquad \mathcal{G}_\lambda = \begin{pmatrix} R_{\lambda 1} & & G_{\lambda ij} \\ & \ddots & \\ G_{\lambda ji} & & R_{\lambda N} \end{pmatrix},$$

$$\mathbf{k} = \begin{pmatrix} k_1(\nu) \\ \vdots \\ k_N(\nu) \end{pmatrix}; \qquad \mathbf{C} = \begin{pmatrix} C_1(\nu) \\ \vdots \\ C_N(\nu) \end{pmatrix}.$$

Remark 3.3.3.2:

(i) With C_j determined by (3.58), the inner solution for $O(\delta^2)$ is determined from (3.51).

(ii) By Remark 3.3.3.1, with C_j determined by (3.58), the $O(\delta^2)$ term for the inner problem for $W_{1,j}$ is a well-posed problem for an arbitrary shape Ω_j. In particular, if $\mathbf{x}_j$ is any point in Ω_{δ_j}, then we must solve uniquely the following problem.

$$\Delta_{\mathbf{y}} W_{1,j} = -\frac{\sigma}{D} \begin{cases} 1 : \mathbf{y} \in \Omega_j \\ 0 : \mathbf{y} \notin \Omega_j \end{cases},$$
$$W_{1,j} \sim k_j \log(|\mathbf{y}|) + C_j + o(1), \quad \text{as } |\mathbf{y}| \to \infty,$$

where C_j is found from (3.58) and $k_j = -\sigma|\Omega_j|/(2\pi D)$. For this general problem, we can set $r_j = 1$ in $\mathcal{P}$ so that $\mathcal{P} = 0$ since in (3.51), we would write $W_{1,j} \sim k_j \log(|\mathbf{y}|) + C_j$ as $|\mathbf{y} \to \infty$ and put $|\mathbf{y}| = |\mathbf{x} - \mathbf{x}_j|/\delta$. Thus, for the general problem, $-2\pi\mathcal{G}_\lambda \mathbf{k} = \mathbf{C}$.

Remark 3.3.3.3: We now compare our theory with results obtained for the annulus $\delta < |\mathbf{x}| < 1$ with $r = |\mathbf{x}|$. For the annulus, we can find an exact solution. Note that this has already been found in (3.21). Expressed differently, the exact solution is

$$v = \begin{cases} (v_E - \sigma)\frac{I_0(\lambda r)}{I_0(\lambda\delta)} + \sigma & : 0 < r < \delta \\ v_E \frac{K_0(\lambda r) - \frac{K_0(\lambda)}{I_0'(\lambda)} I_0(\lambda r)}{K_0(\lambda\delta) - \frac{K_0'(\lambda)}{I_0'(\lambda)} I_0(\lambda\delta)} & : \delta < r < 1 \end{cases},$$

with v_E given as

$$v_E = \lambda\sigma\delta \left[I_0'(\lambda\delta) K_0(\lambda\delta) - \frac{K_0'(\lambda)}{I_0'(\lambda)} I_0(\lambda\delta) I_0'(\lambda\delta) \right].$$

Now, in the outer region with $r_j = 1$, $j = 1$, we have

$$v \sim -2\pi\delta^2 \left(-\frac{\sigma}{2D} \right) G_\lambda(\mathbf{x}; 0) = \frac{\pi\sigma\delta^2}{D} G_\lambda(\mathbf{x}; 0),$$

where for the unit disk the Green's function is given as

$$G_\lambda(\mathbf{x}; 0) = \frac{1}{2\pi} \left[K_0(\lambda r) - \frac{K_0'(\lambda)}{I_0'(\lambda)} I_0(\lambda r) \right].$$

Since $K_0(z) \sim -\log(z/2) - \gamma$ as $z \to 0$ with γ as Euler's constant, we have

$$G_\lambda(\mathbf{x};0) \sim -\frac{1}{2\pi}\log(r) - \frac{1}{2\pi}\left[\log\left(\frac{\lambda}{2}\right) + \gamma + \frac{K_0'(\lambda)}{I_0'(\lambda)}\right] + o(1), \quad \text{as } r \to 0.$$

Thus,

$$R_{\lambda 1} = -\frac{1}{2\pi}\left[\log(\lambda) - \log(2) + \gamma + \frac{K_0'(\lambda)}{I_0'(\lambda)}\right],$$

is the regular part of G_λ at $\mathbf{x} = 0$. In the inner region with $R_{\lambda 1}$ given above, we have from (3.58) that

$$C_1 = \left(\log(\lambda) - \log(2) + \gamma + \frac{K_0'(\lambda)}{I_0'(\lambda)}]\right) k_1, \quad k_1 = -\frac{\sigma}{2D}.$$

Note that with $D = 1$, we can see that this is exactly the constant found in (3.19). Thus, in the inner region, we have for $r = O(\delta)$ that

$$V_1 \sim k_1\delta^2\log(\delta) + \delta^2 \begin{cases} -\frac{\sigma r^2}{4D\delta^2} + C_1 + \frac{\sigma}{4D} & : r \le \delta \\ k_1\log(r) - k_1\log(\delta) + C_1 & : r \ge \delta \end{cases}.$$

We can see that this is the exact inner expansion derived in section 3.3.1 (equations (3.17) and (3.18)) and our analysis for many droplets reduces to a single drop when $N = 1$.

Now we return to the case of N circular drops and we go to higher order to determine non-radially symmetric contributions that result in a non-zero normal velocity.

We return to (3.56), and notice that there is an unmatched term due to the gradient effects. We write the outer solution as (with $\mathbf{x} \to \mathbf{x}_j$),

$$v \sim \delta^2\left[k_j\log(|\mathbf{x} - \mathbf{x}_j|) - 2\pi\left(k_j R_{\lambda j} + \sum_{i\neq j}^{N} k_i G_{\lambda ji}\right) + \mathbf{a}_j\cdot(\mathbf{x} - \mathbf{x}_j)\right],$$

where a_j is given in (3.57).

Note that all the terms except for $\mathbf{a}_j\cdot(\mathbf{x}-\mathbf{x}_j)$ have already been matched. In the inner variable this unmatched term can be expressed as $\delta^3[\mathbf{a}_j\cdot\mathbf{y}+o(1)]$. This suggests that in the inner region near the j^{th} drop we must expand

$$V = \delta^2\log(\delta)k_j + \delta^2 W_{1,j} + \delta^3 W_{2,j} + \ldots$$

Upon substituting into (3.48) we obtain that in all of $\mathbf{y} \in \mathbb{R}^2$ that

$$\Delta_{\mathbf{y}} W_{2,j} = 0, \quad \mathbf{y} \in \mathbb{R}^2; \qquad W_{2,j} \sim \mathbf{a}_j \cdot \mathbf{y} + o(1), \quad \text{as } |\mathbf{y}| \to \infty. \tag{3.59}$$

The $o(1)$ condition at infinity eliminates constant terms and thus, to have a smooth solution in $\mathbb{R}^2$ we must have that $W_{2,j}$ is linear in $\mathbf{y}$. Thus, we have exactly in $\mathbb{R}^2$ that

$$W_{2,j} = \mathbf{a}_j \cdot \mathbf{y}.$$

With this solution we have the three term inner expansion near the j^{th} drop as

$$V = \delta^2 \log(\delta) k_j + \delta^2 \begin{cases} -\frac{\sigma}{4D}\rho^2 + C_j + \frac{\sigma}{4D} r_j^2 & : \rho \le r_j \\ k_j \log(\rho) - k_j \log(r_j) + C_j & : \rho \ge r_j \end{cases} + \delta^3 \mathbf{a}_j \cdot \mathbf{y} + \dots \tag{3.60}$$

This is the key result that will allow us to predict the interface motion starting from an initial configuration of N circular small disjoint droplets of radii $\delta r_1, \dots, \delta r_N$.

The question we are trying to answer is how do the droplets move initially. We know theoretically that for all time $t > 0$ we have that the area of each droplet is preserved in time since

$$\frac{d}{dt} \int_{\Omega_j} 1 \, d\mathbf{x} = \int_{\partial\Omega_j} \dot{\eta}_j \, ds = -\left(\frac{\partial_{s_j} V_0}{A_j(s_j)} \right) \Big|_{\partial\Omega_j} = 0,$$

by periodicity.

We now return to (3.49). The normal velocity with $s_j = \delta r_j \theta$ is

$$\dot{\eta} = -\frac{1}{\delta^2 r_j^2} \frac{\partial_{\theta\theta} V_0}{A_j},$$

where we have used that, to a first order approximation, A_j is a constant independent of θ. Now we use the inner solution to calculate A_j. Recall,

$$A_j(s_j) = \nabla v \cdot \mathbf{n}\big|_{\partial\Omega_{\delta_j}} = -v_r\big|_{r=\delta r_j} = -\delta^2 k_j \frac{1}{r}\Big|_{r=\delta r_j} = \delta \frac{k_j}{r_j}.$$

Now we write the non-radially symmetric terms of v as

$$v = (\dots) + \delta^3 [a_{j1} \rho \cos(\theta_j) + a_{j2} \rho \sin(\theta_j)],$$

where $(\ldots)$ encapsulates the radially symmetric terms and θ_j is the local polar coordinate measured with respect to $\mathbf{y} = 0$ ($\mathbf{x} = \mathbf{x}_j$). Thus, we have

$$\partial_{\theta\theta} V_0 \sim -\delta^3 r_j [a_{j1} \cos(\theta_j) + a_{j2} \sin(\theta_j)], \quad \rho = r_j.$$

Substituting in for A_j and $\partial_{\theta\theta} V_0$, we see that

$$\dot{\eta}_j = -\frac{1}{\delta^2 r_j^2} \frac{-\delta^3 r_j \mathbf{a}_j \cdot \mathbf{e}_{\theta_j}}{-\delta \frac{k_j}{r_j}},$$

where $\mathbf{e}_{\theta_j} = (cos(\theta_j), \sin(\theta_j))$. Simplifying, we have

$$\dot{\eta} = -\frac{\mathbf{a}_j \cdot \mathbf{e}_{\theta_j}}{k_j}.$$

Substituting in for k_j, we arrive at the non-zero normal velocity

$$\dot{\eta} = \frac{2D \mathbf{a}_j \cdot \mathbf{e}_{\theta_j}}{\sigma r_j^2}, \tag{3.61}$$

where $\mathbf{a}_j$ is given in (3.57).

This result shows that the normal velocity to the interface is asymptotically independent of the radius $O(\delta)$. We can write equation (3.61) equivalently as

$$\dot{\eta} = 2\pi \left[\nabla R_\lambda \big|_{\mathbf{x}_j} + \sum_{i \neq j}^{N} \frac{r_i}{r_j} \nabla G_\lambda \big|_{\mathbf{x}_j} \right] \cdot \mathbf{e}_{\theta_j}. \tag{3.62}$$

This is the main result for this section. The initial motion of a collection of small circular droplets of radii $\delta r_1, \ldots, \delta r_N$ is on an $O(1)$ timescale (recall $\dot{\eta}$ is on an $O(1/\epsilon)$ for the general PDE) and is critically influenced by the configuration of all the other drops. Notice the radius factor r_i/r_j. If r_j is large compared to the other drops, then the j^{th} drop moves essentially by $\nabla R_\lambda \big|_{\mathbf{x}_j}$.

Remark 3.3.3.4:

(i) Suppose $\mathbf{x}_1, \ldots, \mathbf{x}_N$ are such that equation (3.62) is identically zero for each j. These locations are an equilibrium state for the dynamics and, in particular, if $r_i = r_c \; \forall \, i$, then the equilibria would be to put N small disks of a common radius at the roots of unity on a ring concentric within the unit disk. There are other 'symmetric configurations' that can be found. These will be touched upon shortly.

(ii) The result (3.62) shows that an initial configuration of N small circular drops will not remain circular as time increases and the boundary of $\partial\Omega_j$ will change as t increases.

(iii) In (3.62), the first term measures the self interaction with the boundary of the domain, $\partial\Omega$. The second term is larger when r_i/r_j is large, i.e. if a small drop of radius r_j is surrounded by larger drops of radii $r_i > r_j$, the small drop will deform the most due to the other drops.

(iv) To determine the direction which the drops move, we first consider a previous result on spot dynamics for the Gray-Scott model as derived in [7]. There, a 1-spot solution with center at $\mathbf{x}_0 \in \Omega \subset \mathbb{R}^2$ satisfies $\mathbf{x}_0(t)$ with

$$\mathbf{x}_0' = -\epsilon^2 k \nabla R_\lambda(\mathbf{x}; \mathbf{x}_0)\big|_{\mathbf{x}=\mathbf{x}_0},$$

for some $k > 0$.

A collection of N spots with centers $\mathbf{x}_0, \ldots, \mathbf{x}_{N-1}$ satisfies

$$\mathbf{x}_j' = -\epsilon k_j \left[S_j \nabla R_\lambda(\mathbf{x}; \mathbf{x}_j)\big|_{\mathbf{x}=\mathbf{x}_j} + \sum_{i \neq j}^{N-1} S_i \nabla G_\lambda(\mathbf{x}; \mathbf{x}_j)\big|_{\mathbf{x}=\mathbf{x}_j} \right],$$

for $j = 0, \ldots, N-1$, and some $k_j > 0$, $S_j > 0$ (see principal result 3.1 in [7]). The dynamics are known to be a repulsive interaction. For a single spot, $\mathbf{x}_0 \to \mathbf{x}_{0e}$ in Ω as $t \to \infty$, where $\mathbf{x}_{0e}$ is the minimum of $R_\lambda(\mathbf{x}; \mathbf{x}_0)$. Thus, the boundary is repelling and spots too close together are pushed away.

Our result, in (3.62), has the opposite sign. Thus, for one droplet aligned with the x-axis in the unit disk we have

$$\dot{\eta}_1 = 2\pi \left[\partial_x R_\lambda\big|_{\mathbf{x}=(x_1,0)} \right] \cos(\theta_j).$$

The bracketed term is positive from results in [7] if $x_1 > 0$. Thus, for $\cos(\theta_j) > 0$, we have $\dot{\eta} > 0$ and $\dot{\eta} < 0$ for $\cos(\theta_j) < 0$. Here, droplet interactions are attractive in the sense that they will deform to each other. In the single droplet case the droplet deforms towards the boundary due to the "mirror" effect of Neumann boundary conditions. A depiction of this can be seen in figure 3.7.

Figure 3.7: A depiction of the results for the case described in Result 3.3.3.4 (iv). We see that the opposite sign for the velocity in the chemotaxis model causes the attractive behavior and thus, a circle off the center deforms and moves towards the boundary.

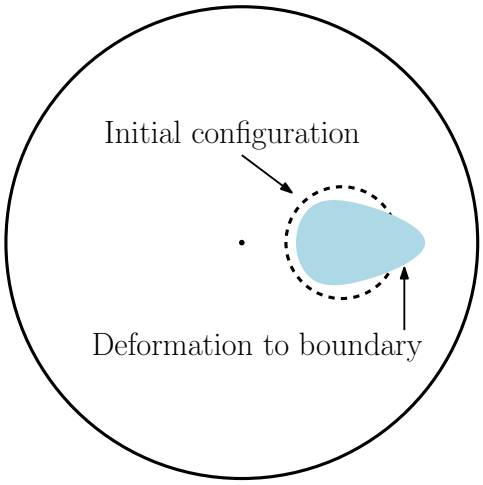

(v) In part (i) of this remark we discussed equilibrium locations for a collection of droplets. To find alternative configurations, we must find points $\mathbf{x}_1, \ldots, \mathbf{x}_N$ for given radii $r_1, \ldots, r_N$, that satisfy $\dot{\eta} = 0$, where $\dot{\eta}$ is given in (3.62). This can be done numerically by evolving the system of ODEs

$$\mathbf{x}_j' = -\left[r_j^2 \nabla R_\lambda\big|_{\mathbf{x}_j} + \sum_{i \neq j}^{N} r_i^2 \nabla G_\lambda\big|_{\mathbf{x}_j} \right], \quad j = 1, \ldots, N,$$

with the given initial positions and radii. Due to the negative sign and analogy with spot dynamics, we will have $\mathbf{x}_j \to \mathbf{x}_{je}$ as $t \to \infty$, where $\mathbf{x}_{je}$ is the equilibrium location and satisfies $\dot{\eta} = 0$.

3.3.4 Arbitrary Shaped Initial Droplet Pattern

We now discuss the case where the initial droplet pattern has N small drops of 'radius' $O(\delta)$ but arbitrary shape. Let $\mathbf{x}_j \in \Omega_{\delta_j}$ be any point in Ω_{δ_j} and all such points are $O(\delta)$ close together.

Let Ω denote the entire region with holes included. We must solve

$$\Delta v - \lambda^2 v = -\frac{\sigma}{D}\begin{cases} 1 & : \mathbf{x} \in \Omega_\delta \\ 0 & : \mathbf{x} \in \Omega \setminus \Omega_\delta \end{cases},$$
$$\frac{\partial v}{\partial n} = 0, \quad \mathbf{x} \in \partial\Omega.$$

We now solve this problem by a matched asymptotic expansion. In the inner region, near the j^{th} drop, we have

$$V \sim \delta^2 \log(\delta) k_j + \delta^2 W_{1,j} + \delta^3 \mathbf{a}_j \cdot \mathbf{y}, \tag{3.63}$$

where $W_{1,j}$ now satisfies (as described in Remark 3.3.3.2),

$$\begin{aligned} \Delta_{\mathbf{y}} W_{1,j} &= -\frac{\sigma}{D}\begin{cases} 1 : \mathbf{y} \in \Omega_j \\ 0 : \mathbf{y} \notin \Omega_j \end{cases}, \\ W_{1,j} &\sim k_j \log(|\mathbf{y}|) + C_j + o(1), \quad \text{as } |\mathbf{y}| \to \infty, \end{aligned} \tag{3.64}$$

where

$$k_j = -\sigma|\Omega_j|/(2\pi D); \qquad C_j = -2\pi(\mathcal{G}_\lambda \mathbf{k})_j.$$

Here, the j subscript for $((G)\mathbf{k})_j$ signifies the j^{th} entry of the vector. The solution to this problem is unique since C_j is specified and was found by matching to the outer solution. Since it is found by solving $\mathbf{C} = -2\pi\mathcal{G}_\lambda \mathbf{k}$, it involves all other droplets.

Note that in (3.63) the $O(\delta^3)$ term is precisely the same as for the N circular droplets. This results from the fact that the problem for $W_{2,j}$ (3.59) is independent of Ω_j. The one key new feature is that we must solve (3.64) for an arbitrary Ω_j and then determine how the shape changes under the surface diffusion law given by equation (3.49). The solution for $W_{1,j}$ can be decomposed as

$$W_{1,j} = \Phi_j + C_j, \tag{3.65}$$

where $\Phi_j(\mathbf{y})$ is the unique solution to

$$\begin{aligned} \Delta_{\mathbf{y}} \Phi_j &= -\frac{\sigma}{D}\begin{cases} 1 : \mathbf{y} \in \Omega_j \\ 0 : \mathbf{y} \notin \Omega_j \end{cases}, \\ \Phi_j &\sim k_j \log(|\mathbf{y}|) + o(1), \quad \text{as } |\mathbf{y}| \to \infty. \end{aligned} \tag{3.66}$$

The $o(1)$ condition above is the condition that makes the PDE uniquely determined. A key feature here is that Φ_j is a local problem in the sense that

it is independent of any interaction with the other drops. The interaction effect with other droplets is simply additive in (3.65).

Lemma 3.3: *The solution to (3.66), with* $d\mathbf{s} = ds_1 ds_2$*, is given as*

$$\Phi_j(\mathbf{y}) = -\frac{\sigma}{2\pi D}\int_{\Omega_j} \log(|\mathbf{y}-\mathbf{s}|)\, d\mathbf{s}$$

Proof: We let $G_f = -\log(|\mathbf{s}-\mathbf{y}|)/2\pi$ satisfy, in the $\mathbf{s}$-plane, the equation for the free space Green's function, $\Delta_{\mathbf{s}} G_f = -\delta(\mathbf{s}-\mathbf{y})$. Now,

$$\begin{aligned} \Delta_{\mathbf{y}}\Phi_j &= -\frac{\sigma}{D}\begin{cases} 1 : \mathbf{s}\in\Omega_j \\ 0 : \mathbf{s}\notin\Omega_j \end{cases}, \\ \Phi_j &\sim k_j \log(|\mathbf{s}|) + o(1), \quad \text{as } |\mathbf{s}|\to\infty. \end{aligned} \tag{3.67}$$

We have

$$\lim_{R\to\infty}\int_{B_R}(G_f\Delta_{\mathbf{s}}\Phi_j - \Phi_j\Delta_{\mathbf{s}}G_f)\, d\mathbf{s} = \lim_{R\to\infty}\int_{\partial B_R}\left(G_f\frac{\partial\Phi_j}{\partial n} - \Phi_j\frac{\partial G_f}{\partial n}\right) d\mathbf{s}, \tag{3.68}$$

where $B_r = \{\mathbf{s} : |\mathbf{s}| = R\}$. The left hand side is

$$\begin{aligned} \lim_{R\to\infty}\left(\int_{B_R} G_f\Delta_{\mathbf{s}}\Phi_j\, d\mathbf{s} + \Phi_j(\mathbf{y})\right) &= \Phi_j(\mathbf{y}) - \frac{\sigma}{D}\int_{\Omega_j} G_f\, d\mathbf{s} \\ &= \Phi_j(\mathbf{y}) + \frac{\sigma}{2\pi D}\int_{\Omega_j}\log(|\mathbf{s}-\mathbf{y}|)\, d\mathbf{s} \end{aligned} \tag{3.69}$$

Now, the right hand side of (3.68) is

$$\begin{aligned} &\lim_{R\to\infty}\int_{\partial B_R}\left(G_f\frac{\partial\Phi_j}{\partial n} - \Phi_j\frac{\partial G_f}{\partial n}\right) d\mathbf{s} = \\ &= \lim_{R\to\infty}\int_{\partial B_R}\left(-\frac{k_j}{2\pi R}\log(|\mathbf{y}-\mathbf{s}|) - (k_j\log(R)+o(1))\frac{\partial G_f}{\partial n}\right) d\mathbf{s}. \end{aligned}$$

But,

$$\log(|\mathbf{s}-\mathbf{y}|)\big|_{\mathbf{s}=R} \sim \log(R) + \frac{\mathbf{y}\cdot\mathbf{s}}{|\mathbf{s}|^2} + O\left(\frac{1}{R^2}\right), \quad \text{for } |\mathbf{s}| = R \gg 1,$$

and

$$\frac{\partial G_f}{\partial n}\Big|_{\mathbf{s}=R} = -\frac{1}{2\pi}\partial_{|\mathbf{s}|}\log(|\mathbf{s}-\mathbf{y}|)\Big|_{\mathbf{s}=R} = -\frac{1}{2\pi}\partial_{|\mathbf{s}|}\left(\log(|\mathbf{s}|) - \frac{\mathbf{y}\cdot\mathbf{s}}{|\mathbf{s}|^2}\right),$$

which yields

$$\frac{\partial G_f}{\partial n}\Big|_{\mathbf{s}=R} \sim -\frac{1}{2\pi R} + O\left(\frac{1}{R^2}\right)$$

Substituting this information into the right hand side of (3.68), we obtain with $\mathbf{s} = R\theta$

$$\lim_{R\to\infty}\int_{\partial B_R}\left(G_f\frac{\partial\Phi_j}{\partial n} - \Phi_j\frac{\partial G_f}{\partial n}\right)d\mathbf{s} =$$
$$= 2\pi\lim_{R\to\infty}\left[\left(-\frac{k_j}{2\pi R}\log(R) + (k_j\log(R) + o(1))\frac{1}{2\pi R}\right)R\right]$$

In the right hand side of this equation we see that the $\log(R)$ terms cancel. Note that it is critical that the additional term on the right hand side be $o(1)$ to ensure the boundary integral vanishes. Thus, since the right hand side of this equation vanishes we obtain the desired result from (3.69).

$$\Phi_j(\mathbf{y}) = -\frac{\sigma}{2\pi D}\int_{\Omega_j}\log(|\mathbf{y}-\mathbf{s}|)\,d\mathbf{s}.$$

We now conclude that

$$W_{1,j} = \frac{\sigma}{2\pi D}\int_{\Omega_j}\log(|\mathbf{s}-\mathbf{y}|)\,d\mathbf{s} + C_j,$$

the exact solution of (3.64).

Remark 3.3.4.1: We would like to verify directly that Φ_j satisfies (3.67). First note that if $\mathbf{y}\notin\Omega_j$, then $\Delta_{\mathbf{y}}\log(|\mathbf{s}-\mathbf{y}|) = 0$ so $\Delta_{\mathbf{y}}\Phi_j = 0$. If $\mathbf{y}\in\Omega_j$, we have

$$\Delta_{\mathbf{y}}\Phi_j = -\frac{\sigma}{2\pi D}\int_{\Omega_j}\Delta_{\mathbf{y}}\log(|\mathbf{s}-\mathbf{y}|)\,d\mathbf{s} = -\frac{\sigma}{D}\int_{\Omega_j}\delta(\mathbf{s}-\mathbf{y})\,d\mathbf{s} = -\frac{\sigma}{D}.$$

To establish the far-field behavior of $\Phi_j(\mathbf{y})$ we let $|\mathbf{y}|\to\infty$ and write

$$\log(|\mathbf{y}-\mathbf{s}|) = \frac{1}{2}\log(|\mathbf{y}-\mathbf{s}|^2) = \frac{1}{2}\log[(\mathbf{y}-\mathbf{s})\cdot(\mathbf{y}-\mathbf{s})] = \frac{1}{2}\log[\mathbf{y}\mathbf{y}^T - \mathbf{s}^T\mathbf{y} - \mathbf{y}^T\mathbf{s} + \mathbf{s}\mathbf{s}^T]$$

Since $\mathbf{s}^T\mathbf{y} = \mathbf{y}^T\mathbf{s}$, we have

$$\begin{aligned}\log(|\mathbf{y}-\mathbf{s}|) &= \frac{1}{2}\log[|\mathbf{y}|^2 - 2\mathbf{y}\cdot\mathbf{s} + |\mathbf{s}|^2] \\ &= \frac{1}{2}\log\left[|\mathbf{y}|^2\left(1 - \frac{2\mathbf{y}\cdot\mathbf{s}}{|\mathbf{y}|^2} + \frac{|\mathbf{s}|^2}{|\mathbf{y}|^2}\right)\right] \\ &= \log(|\mathbf{y}|) + \frac{1}{2}\log\left(1 - \frac{2\mathbf{y}\cdot\mathbf{s}}{|\mathbf{y}|^2} + \frac{|\mathbf{s}|^2}{|\mathbf{y}|^2}\right).\end{aligned}$$

Noting that $\log(1-z) \sim -z$ if $z \to 0$, we have

$$\log(|\mathbf{y}-\mathbf{s}|) \sim \log(|\mathbf{y}|) + \frac{\mathbf{y}\cdot\mathbf{s}}{|\mathbf{y}|^2} + O\left(\frac{1}{|\mathbf{y}|^2}\right), \quad \text{for } |\mathbf{y}| \to \infty.$$

Thus, for $|\mathbf{y}| \gg 1$,

$$\Phi_j(\mathbf{y}) = -\frac{\sigma}{2\pi D}\int_{\Omega_j}\log(|\mathbf{y}-\mathbf{s}|)\,d\mathbf{s} \sim -\frac{\sigma}{2\pi D}\int_{\Omega_j}\left(\log(|\mathbf{y}|) + \frac{\mathbf{y}\cdot\mathbf{s}}{|\mathbf{y}|^2} + O\left(\frac{|\mathbf{s}|^2}{|\mathbf{y}|^2}\right)\right)d\mathbf{s}.$$

So,

$$\Phi_j(\mathbf{y} \sim -\frac{|\Omega_j|\sigma}{2\pi D}\log(|\mathbf{y}|) - \frac{\sigma\mathbf{y}}{2\pi D|\mathbf{y}|^2}\cdot\int_{\Omega_j}\mathbf{s}\,d\mathbf{s}.$$

The second term is indeed $o(1)$ as $\mathbf{y} \to \infty$ and in fact

$$\Phi_j(\mathbf{y}) \sim k_j\log(|\mathbf{y}|) + o(1), \quad \text{as } |\mathbf{y}| \to \infty.$$

In summary, the exact solution to (3.64) is simply

$$W_{1,j} = \frac{\sigma}{2\pi D}\int_{\Omega_j}\log(|\mathbf{s}-\mathbf{y}|)\,d\mathbf{s} + C_j. \tag{3.70}$$

To determine the local change to the interface due to $W_{1,j}$ we write

$$\dot{\eta} = -\left(\frac{\partial_{s_j}V_0}{A_j}\right)_{s_j}, \quad \mathbf{x} \in \partial\Omega_{\delta_j}.$$

We put $s_j = \delta\hat{s}_j$, with $\hat{s}_j \in (0, |\partial\Omega_j|)$, which is the length of $\partial\Omega_j$ measured in the $\mathbf{y}$-variable. This yields

$$\dot{\eta} = -\frac{1}{\delta^2}\left(\frac{\partial_{\hat{s}_j}V_0}{A_j}\right)_{\hat{s}_j}, \quad \mathbf{x} \in \partial\Omega_{\delta_j}. \tag{3.71}$$

We have

$$\partial_{\hat{s}_j} V_0 \approx \delta^2 \partial_{\hat{s}_j} W_{1,j}\big|_{\partial\Omega_j} \sim -\delta^2 \frac{\sigma}{2\pi D} \frac{\partial}{\partial \hat{s}_j} \int_{\Omega_j} \log(|\mathbf{y}(s_j) - \mathbf{s}|)\, d\mathbf{s},$$
$$A_j = \nabla_{\mathbf{x}} v \cdot \mathbf{n} = \frac{1}{\delta} \nabla_{\mathbf{y}} v \cdot \mathbf{n} \sim -\frac{1}{\delta} \delta^2 \frac{\partial W_{1,j}}{\partial n}.$$

Substituting these into the velocity equation (3.71), we obtain

$$\dot{\eta} \sim -\frac{1}{\delta} \left(\frac{\partial_{\hat{s}_j} W_{1,j}}{\partial_{\mathbf{n}} W_{1,j}} \right)_{\hat{s}_j},$$

which shows that $\dot{\eta} = O(1/\delta)$. This means the interface responds quickly to an initial deformation of the non-circular initial shape. This deformation is only due to the drop itself and not the other drops.

Chapter 4

Numerical Results for the Chemotaxis Model

In this chapter we discuss numerical solutions for the volume filling model. This serves as a verification of the analytic results for geometries in which asymptotic analysis is not possible as well as a way to see interface evolution. We solve the quasi-steady problem discussed in previous chapter, where the organism has aggregated into regions of uniform concentration. The problem to solve is

$$\begin{aligned} D\Delta v - v &= -\sigma \begin{cases} 1 : \mathbf{x} \in \Omega_- \\ 0 : \mathbf{x} \in \Omega_+ \end{cases}, \\ \frac{\partial v}{\partial n} &= 0, \quad \mathbf{x} \in \partial\Omega, \end{aligned} \tag{4.1}$$

where $\Omega \subset \mathbb{R}^2$ is some domain and Ω_- is some initial configuration of cell colonies. The inner region may be a single mass or a collection of disjoint groups. Each of these inner regions represent the initial aggregation of the cells in the system and the interface is the boundary of Ω_-, given by Γ.

The main goal is to use the finite element method to solve the steady state equation of the chemical potential and then to calculate the velocity on each interface using our asymptotic results (principal result 3.1). We then pass this information to a level set framework where the velocity is extended in a narrow band around each interface and then evolved in time. With the new location of the interface Γ, the steady state problem is solved once again and the process is repeated.

The level set method was chosen for many reasons. It is known for its ability to easily handle complicated domain evolution where merging or splitting may occur (see [26]). It has been successfully used in applications such as Stefan problems, flame front evolution, and computer vision. Since the chemotaxis equations devolve into a moving boundary problem it seems like the natural framework with which to view it.

4.1 Steady State Solution Using the Finite Element Method

The first step is to solve the steady state problem in (4.1) so the velocity may be calculated. The finite element method was chosen so we can easily fit the mesh to complicated interfaces. Since the forcing term in the problem is a step function it is desirable to have the tessellation respect the inner and outer regions. To achieve this we use two different tessellations, one for the inner and and one for the outer regions, that share the same nodes on their common interface (see figure4.1).

For the tessellation, Per-Olof Persson's distmesh (see [24]) package was used. The first step is to construct Ω_+ and Ω_- separately. We then marry the two tessellations together by adjusting the triangle node numbering in a consistent fashion and appending the additional nodes and triangles onto the original lists. This gives us a single tessellation of Ω with a 'tight' hold on the interface. Note that around the interface we adaptively refine the triangulation for improved accuracy in calculating the velocity.

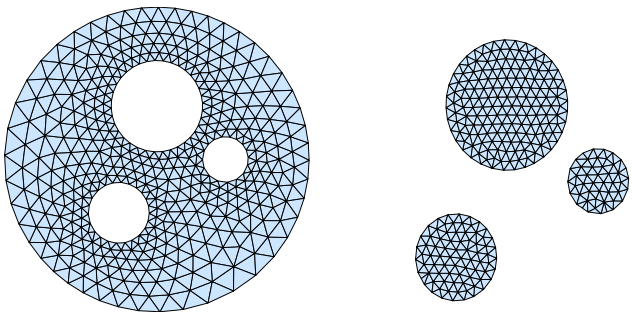

Figure 4.1: An example of a tessellation generated using distmesh and the described methodology.

The steady state problem is solved in a standard manner. We construct the weak form by first assuming that if v solves (4.1), then for any u we have

$$\int_\Omega D\Delta v u \, d\mathbf{x} - \int_\Omega vu \, d\mathbf{x} = -\sigma \int_{\Omega_-} u \, d\mathbf{x}.$$

Applying Green's identity to the first term on the left hand side, we now have

$$-\int_\Omega (D\nabla v \cdot \nabla u + uv) \, d\mathbf{x} + \int_{\partial\Omega} u \frac{\partial v}{\partial n} \, d\mathbf{x} = -\sigma \int_{\Omega_-} u \, d\mathbf{x}.$$

Since v is subject to Neumann boundary conditions, the boundary integral vanishes and we obtain the following weak form of (4.1).

$$\int_\Omega (D\nabla v \cdot \nabla u + uv) \, d\mathbf{x} = \sigma \int_{\Omega_-} u \, d\mathbf{x}.$$

where u is an arbitrary 'trial' function in $H^1(\Omega)$, the Sobolev space given as $H^1(\Omega) = \{u \in L^2(\Omega) : u_{x_1}, u_{x_2} \in L^2(\Omega)\}$.

We use a Galerkin approximation to approximate v and u as

$$v(x,y) = \sum_{i=1}^{N} v_i N_i(x,y); \qquad u(x,y) = \sum_{i=1}^{N} u_i N_i(x,y),$$

where N_i are finite element basis functions. Since u is arbitrary we can set each $u_i = 1$ in turn. The problem to solve, for each i, is

$$\left[\int_\Omega (D\nabla N_i(x,y) \cdot \nabla N_j(x,y) + N_i(x,y)N_j(x,y)) \, d\mathbf{x}\right] v_i = \sigma \int_{\Omega_-} N_j(x,y) \, d\mathbf{x}. \tag{4.2}$$

We approximate the solution by using quadratic basis functions over mapped triangles. For mapped triangles that lie on $\partial\Omega$ or Γ, we use an isoparametric mapping to improve the accuracy with which these curves are represented (see figure 4.2).

The integrals in (4.2) are evaluated by mapping the basis functions to a reference element (see figure 4.2). For a given triangle, the reference map is defined by

$$x = F_1(\omega,\xi) = \sum_{i=1}^{6} x_i \hat{N}_i(\omega,\xi); \qquad y = F_2(\omega,\xi) = \sum_{i=1}^{6} y_i \hat{N}_i(\omega,\xi), \tag{4.3}$$

where x_i and y_i are the vertices of the triangle that correspond to the node where the basis function $N_i(\omega, \xi)$ is one and (ω, ξ) are the reference element coordinates. On the reference element the basis functions can be written explicitly as

$$\begin{gathered}\hat{N}_1 = (1-\omega-\xi)(1-2\omega-2\xi); \qquad \hat{N}_2 = \omega(2\omega-1); \qquad \hat{N}_3 = \xi(2\xi-1), \\ \hat{N}_4 = 4\omega\xi; \qquad \hat{N}_5 = 4\xi(1-\omega-\xi); \qquad \hat{N}_6 = 4\omega(1-\omega-\xi).\end{gathered} \tag{4.4}$$

Applying the map from (4.3) to the integrals in (4.2), we have (for a mapped triangle K and corresponding reference triangle $\hat{K}$),

$$\begin{gathered}D\int_K \nabla N_i \cdot \nabla N_j \, dA = D|\det(J)| \int_{\hat{K}} (J^{-T}\hat{\nabla}\hat{N}_i) \cdot (J^{-T}\hat{\nabla}\hat{N}_j) \, dA, \\ \int_K N_i N_j \, dA = |\det(J)| \int_{\hat{K}} \hat{N}_i \hat{N}_j \, dA; \qquad \int_K N_j \, dA = |\det(J)| \int_{\hat{K}} \hat{N}_j \, dA,\end{gathered}$$

where J is the Jacobian of the map given in (4.3), which can be written explicitly as

$$J = \begin{pmatrix} \partial_\omega \sum_{i=1}^6 x_i \hat{N}_i(\omega,\xi) & \partial_\xi \sum_{i=1}^6 x_i \hat{N}_i(\omega,\xi) \\ \partial_\omega \sum_{i=1}^6 y_i \hat{N}_i(\omega,\xi) & \partial_\xi \sum_{i=1}^6 y_i \hat{N}_i(\omega,\xi) \end{pmatrix}. \tag{4.5}$$

Once on the reference element we use 10-point Gauss quadrature to evaluate the integrals.

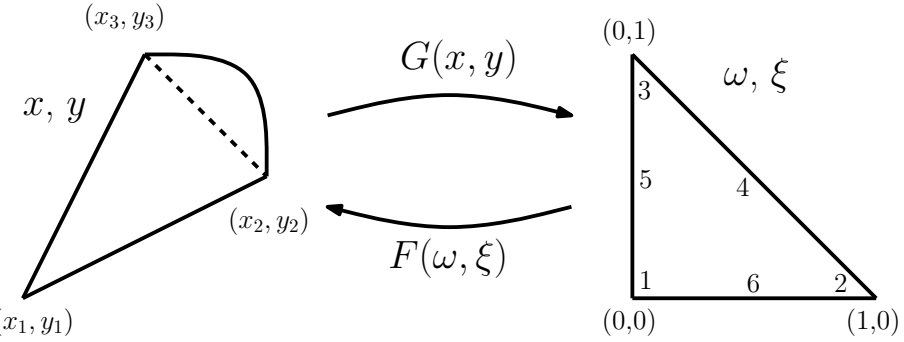

Figure 4.2: A depiction of a triangle with a mapped edge and the reference triangle in ω, ξ space. The dotted line indicates the previously unmapped quadratic or possibly linear triangle edge. $G(x, y)$ is the equivalently written as $F^{-1}(\omega, \xi)$.

Initially, we tried piecewise linear elements but they were not sufficiently accurate for our purposes. Since the velocity on the interface depends upon the arc length of Γ, accuracy of the initial solution and representation of the interface is very important. Quadratic elements were also tried before implementing isoparametric quadratics. Since the interface will typically be curved and not polygonal, mapping the triangle edges that lie on the interface gives us smooth tangent and normal vectors as well as a more accurate representation of the forcing term in (4.1). Since the domain is discretized with special care taken at the interface and boundary, we are able to handle the forcing term properly and maintain $O(h^3)$ accuracy in the L^2 norm.

As a check, we consider problem (4.1) with $\Omega = \{\mathbf{x} : |\mathbf{x}| \leq 1\}$, the unit disk, $\Omega_- = \{\mathbf{x} : |\mathbf{x}| \leq .25\}$, $\sigma = 1$ and $D = 1$. With this given droplet configuration the exact solution, v, can be found and is given in (3.21). The solution is

$$v = \begin{cases} \sigma + AI_0(|\mathbf{x}|\lambda) & : |\mathbf{x}| \leq \delta \\ BI_0(|\mathbf{x}|\lambda) + CK_0(|\mathbf{x}\lambda|) & : \delta < |\mathbf{x}| \leq 1 \end{cases},$$

with A, B, and C given as

$$A = C\left[\frac{(K_0(\delta) - \sigma)I_1(1) + K_1(1)I_0(\delta)}{I_1(1)I_0(\delta)}\right],$$
$$B = C\frac{K_1(1)}{I_1(1)}; \qquad C = \frac{I_1(\delta)\sigma}{\mathcal{W}(K_0(\delta), I_0(\delta))},$$

where $\delta = .25$, $\sigma = 1$ and $\lambda = 1$.

We calculate the numerical solution, V, with quadratic and isoparametric quadratic elements and create a log-log plot of the L^2 error $\|V - v\|_{L^2}$ against the mesh edge length h. Clearly the isoparametric elements are more accurate and converge faster ($O(h^3)$ for isoparametric and $O(h^2)$ for quadratic), as seen in figure 4.3. A surface plot of the numerical solution can be seen in figure 4.4.

4.1.1 Comparison to Asymptotics

The next step is to ensure that the numerical and asymptotic results agree. To this end, we investigate the case where Ω is a circular domain with many circular interfaces analyzed in section 3.3.3. The problem we solve is given in equation (4.1) with $\Omega = \{\mathbf{x} : |\mathbf{x}| \leq 1\}$, $\sigma = 1$, $D = 1$ and $\Omega_- = \{\mathbf{x} : |\mathbf{x} - (-.15, -.45)| \leq \delta\} \cup \{\mathbf{x} : |\mathbf{x} - (.25, .25)| \leq 2\delta\}$. Since the

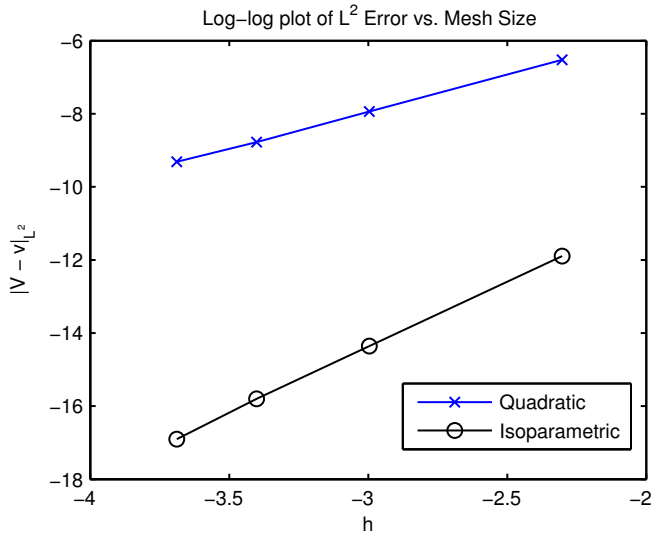

Figure 4.3: Log-log plot of the L^2 error versus mesh size. The isoparametric mapping improves accuracy and leads to a higher convergence rate indicated by the steeper slope. The slopes are 3.67 for the isoparametric elements and 2.02 for quadratic.

problem is solved asymptotically in the limit $\delta \to 0$, we analyze the error for decreasing δ on a fixed initial mesh size $h = .015$.

The derivation of the asymptotic solution can be found in section 3.3.3 and is given as

$$v \approx -\delta^2 2\pi \sum_{i=1}^{N} k_i G_\lambda(\mathbf{x}; \mathbf{x}_j),$$

where G_λ is the reduced-wave Green's function that solves

$$\Delta G_\lambda - \lambda^2 G_\lambda = -\delta(\mathbf{x} - \mathbf{x}_j), \quad \mathbf{x} \in \Omega; \qquad \frac{\partial G_\lambda}{\partial n} = 0, \quad \mathbf{x} \in \partial\Omega.$$

When Ω is a unit disk, as in this case, the reduced-wave Green's function can be found explicitly and is given in appendix B. A surface plot of the numerical solution using this reduced-wave Green's function is given in figure 4.5.

As $\delta \to 0$, the difference between the numerical and asymptotic solution should decrease. This can be seen in table 4.1, where the l^2 norm of the

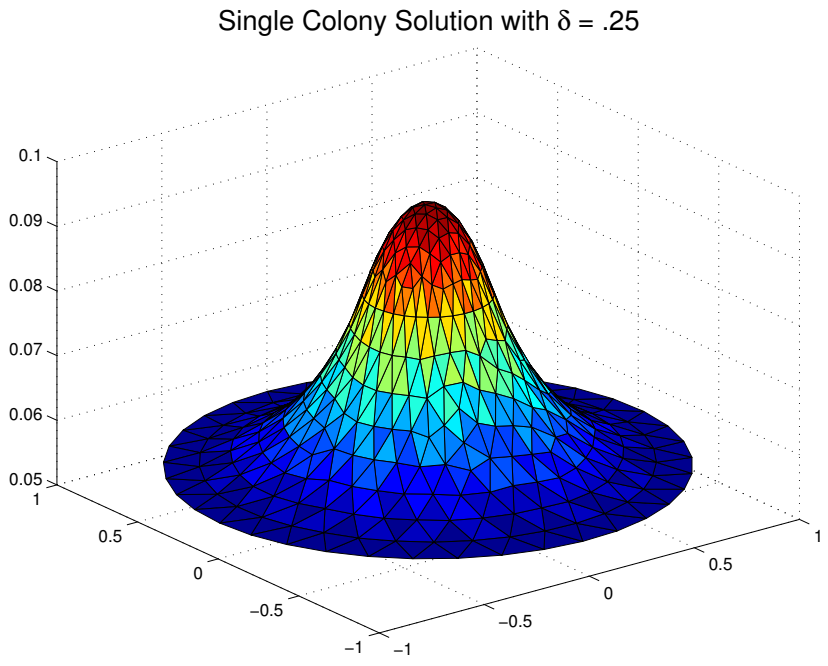

Figure 4.4: The solution to the steady state equation with a single cell colony centered at the origin. Here, $\delta = .25$ and the initial edge length is .05.

difference between solutions is shown for different values of δ. Note that, for a given mesh size, there is a lower bound constraint on δ as there need to be sufficient degrees of freedom in the FEM model to represent the interior regions accurately.

This result helps to confirm the asymptotic solutions presented in section 3.3.3 as well as the accuracy of the numerical computations.

4.2 Calculating the Interface Velocity

Recall our asymptotic result,

$$\dot{\eta} = -\Big(\frac{\partial_s V_0}{A_1(s)}\Big)_s = -\Big(\frac{v_s}{\nabla v \cdot \mathbf{n}}\Big)_s,$$

where V_0 is the first term in the inner expansion of (4.1) and A_1 arises from the second term. This is the velocity we need to calculate in order to use

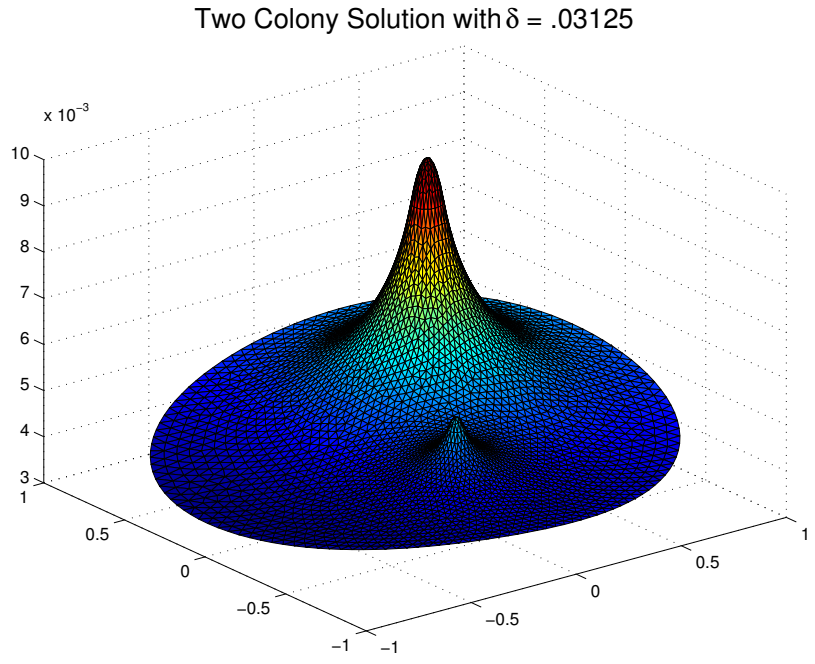

Figure 4.5: The solution to the steady state equation with two cell colonies located at [-.15, -.45] and [.25, .25] with radii of δ and 2δ respectively. Here, $\delta = .03125$.

the level set method and capture interface motion.

The arc length derivatives are calculated by determining the tangent to the interface from the isoparametric mapping (4.3) and taking the dot product of that with the gradient of v. This is because $\partial_s f(\mathbf{x}) = \nabla f(\mathbf{x}) \cdot \mathbf{t}$, where $\mathbf{t}$ is the tangent vector of the curve at the point $\mathbf{x}$. The gradient is calculated using the finite element framework. For a given triangle K and point $(x, y) \in K$, the gradient is defined as

$$\nabla v(x, y) = \sum_{i=1}^{6} v_i \nabla N_i(x, y),$$

where $N_i(x, y)$ are the non-zero basis functions on that triangle. We can take advantage of the reference element to say that the gradient is

δ	difference (l^2)
.25000	3.3275
.12500	.44805
.06250	.05868
.03125	.00977

Table 4.1: A table of the error for decreasing values of δ. The error quickly decreases as δ decreases, coinciding with the asymptotic limit of $\delta \ll 1$.

$$\nabla v(x,y) = J^{-T} \sum_{i=1}^{6} v_i \hat{\nabla} \hat{N}_i(\omega, \xi),$$

where $\hat{N}_i(\omega, \xi)$ are the local basis functions and J^{-T} is the inverse transpose of the Jacobian of the reference map. The reference basis functions are given in (4.4) and the Jacobian is given in (4.5). The normal vector $\mathbf{n}$ is calculated using an outward normal by taking the vector perpendicular to the tangent $\mathbf{t}$.

Since the gradient and normal vectors are not well defined at the vertices of a triangle we instead only calculate the velocity at the mapped quadratic nodes that sit between two vertices that lie on the interface. To calculate the velocity elsewhere we pass a periodic spline through those points and interpolate. This gives us the normal velocity at all of the nodes on the interface and in principle anywhere on the curve.

To check the accuracy of the velocity, we again look to the problem problem (4.1) with $\Omega = \{\mathbf{x} : |\mathbf{x}| \leq 1\}$, the unit disk, $\Omega_- = \{\mathbf{x} : |\mathbf{x}| \leq .25\}$, $\sigma = 1$ and $D = 1$. Since the solution is independent of θ, the arc length derivative will be 0 and thus the velocity is 0. We calculate the velocity on the interface with quadratic and isoparametric elements and use the maximum value as a measure of accuracy. Figure 4.6 is a log-log plot of the maximum velocity value versus h, the initial mesh size. The convergence rates (slopes) are 1.24 and 1.68 for the quadratic and isoparametric elements, respectively.

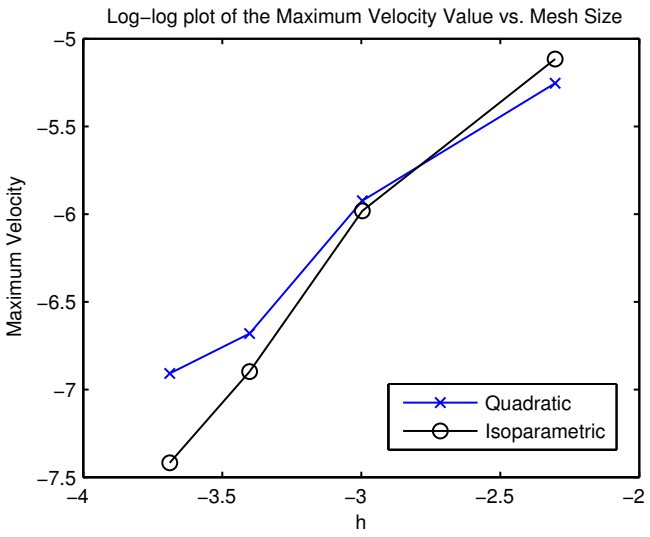

Figure 4.6: Log-log plot of maximum velocity value on the interface versus mesh size. Once again the isoparametric elements provide an improvement in accuracy.

4.3 Interface Evolution Using the Level Set Method

The level set method was developed by Osher and Sethian in [21] and it offers an accurate and robust way of evolving interfaces. The formulation for the level set method is as follows. Given a normal velocity field $\mathcal{V}$, we evolve the surface $z = \phi(x, y, t)$ according to the hyperbolic conservation law

$$\phi_t + \mathcal{V}|\nabla\phi| = 0,$$

where $\phi(x, y, t) = 0$ defines the moving interface we want to track. At the first step ϕ is initialized as a signed distance function that, at each point in space, describes the distance to the interface. Since the level set equation requires a normal velocity field for *all* level sets, we need to build an extension velocity off the interface. Thus, before we proceed with the evolution, we need to construct this signed distance function and extension velocity field.

As an example, a circular interface of radius R can be represented as the signed distance function

$$\phi(x, y) = \sqrt{x^2 + y^2} - R.$$

An interface comprised of a collection of disjoint regions can be represented as a union of a collection of signed distance functions ϕ_i, where each ϕ_i is an embedding of a simple closed curve. The value for $\phi(x, y) = \bigcup_i \phi_i(x, y)$, at a point (x, y) in space, is given by $\phi(x, y) = \min_i(\phi_i(x, y))$. This simple fact allows one to represent complicated domain configurations as a minimum over much simpler ones.

The level set equation is typically solved on a rectangular grid with uniform spacing. We chose to do the same and thus we embed the finite element mesh in a square domain and impose artificial periodic boundary conditions. Since curve evolution only requires local information, the boundary effects never come into play. We will now take a deeper look at more specific points of the implementation.

4.3.1 The Signed Distance Function

Evolution by the level set equation does not strictly require a signed distance function but a signed distance function has many nice properties that improve the accuracy of numerical computations. A signed distance function, ϕ, gives the shortest distance from a point $\mathbf{x}$ to the boundary $\phi = 0$ and also has the property that $|\nabla\phi| = 1$. This normalized gradient diminishes the negative effects that large variations in the gradient may have on numerical computations. This is why a signed distance function is often chosen.

Throughout evolution, the level set equation can have a distorting effect on the interface, causing very steep or flat gradients (see [18]). This means small perturbations in the velocity or interface can have large and unphysical effects on the solution. This problem is ameliorated by reinitializing ϕ as a signed distance function at every iteration. In order to reinitialize a level set function into a signed distance function we evolve the following reinitialization equation proposed in [28] to a steady state.

$$\phi_t = \text{sign}(\phi)(1 - |\nabla\phi|).$$

Typically, very few iterations are required for a reasonably accurate reinitialization.

For points within one grid space of the interface we use a subcell fix (see figure 4.7). Russo and Smereka in [25] explain that for these 'close' points, a standard discretization will not remain upwind. Thus, for the

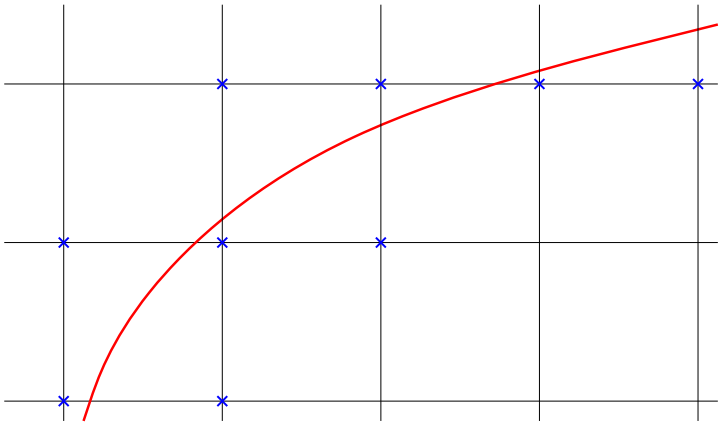

Figure 4.7: An example of a set of points (identified by the crosses) one grid node away from an interface.

point (i, j) on the n^{th} iteration, the subcell fix changes the right hand side of the reinitialization equation given above to

$$\text{sign}(\phi^0_{i,j})|\phi^n_{i,j}| - D_{i,j},$$

where $\phi^k_{i,j} = \phi(x_i, y_j, t_k)$ and $D_{i,j}$ is an approximation of the distance from the node (x_i, y_j) to the interface. $D_{i,j}$ is given by

$$D_{i,j} = h\frac{\phi^0_{i,j}}{\Delta\phi^0_{i,j}}$$

$$\Delta\phi^0_{i,j} = \sqrt{(D_x\phi^0_{i,j})^2 + (D_y\phi^0_{i,j})^2}$$

where h is the grid spacing, $D_x\phi^0_{i,j}$ and $D_y\phi^0_{i,j}$ are the maximum absolute value of a small parameter ϵ, along with the central, forward, and backward difference operators in the x and y directions, respectively. $\Delta\phi^0_{i,j}$ is given as above because merging or breaking interfaces may result in small values for the denominator and this formulation keeps the distance, $D_{i,j}$, numerically robust. Note that this fix is only done for points within one grid space away from the interface and for all others we use Godunov's method.

An example of the effectiveness of reinitialization with a subcell fix can be is seen in figure 4.8

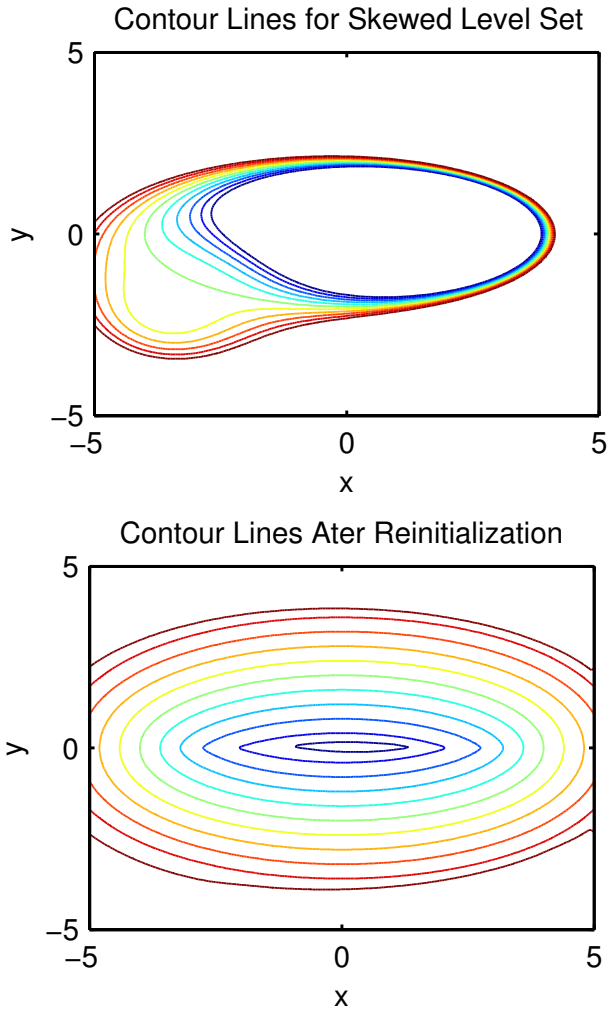

Figure 4.8: An example where reinitialization, particularly with a subcell fix, is very effective at correcting defects in a level set function. Here, $\phi = f * (\sqrt{(x/4)^2 + (y/2)^2} - 1)$, where $f = .1 + (x + 3.5)^2 + (y + 2)^2$.

4.3.2 Regular Grid Initialization and Velocity Extension

As mentioned previously, the level set equation is solved on a regular grid. Since the velocity is only defined on the interface, it needs to be interpolated to this grid and then extended outward in a reasonable fashion. The only strict stipulation [26] imposes upon this extension is that it be continuous at the interface. This can be done in the manner suggested in [17]. First, the velocity is extended to the rest of the triangulated mesh by solving the following equation.

$$\begin{aligned} \Delta\mathcal{V} = 0, \quad \mathbf{x} \in \Omega \setminus \Gamma; \qquad \mathcal{V} = \dot{\eta}, \quad \mathbf{x} \in \Gamma \\ \left[\frac{\partial \mathcal{V}}{\partial n}\right] = 0, \quad \mathbf{x} \in \Gamma; \qquad \frac{\partial \mathcal{V}}{\partial n} = 0, \quad \mathbf{x} \in \partial\Omega. \end{aligned} \tag{4.6}$$

We solve Laplace's equation with Dirichlet boundary conditions away from the interface and initialize the velocity that was already solved for on the nodes corresponding to the interface. We also enforce a zero jump condition in the normal derivative on the interface to impose differentiability. Since this system is overdetermined it is solved in the least squares sense using the normal equations.

The reason we extend the velocity in this way is because, in a weak sense, we enforce the fact that $\nabla\phi \cdot \nabla\mathcal{V} = 0$. To show this, consider the integral

$$\int_\Omega \phi \Delta\mathcal{V}\, d\mathbf{x} = 0,$$

which is true because of (4.6). This can be decomposed into a sum of two integrals,

$$\int_{\Omega_-} \phi \Delta\mathcal{V}\, d\mathbf{x} + \int_{\Omega_+} \phi \Delta\mathcal{V}\, d\mathbf{x} = 0,$$

Applying Green's identity, we have

$$-\int_\Omega \nabla\phi \cdot \nabla\mathcal{V}\, d\mathbf{x} + \int_{\partial\Omega} \phi \frac{\partial \mathcal{V}}{\partial n}\, d\mathbf{x} - \int_{\partial\Omega_+} \phi \frac{\partial \mathcal{V}}{\partial n}\, d\mathbf{x} + \int_{\partial\Omega_-} \phi \frac{\partial \mathcal{V}}{\partial n}\, d\mathbf{x} = 0$$

where the sign for the last two integrals is opposite because of the different normal directions. The last two integrals vanish due to the imposed jump condition on the interface and the second integral vanishes because of the Neumann boundary conditions. Thus, we have

$$\int_\Omega \nabla\phi \cdot \nabla\mathcal{V}\, d\mathbf{x} = 0,$$

and therefore, in a weak sense, we have $\nabla\phi \cdot \nabla\mathcal{V} = 0$. The reason why this condition is important is because it helps maintain ϕ as a signed distance function. To see this, suppose that initially $|\nabla\phi| = 1$ and we evolve the interface using the level set equation $\phi_t + \mathcal{V}|\nabla\phi| = 0$. Now, consider

$$\frac{d|\nabla\phi|^2}{dt} = 2\nabla\phi \cdot \frac{d}{dt}\nabla\phi = -2(\nabla\phi \cdot \nabla\mathcal{V}|\nabla\phi| + \nabla\phi \cdot \nabla|\nabla\phi|\mathcal{V}).$$

Since $|\nabla\phi| = 1$, we have that $\nabla|\nabla\phi| = 0$. Now, with $\nabla\phi \cdot \nabla\mathcal{V} = 0$, we have that

$$\frac{d|\nabla\phi|^2}{dt} = 0,$$

and therefore $|\nabla\phi| = 1$ for all time as it is a unique solution to the ODE. This is why we impose $\nabla\phi \cdot \nabla\mathcal{V} = 0$; having ϕ as a signed distance function, as mentioned previously, improves numerical accuracy and robustness significantly.

Once the velocity has been extended to the rest of the triangulated domain we can initialize it to a set of points on the regular grid. We choose these points by selecting those that lie within a certain small distance (given by ϕ) from the interface, $\phi = 0$. The finite element method gives us a natural interpolation scheme; we find which triangle a mesh point lies in and interpolate using the basis functions for that triangle. For the rest of the points in the domain we set the velocity to zero.

Once the velocity has been initialized we can smooth the jump between initialized and non initialized grid points with the velocity extension equation. This extends the initial set of points with non-zero velocity further outwards and alleviates discontinuities. The velocity extension equation is

$$\frac{\partial\mathcal{V}}{\partial t} + \text{sign}(\phi)\frac{\nabla\phi}{|\nabla\phi|} \cdot \nabla\mathcal{V} = 0.$$

This equation advects the initial velocity away from the front in the proper upwind direction (see [6]), maintains continuity between the interfacial velocity and extension velocity at the interface, and in equilibrium has the property that $\nabla\phi \cdot \nabla\mathcal{V} = 0$. This property, once again, helps maintain ϕ as a signed distance function and works in conjunction with the finite element extension method described in (4.6).

Since the velocity depends upon the solution to the steady state PDE given in (4.1) and the shape of the interface, it is only valid on a very small timescale for the level set equation. This means we only need to extend the

velocity to a narrow band around the interface as we are forced to discard it and re-solve the steady state equation. An example of an interface velocity curve and the corresponding extension can be seen in 4.9

4.3.3 Interface Evolution

Finally we come to the interface evolution step. Here, we solve the level set equation

$$\phi_t + \mathcal{V}|\nabla\phi| = 0,$$

for a small time step before recovering the interface and passing the new configuration back to the steady state equation (4.1). The interface is recovered by passing a periodic spline through the oriented collection of points that represent the zero level set $\phi(x, y, t) = 0$ and then sampling this spline at evenly spaced values along the curve.

As ϕ moves towards equilibrium the values of the velocity field will decrease. Since we need to interpolate the velocity from the interface to a regular grid, the interpolation process will cause unphysical results when the interpolation error is the same order as the velocity. To fix this problem and continue with the evolution we can switch to a simpler front tracking method when the maximum velocity value falls below some tolerance based on grid size. By this stage the level set method will have handled the topological changes and non-convex interfaces that are so difficult to capture with front tracking.

Front tracking is very simple to implement and only requires that one calculate the normal vector for nodes on the interface and advance these points in that direction, scaled by the velocity $\dot{\eta}$.

4.3.4 Discretizations

Following the intuition given in [6], we use a third-order total variation diminishing Runge-Kutta scheme for solving the reinitialization, level set and extension velocity equations. This scheme was chosen to avoid temporal instabilities arising from the discretization. Consider the following general equation

$$\phi_t = \mathcal{L}(\phi),$$

where $\mathcal{L}$ is the spatial operator. The third-order TVD scheme is then given as

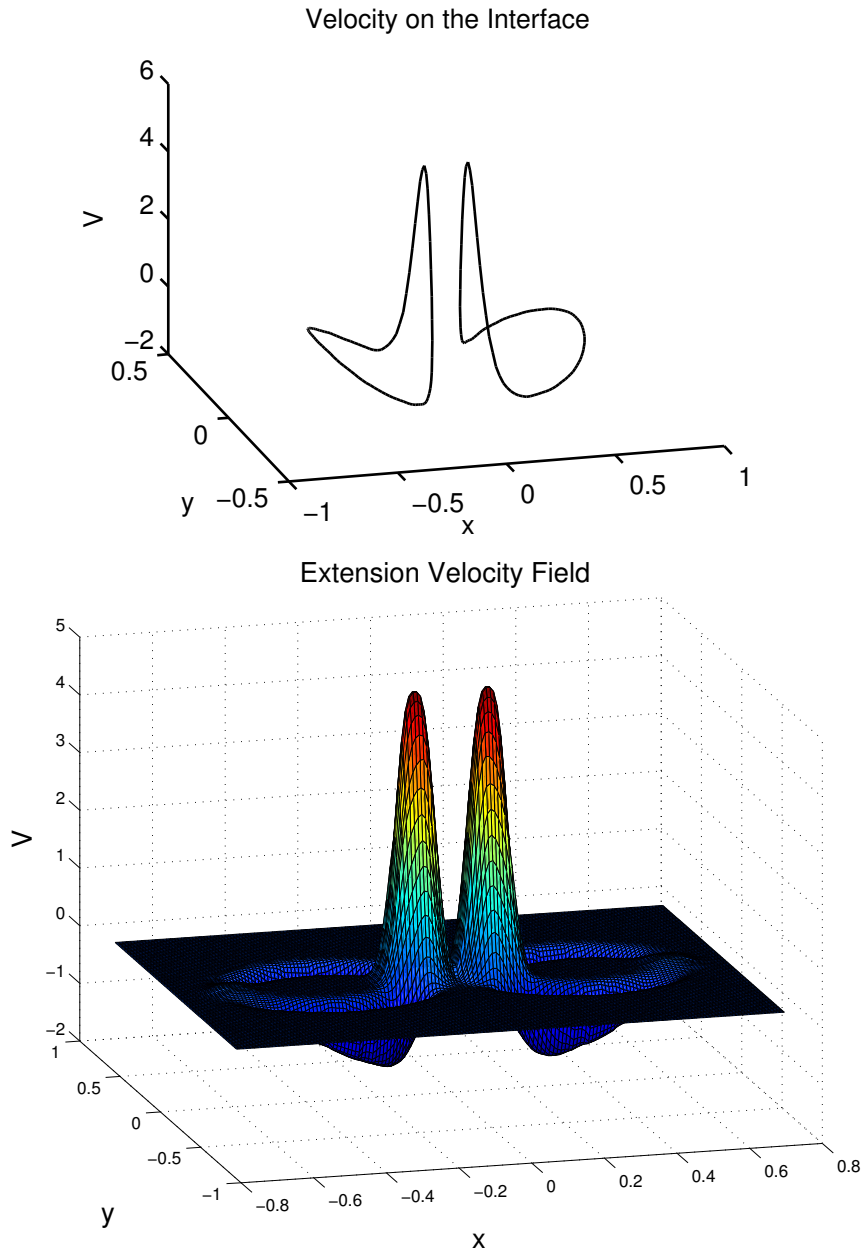

Figure 4.9: An example of a normal velocity curve on the interface and the resulting narrow band extension.

$$\begin{aligned}
\phi^{(1)} &= \phi^{(0)} + \Delta t L(\phi^{(0)}),\\
\phi^{(2)} &= \tfrac{3}{4}\phi^{(0)} + \tfrac{1}{4}\phi^{(1)} + \tfrac{1}{4}\Delta t L(\phi^{(1)}),\\
\phi^{(3)} &= \tfrac{1}{3}\phi^{(0)} + \tfrac{2}{3}\phi^{(2)} + \tfrac{2}{3}\Delta t L(\phi^{(2)}),
\end{aligned}$$

where L is the discrete spatial operator.

For the spatial discretization we again follow [6]. Consider the spatial operator of the level set equation, given as

$$\mathcal{L}(\phi) = -\mathcal{V}|\nabla\phi|.$$

This is discretized using Godunov's method to make sure upwinding is handled properly. Godunov's method gives us

$$L(\phi) = -\max(\mathcal{V},0)\nabla^+ - \min(\mathcal{V},0)\nabla^-,$$

where

$$\begin{aligned}
\nabla^+ =&[\max(\max(D^{+x}\phi,0)^2, \min(D^{-x}\phi,0)^2)+\\
&\max(\max(D^{+y}\phi,0)^2, \min(D^{-y}\phi,0)^2)]^{1/2},\\
\nabla^- =&[\max(\max(D^{-x}\phi,0)^2, \min(D^{+x}\phi,0)^2)+\\
&\max(\max(D^{-y}\phi,0)^2, \min(D^{+y}\phi,0)^2)]^{1/2},
\end{aligned}$$

with $D^{\pm x}$ representing the forward and backward difference operators in the x direction, respectively. To improve accuracy the forward and backward difference operators are discretized using the second-order ENO scheme found in [18]. The schemes are

$$D^{+x}\phi_{i,j} = \frac{\phi_{i+1,j} - \phi_{i,j}}{h} - \frac{h}{2}\text{minmod}(D^{xx}\phi_{i,j}, D^{xx}\phi_{i+1,j}),$$

$$D^{-x}\phi_{i,j} = \frac{\phi_{i,j} - \phi_{i-1,j}}{h} + \frac{h}{2}\text{minmod}(D^{xx}\phi_{i,j}, D^{xx}\phi_{i-1,j}),$$

where D^{xx} is the standard central difference approximation to the second derivative and the minmod function returns the argument with the smaller absolute value. These are all reproduced in an analogous fashion for the y direction.

The reinitialization and velocity extension equations are handled with similar discretizations, also using Godunov's method. For the sign function that arises in these equations, we use a smoothed version to alleviate any numerical issues given as

$$\text{sign}(\phi) = \frac{\phi}{\sqrt{\phi^2 + h^2}},$$

where h is the grid spacing.

4.4 Results

In this section we present a few canonical results from which the behavior of many different configurations can be explained. We also verify some of the asymptotic results found in section 3.3.2, 3.3.3 and 3.3.4, where instabilities and different timescales are present. In all examples the outer domain Ω is a circle of radius one centered at the origin and the level set equation is solved on a regular grid with 200 grid points in each direction.

4.4.1 Off-Center Circle

Figure 4.10 is an example of interface evolution where Γ is an off-center circle. Here, $\Omega_- = \{\mathbf{x} : |\mathbf{x} - (.25, .25)| \leq .25\}$, $\sigma = 1$ and $D = 1$.

The reason the drop moves away from the center is due to the Neumann boundary conditions on the domain wall which creates a mirroring effect. The droplet is attracted to its image droplet and 'reaches' out towards it. This also confirms the analysis from section 3.3.3, in particular remark 3.3.3.4 (iv), where it was found that when off-center the drop initially bulges outwards. With this level set formulation it would be hard to capture exactly what occurs when it reaches the boundary due to our embedding the circular domain in a regular gridded square.

We also plot the area loss versus iteration count (area at current iteration - initial area) in figure 4.11. This is a rough metric for accuracy of the level set method in this case when there is no exact solution. Despite losing area per time step the total loss remains small.

4.4.2 Two Axisymmetric Perturbed Circles

In figures 4.12 through 4.15 we examine the case of two axisymmetric perturbed circles, where the perturbation is relatively small. In polar coordinates the shapes are given by $r = .0175(\cos(6\theta) + 12)$ with a shift of .45 and $-.45$ in the x direction. Here, $D = 1$ and $\sigma = 1$.

The evolution of this example can be broken into four phases. The first phase is that in which the perturbations rapidly smooth out to a circular shape (figure 4.12). The second phase is the much slower evolution of the two

circles moving together and eventually merging into one mass (figure 4.13). The third phase is the barbell shape of the two merged circles smoothing out into an ellipse (figure 4.14). Finally, the last phase is the equilibrium state of a circular drop centered in Ω at the origin (figure 4.15).

These four phases serve as canonical results that explain the chemotactic evolution process for many different droplet configurations. For typical parameter values, perturbations to circles will smooth out and drops will move towards each other and merge into one large group. The behavior is very similar to that of the Ostwald ripening in this regard.

The slow merging in the second and third phases relative to the quick smoothing in the first suggests that the two evolution processes happen on different timescales. This confirms the asymptotic result derived at the end of section 3.3.4.

4.4.3 Asymptotic Result: Boundary Effects Cause Instabilities

In figure 4.16, we confirm the asymptotic result in section 3.3.2, remark 3.3.2.1. In this case, $\Gamma = r_0 + \delta\cos(n\theta)$ was shown to be unstable when r_0 was above some critical value that depends upon n and λ. Instead of returning to a circular shape as in figures 4.12 through 4.15, we have growth of the perturbation. This instability is due to effects of the domain boundary and Neumann boundary conditions, which cause the drop to reach outwards towards its mirror image. Notice that the entirety of the perturbation does not grow, only the sides that reach out beyond $r = .5$.

The parameter values selected that satisfy this condition are $D = 250$, $r_0 = .65$, $\delta = .15$, $n = 2$ and $\sigma = 1$. Figure 4.16 highlights this instability and the aforementioned growth of the perturbation.

4.4.4 Asymptotic Result: Perturbations to Small Drop Decay Faster Than Perturbations to Large Drop

Figure 4.17 is a confirmation of the result from section 3.3.2, specifically equation (3.46). Here, we assumed that the interface, Γ, is a near circle given by $r = r_0 + \delta\cos(n\theta)$. In the limit where $\delta \ll r_0 \ll 1$ and $\lambda = 1/\sqrt{D} = O(1)$ (D from (4.1)), we have that a perturbation flattens out with velocity proportional to $O(\delta/r_0^2)$. This indicates that a small circle with a size δ perturbation should flatten out faster than a larger circle with the same size perturbation.

For the steady state PDE, we set $D = 1$ and $\sigma = 1$. The interface for

the small near-circle is given by $r = .25 + .05\cos(6\theta)$ and large near-circle is $r = .5 + .05\cos(6\theta)$. Figure 4.17 shows that the smaller near-circle returns to an equilibrium state faster than its larger counterpart.

4.4.5 Asymptotic Result: High Frequency Perturbations Decay Faster Than Low Frequency Perturbations

Figure 4.18 is a confirmation of the result from section 3.3.2, equation (3.47). Here, we assumed that the interface, Γ, is a near circle given by $r = r_0 + \delta\cos(n\theta)$. In the limit where D and ρ_0 are fixed and $n \to \infty$, where n is the order of the perturbation, we have that the perturbations flatten with velocity proportional to $O(n^2)$. This means a high frequency perturbation will decay faster than a lower frequency one for the same r_0 and δ.

For the steady state PDE, we set $D = 1$ and $\sigma = 1$. The high frequency interface is given by $r = .35 + .05\cos(9\theta)$ and the low frequency is $r = .35 + .05\cos(6\theta)$. Figure 4.18 shows that the higher the frequency, the faster the perturbations decay.

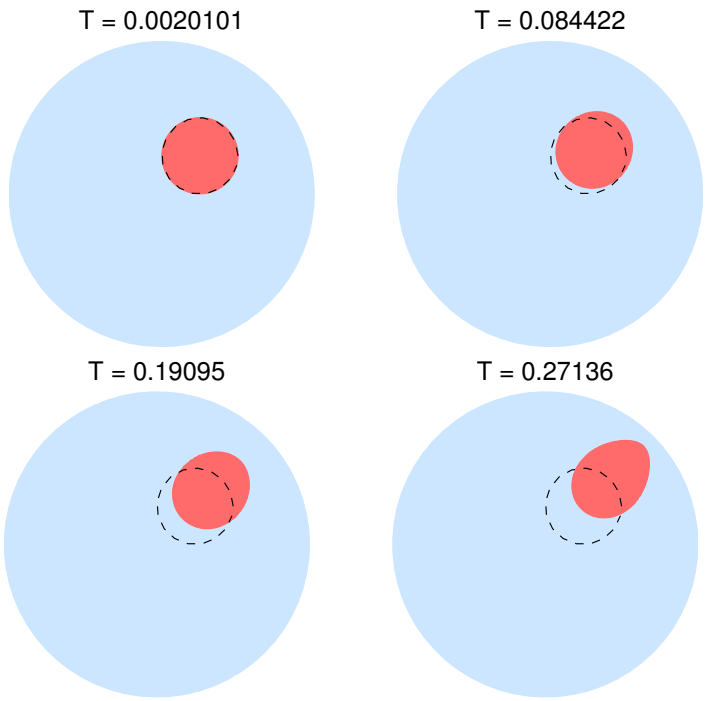

Figure 4.10: Off-circle example. Blue is the outer domain, the dotted black line is the initial position and dark red is the moving drop. For the triangulated mesh we start with an initial edge size of .05 with 100 fixed nodes on the interface. The time step for reinitialization, constructing the extension velocity and solving the level set equation was chosen to be $h/5$, where h is the regular grid mesh size.

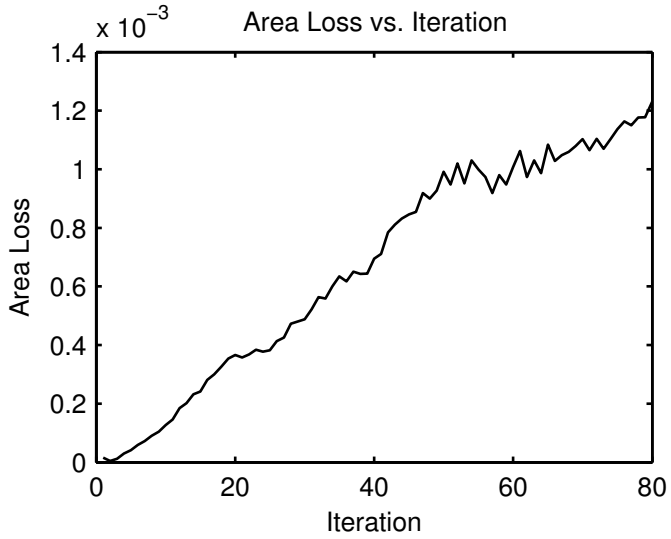

Figure 4.11: Plot of area loss versus iteration count for the off-center circle example. Area is lost at each iteration but remains small.

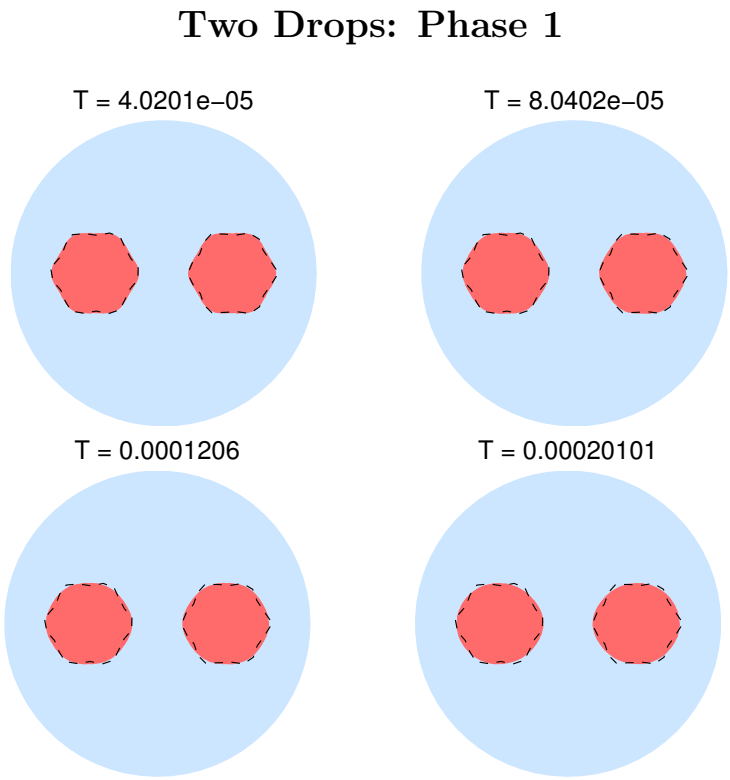

Figure 4.12: Phase 1 of the two perturbed circle example. Blue is the outer domain, the dotted black line is the initial position and dark red is the moving drop. For the triangulated mesh we start with an initial edge size of .05 with 100 fixed nodes on each interface. The time step for reinitialization, constructing the extension velocity and solving the level set equation was chosen to be $h/5$, where h is the regular grid mesh size.

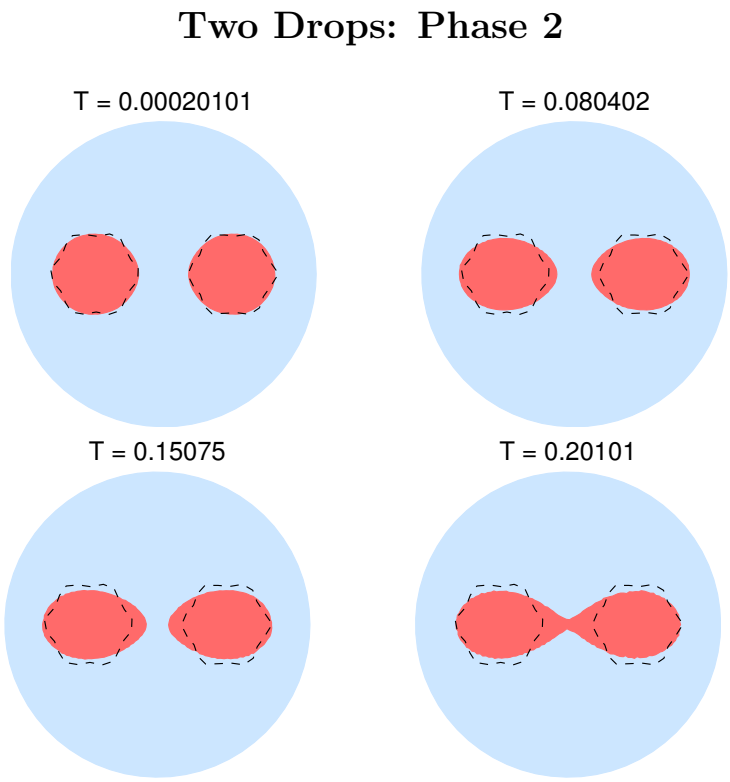

Figure 4.13: Phase 2 of the two perturbed circle example. Blue is the outer domain, the dotted black line is the initial position and dark red is the moving drop. For the triangulated mesh we start with an initial edge size of .05 with 100 fixed nodes on each interface which becomes 200 fixed nodes when the domains merge. The time step for reinitialization, constructing the extension velocity and solving the level set equation was chosen to be $h/5$, where h is the regular grid mesh size.

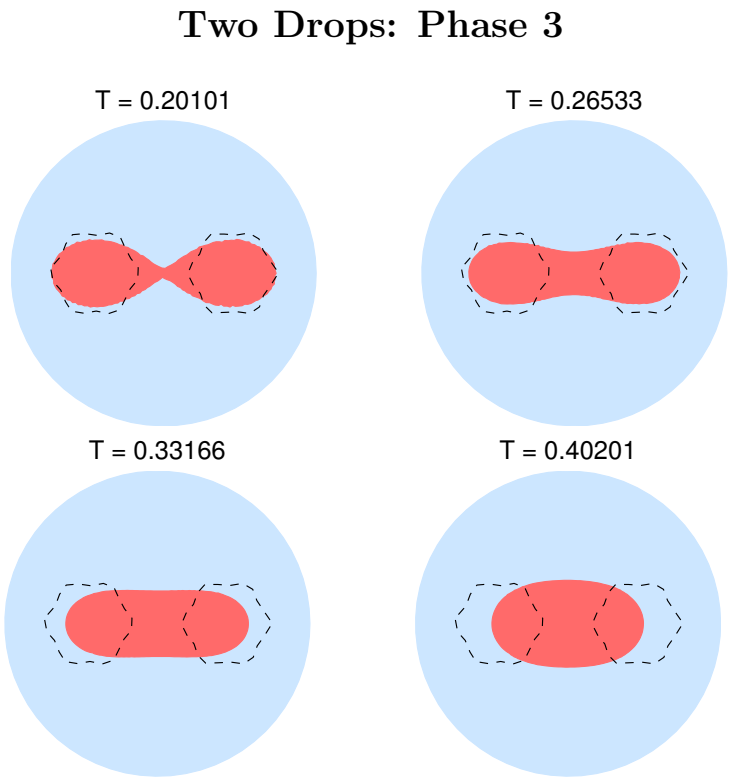

Figure 4.14: Phase 3 of the two perturbed circle example. Blue is the outer domain, the dotted black line is the initial position and dark red is the moving drop. For the triangulated mesh we start with an initial edge size of .05 with 200 fixed nodes on the interface. The time step for reinitialization, constructing the extension velocity and solving the level set equation was chosen to be $h/5$, where h is the regular grid mesh size.

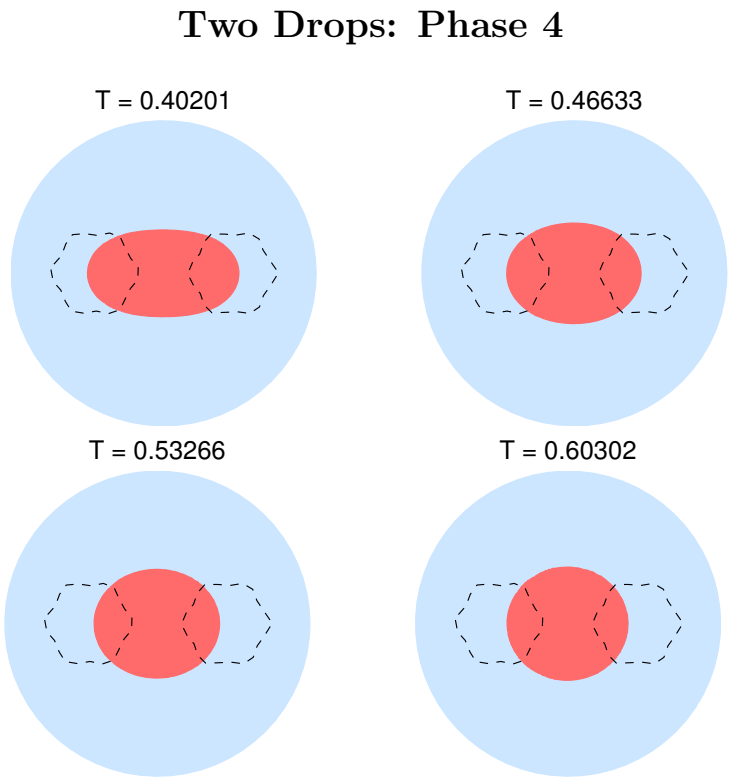

Figure 4.15: Phase 4 of the two perturbed circle example. Blue is the outer domain, the dotted black line is the initial position and dark red is the moving drop. For the triangulated mesh we start with an initial edge size of .05 with 200 fixed nodes on the interface. The time step for reinitialization, constructing the extension velocity and solving the level set equation was chosen to be $h/5$, where h is the regular grid mesh size.

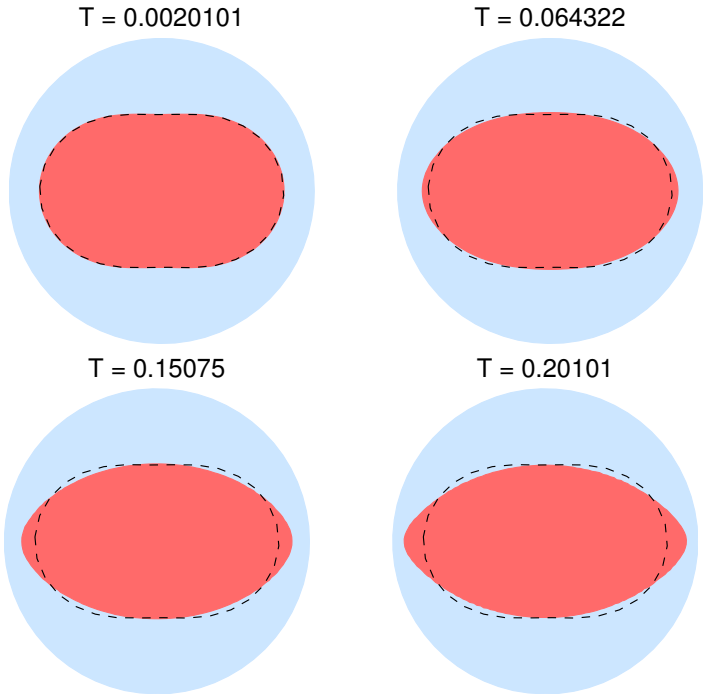

Figure 4.16: An example of an unstable perturbation due to boundary effects. Blue is the outer domain, the dotted black line is the initial position and dark red is the moving drop. For the triangulated mesh we start with an initial edge size of .05 with 180 fixed nodes on the interface. The time step for reinitialization, constructing the extension velocity and evolution of the level set equation was selected as $h/5$, where h is the regular grid mesh size.

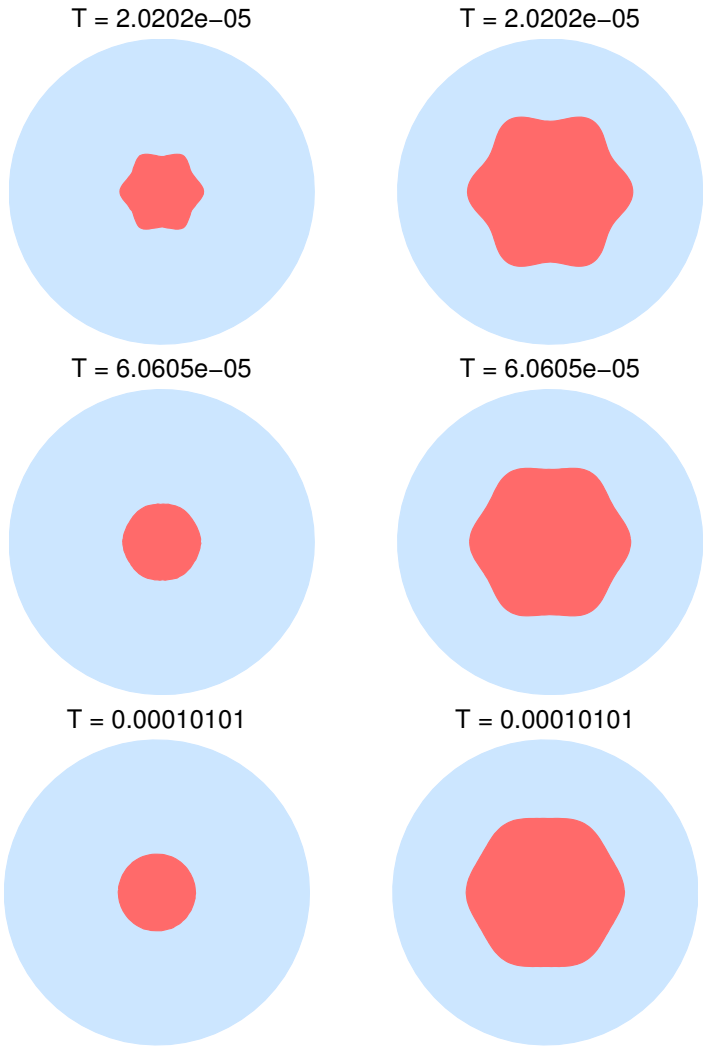

Figure 4.17: Different sized perturbed circle example. Blue is the outer domain and dark red is the moving drop. For the triangulated mesh we start with an initial edge size of .05 with 100 fixed nodes on the interface when $r_0 = .25$ (left) and 200 fixed nodes on the interface when $r_0 = .5$ (right). The time step for reinitialization and constructing the extension velocity was selected as $h/5$, where h is the regular grid mesh size. In order to capture the quick perturbation-flattening effects, the time step for the level set equation was $h^2/5$.

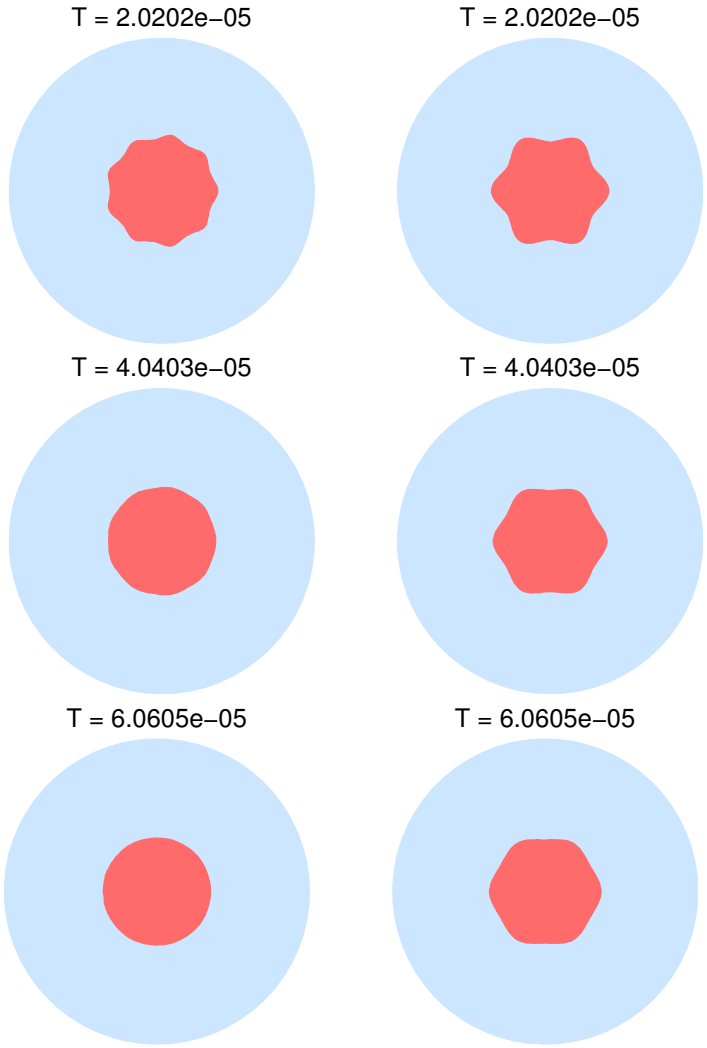

Figure 4.18: Different frequency perturbed circle example. Blue is the outer domain and dark red is the moving drop. For the triangulated mesh we start with an initial edge size of .05 with 150 fixed nodes on the interface. The time step for reinitialization and constructing the extension velocity was selected as $h/5$, where h is the regular grid mesh size. In order to capture the quick perturbation-flattening effects, the time step for the level set equation was $h^2/5$.

Chapter 5

Conclusion

In this thesis we studied the interfacial motion present in the two-dimensional Ostwald ripening and volume-filling chemotaxis systems. For both problems, we derive the governing partial differential equation model and use the method of matched asymptotic expansions to determine the laws which dictate motion. After this motion law is derived, we verify the result against intuition and expected behavior with numerical simulations and specific examples.

The Ostwald ripening system is derived as the late-stage dynamics of the Cahn-Hilliard equation and results in a Mullins-Sekerka free boundary problem. We consider a collection of N small circular droplets in a domain, $\Omega \subset \mathbb{R}^2$. We construct an inner and outer solution to the problem and enforce matching to derive a system of ordinary differential equations which describe the motion of the radius of each drop, to leading order. Following this, we improve our solution, solving the problem to terms of all logarithmic order where, at this order, the interaction is captured by a Neumann Green matrix. The system of ordinary differential equations is improved and now requires solving a linear algebraic system involving the radius of each drop and the Neumann Green's function. The system is seen to be area preserving, perimeter reducing, and have the finite time extinction property where the smallest droplet vanishes in finite time. These properties push the system towards an equilibrium state of a single, large drop that holds all of the initial mass. We verify the derived system of ordinary differential equations with a simple two drop numerical simulation.

For our study on the volume-filling chemotaxis system, we derive the model by assuming an organism exhibits a random walk on a one-dimensional infinite lattice with preferred movement in the direction of a chemical gradient. Volume-filling is included with a monotone decreasing function which decays to zero when the concentration of the organism reaches the normalized maximum value of one. We define the interface, Γ, as a collection of simple closed curves which separate regions with concentration one and concentration zero of the organism. In the limit of small diffusive forces, we use a boundary fitted coordinate system and matched asymptotic expansions to

derive a surface diffusion law that describes the velocity on this interface. The velocity is then used to determine the behavior in a few specific cases.

In the case of two concentric circles, the velocity is identically zero and we are in a stable equilibrium. This is confirmed by solving the problem exactly as well as with a matched asymptotic expansion when the initial mass of the system is small. Next, we examine what occurs when the circular shape of the droplet is perturbed. In the limit of a high frequency perturbation or large chemical diffusion, we see the velocity stabilizing the system. When in the limit of small diffusive forces, we cannot confirm the system stabilizes but if any instability occurs it will be very weak. The third case is that of many small circular interfaces. Here the movement is critically influenced by the configuration of all other drops due to gradient terms in the Green's function. We see that there is a weakness in the model as the equations dictate an unphysical stable equilibrium of N small disks of a common radius located at the roots of unity on a ring concentric within the unit disk. We also determine that a single off-center drop will move away from the center, in the direction of its image across the domain wall. This case also shows that a small drop will deform the most and a collection of N small circular drops will not remain circular. In the final case study we derive information about the velocity for N small arbitrarily shaped drops. Here we see that, to leading order, the drops are influenced not by interaction among themselves but due to their arbitrary shape.

We analyze and verify the asymptotic results with numerical simulations, making use of the finite element and level set methods to capture complicated geometries and merging of interfaces. An interface-fitted mesh is used along with isoparametric quadratic elements in the finite element method to solve the steady state partial differential equation with sufficient accuracy. We use this solution to numerically calculation the velocity on each interface. This interfacial velocity is then interpolated to a regular-gridded domain and extended outwards for use with the level set method. The level set method robustly handles the evolution and merging of each interface by describing them as a signed distance function. This process is repeated by recovering the interface and again solving the steady state problem. We confirm many of the asymptotic results as well as show a set of canonical drop interactions.

The analysis of these two systems suggest many open problems and future work. For Ostwald ripening, we would like to extend the work in [8] to two dimensions. Here, they consider the Mullins-Sekerka free boundary problem with kinetic drag. We would also like to extend the equations of motion in Ostwald ripening to incorporate perturbations to the circu-

lar shapes. In the chemotaxis model we assumed the volume-filling term was $q(u) = 1 - u$. The surface diffusion law can be extended to include a more general volume-filling term. For chemotaxis, numerical simulations revealed boundary effects when the radius of a near-circular drop was beyond a certain critical value. This phenomenon was only observed and not characterized; it would be interested to see analytic results verifying these simulations. Additionally, we conjecture in section 3.1, conjecture 3.1 that the denominator of the surface diffusion law must be positive. Proving this is important for completeness of understanding the surface diffusion in chemotaxis. Finally, the analysis on a collection of arbitrarily shaped small initial droplets concludes with a local solution that is independent of any interaction with the other drops. Extending this analysis to higher orders will answer the question of whether the system leads to a circular shape on a longer timescale.

Bibliography

[1] Milton Abramowitz and Irene A. Stegun, editors. *Handbook of Mathematical Functions with Formulas, Graphs, and Mathemtical Tables*. Dover Publications, New York, 1972.

[2] Nicholas D. Alikakos, Giorgio Fusco, and Georgia Karali. Ostwald ripening in two dimensions- the rigorous derivation of the equations from the mullins-sekerka dynamics. *Journal of Differential Equations*, 205:1–49, 2004.

[3] Howard C. Berg. *E. coli in Motion*. Biological and Medical Physics, Biomedical Engineering. Springer, New York, 2004.

[4] John W. Cahn. On spinodal decomposition. *Acta Meterialia*, 9(795-801), 1961.

[5] John W. Cahn and John E. Hilliard. Free energy of a nonuniform system. i. interfacial free energy. *The Journal of Chemical Physics*, 28, 1958.

[6] S. Chen, B. Merriman, S. Osher, and P. Smereka. A simple level set method for solving stefan problems. *Journal of Computational Physics*, 135(CP975721), 1997.

[7] W. Chen and M. J. Ward. The stability and dynamics of localized spot patterns in the two-dimensional gray-scott model. *SIAM Journal of Applied Dynamical Systems*, 10(2):582–666, 2011.

[8] Shibin Dai, Barbara Niethammer, and Robert L. Pego. Crossover in coarsening rates for the monopole approximation of the mullins-sekerka model with kinetic drag. *Proceedings of the Royal Society of Edinburgh*, 140:553–571, 2010.

[9] H. J. Eberl, D. F. Parker, and M. C. M. van Loosdrecht. A new deterministic spatio-temporal continuum model for biofilm development. *Journal of Theoretical Medicine*, 3:161–175, 2001.

[10] Thomas Hillen and Kevin Painter. Global existence for a parabolic chemotaxis model with prevention of over-crowding. *Adv. Appl. Math*, 26:280–301, 2001.

[11] Thomas Hillen and Kevin Painter. Volume-filling and quorum-sensing in models for chemosensitive movement. *Canadian Applied Mathematics Quarterly*, 10:501–543, 2002.

[12] Thomas Hillen and Kevin Painter. A users guide to pde models for chemotaxis. *Journal of Mathematical Biology*, 58:183–217, 2009.

[13] D. Horstmann. Lyapunov functions and l^p-estimates for a class of reaction-diffusion systems. *Coll. Math*, 87:113–127, 2001.

[14] D. Horstmann. From 1970 until present: the keller-segel model in chemotaxis and its consequences. *I. Jahresberichte DMV*, 105:103–165, 2003.

[15] E. F. Keller and L. A. Segel. Model for chemotaxis. *Journal of Theoretical Biology*, 30:225–234, 1971.

[16] R. Kowalczyk. Preventing blow-up in a chemotaxis model. *J. Math. Anal. Appl.*, 305:566–588, 2005.

[17] Bo Li and John Shopple. An interface-fitted finite element level set method with applications to solidification and solvation. *Commun. Comput. Phys.*, 10(1):32–56, July 2011.

[18] Chohong Min. On reinitializing level set functions. *Journal of Computational Physics*, 229:2764–2772, 2010.

[19] Derek Van Orden and Vitaliy Lomakin. Rapidly convergent representations for periodic green's functions of a linear array in layered media. *IEEE Transactions on Atennas and Propagation*, 60(2), February 2012.

[20] K. Osaki and A. Yagi. Finite dimensional attractor for one-dimensional keller-segel equations. *Funkcial. Ekvac*, 44:441–469, 2001.

[21] S. Osher and J. A. Sethian. Fronts propagating with curvature dependent speed: Algorithms based on hamilton-jacobi formuatlion. *Journal of Computational Physics*, 1988:12–49, 1988.

[22] C. S. Patlak. Random walk with persistence and external bias. *The Bulletin of Mathematical Biophysics*, 15:331–338, 1953.

[23] R. L. Pego. Front migration in the nonlinear cahn-hilliard equation. *Proceedings of the Royal Society of London. series A, Mathematical and Physical Science*, 422:261–278, 1989.

[24] Per-Olof Persson and Gilbert Strang. A simple mesh generator in matlab. *SIAM Review*, 46(2):329–345, June 2004.

[25] Giovanni Russo and Peter Smereka. A remark on computing distance functions. *Journal of Computational Physics*, 163:51–67, 2000.

[26] J. A. Sethian. *Level Set Methods and Fast Marching Methods: Evolving interfaces in Computational geometry, fluid mechanics, computer vision, and material science.* Cambridge Monographs on Applied and Computational Mathematics. Cambidge University Press, 1999.

[27] Roy H. Stogner, Graham F. Carey, and Bruce T. Murray. Approximation of cahn-hilliard diffuse interface models using parallel adaptive mesh refinement and coarsening with c^1 elements. *International Journal for Numerical Methods in Engineering*, 64:1–19, 2006.

[28] Mark Sussman, Peter Smereka, and Stanley Osher. A level set approach for computing solutions to incompressible two-phase flow. *Journal of Computational Physics*, 114:146–159, 1994.

[29] M. Winkler. Absence of collapse in a parabolic chemotaxis model with signal-dependent sensitivity. *Math. Nachr.*, 283:1664–1673, 2010.

[30] D. Wrzosek. Global attractor for a chemotaxis model with prevention of overcrowding. *Nonlin. Ana.*, 59:1293–1310, 2004.

Appendix A

Boundary Fitted Coordinates

Here we derive the boundary fitted coordinate system used in the chemotaxis model. Let η be the minimal distance from a point in some domain Ω to boundary $\partial\Omega$. We choose η such that $\eta > 0$ inside Ω and $\eta < 0$ outside Ω. Assuming Ω is smooth, there exists have a unit tangent vector $\mathbf{t}$ and unit (inward) normal vector $\mathbf{n}$ at each point on $\partial\Omega$.

We can parametrize $\partial\Omega$ by arc length giving us $(\gamma_1(s), \gamma_2(s))$ as the parametrization. We also know that the normal vector and tangent vector are related through curvature, κ. That is, $\frac{d\mathbf{t}}{ds} = \kappa\mathbf{n}$. κ is positive for convex sets, as seen from inside.

Let (x_1, x_2) be any point near $\partial\Omega$ in cartesian coordinates (the notion of near is clarified below). The change of variables becomes

$$\begin{aligned} x_1 &= \gamma_1(s) + \eta n_1(s); \qquad & \mathbf{n} &= (n_1, n_2), \\ x_2 &= \gamma_2(s) + \eta n_2(s); \qquad & \mathbf{t} &= (\gamma_1', \gamma_2'). \end{aligned}$$

Differentiating with respect to x_1 and x_2 and letting $\mathbf{e_{x_1}} = (1, 0)$ and $\mathbf{e_{x_2}} = (0, 1)$ we wind up with

$$\begin{aligned} \mathbf{e_{x_1}} &= \boldsymbol{\gamma}'(s)\frac{\partial s}{\partial x_1} + \frac{\partial \eta}{\partial x_1}\mathbf{n} + \eta\mathbf{n}'(s)\frac{\partial s}{\partial x_1}, \\ \mathbf{e_{x_2}} &= \boldsymbol{\gamma}'(s)\frac{\partial s}{\partial x_2} + \frac{\partial \eta}{\partial x_2}\mathbf{n} + \eta\mathbf{n}'(s)\frac{\partial s}{\partial x_2}. \end{aligned} \tag{A.1}$$

Since $\mathbf{n}$ is a unit vector, $\mathbf{n} \cdot \mathbf{n} = 1$ and thus

$$\frac{d}{ds}(\mathbf{n} \cdot \mathbf{n}) = 2\frac{d\mathbf{n}}{ds} \cdot \mathbf{n} = 0.$$

This means that $d\mathbf{n}/ds$ is perpendicular to $\mathbf{n}$ and thus we have $d\mathbf{n}/ds = \alpha\mathbf{t}$ for some α to be found. To find α we take two derivatives with respect to s of $\mathbf{t}$, giving us

$$\frac{d^2\mathbf{t}}{ds^2} = \kappa'(s)\mathbf{n} + \kappa\frac{d\mathbf{n}}{ds}.$$

Taking the dot product of above with respect to $\mathbf{t}$ we arrive at

$$\mathbf{t} \cdot \frac{d^2\mathbf{t}}{ds^2} = 0 + \kappa \mathbf{t} \cdot \frac{d\mathbf{n}}{ds} = \kappa\alpha \mathbf{t} \cdot \mathbf{t} = \kappa\alpha.$$

Since, as stated above, $d\mathbf{t}/ds = \kappa\mathbf{n}$ and $\mathbf{n}$ is perpendicular to $\mathbf{t}$, $\mathbf{t} \cdot (d\mathbf{t}/ds) = 0$. Thus, consider

$$0 = \frac{d}{ds}\left[\frac{d\mathbf{t}}{ds} \cdot \mathbf{t}\right] = \mathbf{t} \cdot \frac{d^2\mathbf{t}}{ds^2} + \frac{d\mathbf{t}}{ds} \cdot \frac{d\mathbf{t}}{ds} = \kappa\alpha + \kappa^2 \mathbf{n} \cdot \mathbf{n} = \kappa(\alpha + \kappa).$$

Since $\kappa \neq 0$, we have that $\alpha = -\kappa$. Substituting the information we just derived into the equation A.1 for $\mathbf{e_{x_1}}$ and $\mathbf{e_{x_2}}$ we wind up with

$$\begin{aligned}
\mathbf{e_{x_1}} &= (1 - \kappa\eta)\frac{ds}{dx_1}\mathbf{t}(s) + \frac{d\eta}{dx_1}\mathbf{n}(s), \\
\mathbf{e_{x_2}} &= (1 - \kappa\eta)\frac{ds}{dx_2}\mathbf{t}(s) + \frac{d\eta}{dx_2}\mathbf{n}(s).
\end{aligned}$$

Now, taking the dot product of these two equations with respect to $\mathbf{t}$ we wind up with

$$\nabla s = \left(\frac{ds}{dx_1}, \frac{ds}{dx_2}\right) = \frac{\mathbf{t}}{1 - \kappa\eta} \tag{A.2}$$

Similarly, by taking the dot product of the two equations with $\mathbf{n}$ we wind up with

$$\nabla \eta = \left(\frac{d\eta}{dx_1}, \frac{d\eta}{dx_2}\right) = \mathbf{n}. \tag{A.3}$$

This implies that η, the distance, must satisfy $\eta < 1/\kappa$. This is the precise definition of a point being near the boundary.

With this in hand we take an arbitrary function $u(x_1, x_2)$ and write ∇u in terms of the new coordinates. This gives us

$$\begin{aligned}
\nabla u &= u_{x_1}\mathbf{e_{x_1}} + u_{x_2}\mathbf{e_{x_2}} \\
&= (u_s s_{x_1} + u_\eta \eta_{x_1})[(1 - \kappa\eta)s_{x_1}\mathbf{t} + \eta_{x_1}\mathbf{n}] \\
&\quad + (u_s s_{x_2} + u_\eta \eta_{x_2})[(1 - \kappa\eta)s_{x_2}\mathbf{t} + \eta_{x_2}\mathbf{n}].
\end{aligned}$$

Expanding and rearranging, we wind up with

$$\begin{aligned}
\nabla u = (1 - \kappa\eta)u_s\mathbf{t}(s_{x_1}^2 + s_{x_2}^2) + u_\eta\mathbf{n}(\eta_{x_1}^2 + \eta_{x_2}^2) \\
+ u_s\mathbf{n}(s_{x_1}\eta_{x_1} + s_{x_2}\eta_{x_2}) + (1 - \kappa\eta)u_\eta\mathbf{t}(s_{x_1}\eta_{x_1} + s_{x_2}\eta_{x_2}).
\end{aligned}$$

Realizing that $s_{x_1}\eta_{x_1} + s_{x_2}\eta_{x_2} = \nabla s \cdot \nabla \eta = 0$, we have

$$\nabla u = \|\nabla s\|^2(1-\kappa\eta)u_s\mathbf{t} + \|\nabla\eta\|^2 u_\eta \mathbf{n},$$

but, since we have expressions for ∇s and $\nabla \eta$ (A.2 and A.3), we can simplify further

$$\nabla u = \frac{u_s}{1-\kappa\eta}\mathbf{t} + u_\eta \mathbf{n}. \tag{A.4}$$

We would also like to see how Δu changes under this new coordinate system. We begin by calculating $\Delta\eta$ as

$$\Delta\eta = \frac{d\mathbf{n}}{ds}\cdot\nabla s = -\kappa\mathbf{t}\cdot\frac{\mathbf{t}}{1-\kappa\eta} = -\frac{\kappa}{1-\kappa\eta}. \tag{A.5}$$

We do the same for Δs to give us

$$\Delta s = \frac{\mathbf{t}'(s)\cdot\nabla s}{1-\kappa\eta} + \mathbf{t}\cdot\nabla\left(\frac{1}{1-\kappa\eta}\right).$$

We know that $\nabla s = \mathbf{t}/(1-\kappa\eta)$ from A.2 so the first term on the right hand side vanishes by the fact that $\mathbf{t}'\cdot\mathbf{t} = 0$. We wind up with

$$\Delta s = \mathbf{t}\cdot\left[\frac{\kappa'\eta\nabla s + \kappa\nabla\eta}{(1-\kappa\eta)^2}\right].$$

From A.3, we know that $\nabla\eta = \mathbf{n}$ and $\mathbf{n}$ is perpendicular to $\mathbf{t}$ so the second term in the numerator vanishes. Substituting in for ∇s we arrive at

$$\Delta s = \mathbf{t}\cdot\left[\frac{\kappa'\eta\mathbf{t}}{(1-\kappa\eta)^3}\right] = \frac{\kappa'\eta}{(1-\kappa\eta)^3}. \tag{A.6}$$

We are now in a position to finish the calculation. Taking a dot product of the gradient in the boundary fitted coordinate system and ∇u from A.4, we have

$$\Delta u = u_{\eta\eta}\|\nabla\eta\|^2 + u_{ss}\|\nabla s\|^2 + 2u_{s\eta}\nabla s\cdot\nabla\eta + u_\eta\Delta\eta + u_s\Delta s.$$

Substituting in for $\nabla\eta$, ∇s, $\Delta\eta$ and Δs from A.3, A.2, A.5 and A.6, we can simplify to

$$\Delta u = u_{\eta\eta} - \frac{\kappa}{1-\kappa\eta}u_\eta + \frac{1}{(1-\kappa\eta)^2}u_{ss} + \frac{\kappa'\eta}{(1-\kappa\eta)^3}u_s,$$

or, written in a slightly different way, we arrive at our final equation

$$\Delta u = u_{\eta\eta} - \frac{\kappa}{1-\kappa\eta} u_\eta + \frac{1}{1-\kappa\eta} \frac{d}{ds} \left(\frac{u_s}{1-\kappa\eta} \right).$$

Appendix B

Green's Function for the Unit Disk

This work was taken from a paper [7]. We want to find the Green's function corresponding to the PDE given below in the domain $\Omega = \{\mathbf{x} : |\mathbf{x}| \leq 1\}$.

$$\Delta G_\lambda - \lambda^2 G_\lambda = -\delta(\mathbf{x} - \mathbf{x}_0), \quad \mathbf{x} \in \Omega; \qquad \frac{\partial G_\lambda}{\partial n} = 0, \quad \mathbf{x} \in \partial\Omega, \tag{B.1}$$

where $\lambda = 1/\sqrt{D}$.

The first step is to switch to polar coordinates. The PDE above becomes

$$\partial_{\rho\rho} G_\lambda + \frac{1}{\rho}\partial_\rho G_\lambda + \frac{1}{\rho^2}\partial_{\theta\theta} G_\lambda - \lambda^2 G_\lambda = -\frac{1}{\rho}\delta(\rho - \rho_0)\delta(\theta - \theta_0),$$

where the boundary conditions become $G_\lambda(\rho, \theta+2\pi) = G_\lambda(\rho, \theta)$, $\partial_\rho G_\lambda(1, \theta) = 0$ and G_λ has the proper log singularity as $\rho \to 0$.

This can be solved by making use of the complex Fourier series. We have

$$G_\lambda(\rho, \theta; \rho_0, \theta_0) = \frac{1}{2\pi}\sum_{n=-\infty}^{\infty} \bar{G}_{\lambda,n}(\rho; \rho_0, \theta_0) e^{-in\theta},$$

$$\bar{G}_{\lambda,n}(\rho; \rho_0, \theta_0) = \int_0^{2\pi} e^{in\theta} G_\lambda(\rho, \theta; \rho_0, \theta_0) d\theta.$$

Substituting this in leads us to

$$\begin{gathered}\partial_{\rho\rho}\bar{G}_{\lambda,n} + \frac{1}{\rho}\partial_\rho \bar{G}_{\lambda,n} - \frac{n^2}{\rho^2}\bar{G}_{\lambda,n} - \lambda^2 \bar{G}_n = \frac{1}{\rho}\delta(\rho - \rho_0)e^{in\theta_0}, \quad 0 < \rho < 1, \\ \bar{G}_{n\rho}(1; \rho_0, \theta_0) = 0; \qquad \bar{G}_n(0; \rho_0, \theta_0) < \infty.\end{gathered} \tag{B.2}$$

The solution to this is

$$\bar{G}_{\lambda,n}(\rho; \rho_0, \theta_0) = \left[K_n(\rho_> \lambda) - \frac{K_n'(\lambda)}{I_n'(\lambda)} I_n(\rho_> \lambda)\right] e^{in\theta_0} I_n(\rho_< \lambda),$$

where this can be found by solving equation B.2 on either side of ρ_0 and then enforcing continuity and the jump condition. Here, $\rho_< = \min(\rho_0, \rho)$ and $\rho_> = \max(\rho_0, \rho)$. Thus, the full solution to B.1 is

$$G_\lambda(\rho, \theta; \rho_0, \theta_0) = \frac{1}{2\pi} \sum_{n=-\infty}^{\infty} e^{-in(\theta-\theta_0)} \left[K_n(\rho_>\lambda) - \frac{K_n'(\lambda)}{I_n'(\lambda)} I_n(\rho_>\lambda) \right] I_n(\rho_<\lambda). \tag{B.3}$$

We wish to improve the convergence of this series which is known to converge slowly ([19]). Consider the free space Green's function Fourier representation,

$$G_f(\rho, \theta; \rho_0, \theta_0) = \frac{1}{2\pi} K_0(R\lambda) = \frac{1}{2\pi} \sum_{n=-\infty}^{\infty} e^{-in(\theta-\theta_0)} K_n(\rho_>\lambda) I_n(\rho_<\lambda),$$

where $R = \sqrt{\rho^2 + \rho_0^2 - 2\rho\rho_0 \cos(\theta - \theta_0)}$. At this point the $\rho_<$ and $\rho_>$ notation can be dropped and replaced with ρ_0 and ρ. Rewriting the term above in B.3, we see that

$$G(\rho, \theta; \rho_0, \theta_0) = \frac{1}{2\pi} K_0(R\lambda) - \frac{1}{2\pi} \sum_{n=-\infty}^{\infty} e^{-in(\theta-\theta_0)} \frac{K_n'(\lambda)}{I_n'(\lambda)} I_n(\rho_0\lambda) I_n(\rho\lambda).$$

To approximate this numerically we truncate the infinite series. Before doing this, realizing that $K_n(z) = K_{-n}(z)$ and $I_n(z) = I_{-n}(z)$ we can rewrite the infinite sum to instead go from $n = 0, 1, 2, \ldots$. If we rewrite the exponential term using Euler's formula the sine terms will cancel and gives us

$$\begin{aligned} G(\rho, \theta; \rho_0, \theta_0) = {} & \frac{1}{2\pi} K_0(R\lambda) - \frac{1}{2\pi} \frac{K_0'(\lambda)}{I_0'(\lambda)} I_0(\rho_0\lambda) I_0(\rho\lambda) \\ & - \frac{1}{\pi} \sum_{n=1}^{M} \cos(n(\theta - \theta_0)) \frac{K_n'(\lambda)}{I_n'(\lambda)} I_n(\rho_0\lambda) I_n(\rho\lambda), \qquad 0 < \rho < 1. \end{aligned}$$

Numerically, this can be implemented with MATLAB's built in $K_n(z)$ and $I_n(z)$ and using the recurrence relations, $\partial_z K_n(z) = -(K_{n-1}(z) + K_{n+1}(z))/2$ and $\partial_z I_n(z) = (I_{n-1}(z) + I_{n+1}(z))/2$ for the modified Bessel function derivatives. Terms in the infinite sum are calculated until the next

ρ	ρ_0	M	P_M
.08	.08	32	-9.7502e-09
.05	.08	17	-4.9680e-09
.05	.05	12	-2.4060e-09
.02	.08	9	-3.6761e-09

Table B.1: This table shows the convergence rate for the improved Green's function for select values of ρ and ρ_0. M is the number of iterations required to reach the specified tolerance of 1e-8 for P_M. D = 1 and $\theta = \theta_0$.

term is below some tolerance, say 1e-8. Under these conditions the Green's function for the unit disk converges very quickly, in as few as 9 iterations for some values of ρ and ρ_0. The required number of iterations and P_M for the final term in the sum for different values of ρ and ρ_0 are given in table B.1.